2013 | Faculteit Wetenschappen

DOCTORAATSPROEFSCHRIFT

QCM-based biomimetic sensors for the detection of nicotine, histamine, and malachite green in body fluids and environmental samples.

Proefschrift voorgelegd tot het behalen van de graad van doctor in de wetenschappen

Jan Alenus

Promotor: prof. dr. Patrick Wagner
Copromotor: prof. dr. Thomas J. Cleij

D/2013/2451/29

universiteit hasselt

Chairman:	Prof. Dr. J. MANCA UHasselt
Promotor:	Prof. Dr. P. Wagner UHasselt
Co-promotor:	Prof. Dr. T.J. Cleij Uhasselt and Maastricht University
Members of the jury:	Prof. Dr. K. De Wael Universiteit Antwerpen
	Prof. Dr. S. Ingebrandt University of Applied Sciences Kaiserslautern
	Dr. T. Wagner Aachen University of Applied Sciences
	Dr. R. Thoelen XIOS
	Dr. A. Ethirajan Uhasselt

universiteit hasselt

Table of Contents

Acknowledgements

In the four years working on this thesis, I had the pleasure to be working with some exceptional people. I would like to thank these people for their time and effort.

In de eerste plaats zou ik mijn promotor Prof. Dr. Patrick Wagner willen bedanken. Door zijn boeiende lessen in de opleiding biomedische wetenschappen was de keuze voor mijn bachelor stage in de biosensor groep snel gemaakt. Na deze uiterst leerzame en amusante stage was de keuze voor de master Bioelektronica en Nanotechnologie nog sneller gemaakt. In deze master heb ik door u lessen mij kunnen gooien in de meer fysische aspecten van de wetenschap. Ik was dan ook zeer blij dat ik dit doctoraat in de biosensor groep kon beginnen. Paddi, bedankt om de interesse in biosensoren op te wekken, voor alle goede raad, geweldige ideeën, vele mopjes en zo veel meer.

Uiteraard bedank ik dan ook de tweede helft van de leiders van de master bioelektronica en nanotechnologie, mijn copromotor Prof. Dr. Thomas J. Cleij. Dank u om mij de chemische (en vooral polymeer) kant van de wetenschap te laten ontdekken en voor de heldere ideeën om MIP sensoren vooruit te helpen.

Dit werk had niet kunnen gebeuren zonder de goede hulp en bereidwilligheid van de collega's bij de chemie afdeling. Ten eerste bedank ik Dr. Frederik Horemans die alle MIPs die in dit werk gebruikt zijn ontwikkeld heeft. Dank u voor het maken en optimaliseren van de ontelbare MIPs. Ook zou ik Ans Weustenraed willen bedanken voor het aanmaken van extra MIP batches als de huidige voorraad opgemeten was. Ik wens u veel succes met het afronden van jouw doctoraat.

De eerste maanden van mijn doctoraat werd ik opgevangen en opgeleid door Dr. Ronald Thoelen. Ronald, een dikke merci voor mij te introduceren in de

wondere wereld van sensoren, voor het delen van u kennis en inzichten. Ook na het behalen van uw doctoraat stond gij klaar om elke vraag te beantwoorden en te helpen waar het kon.

I would also like to thank Dr. Anitha Ethirajan for the pleasant talks and meetings which gave new insights and pushed the research into a higher gear.

Aan een doctoraat werk je dus duidelijk niet alleen. Alle ideeën moeten natuurlijk ook praktische mogelijk gemaakt worden. Daarom een dikke merci aan Johnny Baccus en Johan Soogen die elke idee kunnen omzetten in respectievelijk een Solidworks tekening en teflon meetcellen. Werken in een laboratorium kan natuurlijk niet zonder de nodige materialen, bedankt Hilde en Christel voor alle voorzieningen. Graag zou ik dan ook nog Dr. Jan D'haen en Bart Ruttens willen bedanken voor alle SEM beelden. Ook een dank u wel gaat uit naar Jan, Lieven en Erik voor alle hulp en vragen over elektronica en IT. Gelukkig werd ook alles administratief in goede banen geleidt door het secretariaat, merci Lea, Relinde en Marina.

Ook de vele studenten die stage liepen en meehielpen moet ik bedanken voor hun enthousiasme en werklust. Merci Kelly, Daniëlle, Kasper, Martijn and Ruben. A special thanks goes out to Pavel Galar for his seemingly effortless work and the great times we had during his stay in Belgium. He also finally learned that Czech beer is not the best beer in world (but it is still pretty good).

Dan wil ik zeker nog mijn mede doctoraatsstudenten bedanken voor alle hulp en zeker voor alle leuke tijden tijdens mijn doctoraat. Mijn eerste bureaugenoten Lars en Bert, merci om alle problemen van doctoraatstudenten te delen maar zeker ook bedankt voor alle goede raad en de leuke tijd die we beleefd hebben in de te kleine bureau. Ook bedankt aan de oude garde die voor mij begonnen zijn: Evi, Wouter, Rob, Ronald, Stoffel, Sylvia merci voor de geweldige tijden zowel op het IMO als ook in de

cafetaria op vrijdagavond, het Hemelrijck, de Ambi en vele andere momenten.
Maar zeker ook een dikke Merci aan de mensen die na mij zijn begonnen. Ook jullie hebben het IMO verblijf geweldig gemaakt. Matthi, Kasper, Mohammed, Kathia, Bart en Marloes bedankt voor alle geweldig amusante tijden die we beleefd hebben, ik zal ze nooit vergeten.
Ik zou Marloes en Bart ook nog zeker willen bedanken om tijdens de laatste loodjes van dit doctoraat er mee voor te zorgen dat het mooi afgerond wordt.

Ik zou ook mijn mama en mijn zus willen bedanken voor de onvoorwaardelijke steun en vertrouwen dat ik altijd van hen gekregen heb. Zonder jullie steun was het niet mogelijk geweest om dit avontuur af te ronden.

Als laatste zou ik deze thesis willen opdragen aan mijn papa. Mijn papa gaf mij alle vertrouwen in alle keuzes die ik maakte en daar wil ik hem voor bedanken. Hij liet mij altijd mijn eigen weg gaan en ik hoop dat ik hem trots zal maken in alles wat ik doe.

Acknowledgements

Abstract

The need for fast monitoring of compounds is increasing in medicine, food safety and environmental safety. This can be accomplished with the use of sensors which are highly sensitive and selective. Biosensors can fulfill these requirements with an array of different natural recognition elements such as DNA, antibodies, enzymes, cells, etc. The biggest concerns about these sensors are the cost, shelf life and their inability to be used in extreme pH or temperature environments. Synthetic recognition elements can achieve the criteria of the biosensors. However, without their major drawbacks. Molecular imprinted polymers (MIP) are a great candidate as a recognition element. Sensors that use synthetic recognition element are called biomimetic sensors. In this work, biomimetic sensors are created that use MIPs for recognition of histamine, malachite green and L-nicotine.

The principle of a MIP is the creation of a mold around a target molecule. After removal of this target, the mold can only rebind that target. To achieve this, a target molecule is mixed together with functional monomers (e.g. methacrylic acid) and crosslinking monomers (e.g. ethylene glycol dimethacrylate) in a fluid. The functional monomers will form connections with the target molecules. The cross linking monomers are then polymerized so the functional monomers are held into place in an established position. This bulk polymer is crushed and sieved in order to obtain small micro particles. When the target molecule is extracted from these particles, a custom made synthetic recognition element is achieved which can rebind its target molecule. For reasons of control, a non imprinted polymer (NIP) is created in the same way save the use of the target molecules thus creating a NIP which only will bind in a non specific way.

The effectiveness of the created MIP is first tested using (Ultraviolet/Visible) UV/Vis spectroscopy. MIPs are mixed with a solution containing a known concentration of the target molecule. The MIPs will bind a certain amount of

the target molecule present. The MIPs (and thus the target molecule) are then removed from the solution and the remaining target molecules are measured with UV/Vis spectroscopy. This result is compared with a previously measured baseline, so the bound concentration of target molecule is known. UV/Vis is a reliable technique for preliminary testing. However, it can only measure in relative high concentrations (miliMolar range). The NIP is tested with the same protocol. Besides the NIP as a control for sensitivity, other similar compounds are used as selectivity control. Histidine is an amino acid from which histamine is metabolized and is thus an excellent control. Cotinine is the metabolite from L-nicotine and is also used as a control.

Once the MIPs is optimized for their target molecules, they are implemented into a sensor setup. In this work, impedance spectroscopy and gravimetric detection via a quartz crystal microbalance are used. Implementation of the MIPs occurs via immobilization on a polymer layer which was applied on the electrode surface. The polymer used is dependent on the read out technique. With impedance spectroscopy the conjugated polymer OC_1C_{10}-PPV is used while the Quartz crystals used for gravimetric detection are coated with PVC (polyvinyl chloride).

Impedance spectroscopy is a very sensitive technique that measures changes in impedance (electrical resistance) in a frequency spectrum over time. Measurements are performed in the lower frequency ranges as binding of the target molecules to the MIP induces capacitive changes in the recognition layer. It is possible to measure up to 4 different channels, which allows for differential measurements. Histamine measurements were performed in PBS (phosphate buffered saline) in the nanomolar range. Upon binding of histamine to the MIP, the impedance increased significantly while the NIP showed no change. Histidine also showed no impedance change, proving that the MIP is very selective towards histamine. After these successful measurements in PBS, tune brine was spiked with histamine and measured in PBS. Despite the complex fluid, the MIP was able to selectively bind histamine while the NIP showed no significant response. Malachite

green was also successfully detected in the nanomolar range while the NIP showed a lower response.

Gravimetric detection uses a quartz crystal that vibrates at a certain predetermined frequency, the resonance frequency. When the target molecule binds to the MIP, the resonance frequency will decrease linearly with the added mass. This sensor setup is used to measure histamine in deionized water in the micromolar range. The MIP was able to bind 4 times the amount of histamine than the NIP. Malachite green was also successfully tested with QCM in the nanomolar range, which is low for the QCM read out technique. These measurements were performed in water with a pH value of pH 3. L-nicotine was measured with QCM-D (quartz crystal microbalance – dissipation). Dissipation is the amount of energy the crystal dissipates after a crystal excitation. The dissipation will change when softer material is bound to the crystal surface. Measurements were performed in deionized water and in PBS. The amount of L-nicotine that can be bound in deionized water is greater than in PBS. This is due to the ions present in the PBS as they inhibit the interactions between L-nicotine and the MIP. Lower concentrations of PBS showed an increase in the binding potential of the MIP towards L-nicotine. When measured in PBS, the optimal pH value was pH 9. The dissipation changes of the MIP upon binding of L-nicotine were also significantly higher than the NIP in deionized water and PBS. The L-nicotine MIP was also tested with spiked urine and saliva. These test showed that the MIP was able to bind L-nicotine despite being in a complex matrix. As a final test, the saliva of a subject who chewed nicotine gum (4 and 2 mg L-nicotine) and chewing tobacco was collected and measured with the QCM-D. The MIP was able to differentiate between the 4 mg and 2 mg saliva sample. The MIP was also successful in binding the L-nicotine from the chewing tobacco samples.

This work has proven that molecular imprinted polymers are promising candidates for future sensor applications. The MIP was able to function in various complex matrices without losing its sensitivity. Further investigation could implement the MIPs in other more sensitive read out techniques that

allow for easier miniaturization, creating a hand held diagnostic tool for the future.

Nederlandse samenvatting

De nood om snel stoffen te kunnen detecteren is snel aan het groeien in de zowel de medische wereld, voedsel veiligheid als in de natuur. Dit kan bewerkstelligd worden met de hulp van sensoren die gevoelig en selectief zijn. Biosensoren voldoen aan deze eisen met behulp van verschillende natuurlijke herkenningselementen zoals, DNA, antilichamen, enzymen, cellen etc. Het grootste nadeel van deze natuurlijke herkenningselementen zijn de kostprijs, duurzaamheid en hun gebruikslimiet. Deze kunnen namelijk niet gebruikt worden in omgevingen met een hoge of lage pH waarde of met een hoge of lage temperatuur. Synthetische herkenningselementen kunnen wedijveren met de natuurlijke herkenningselementen maar zonder de grote nadelen. Molecular imprinted polymers (MIPs) zijn een sterke kandidaat als synthetisch herkenningselement. Sensoren die gebruik maken van synthetische herkenningselementen worden biomimetische sensoren genoemd. In dit werk zijn biomimetische sensoren gecreëerd die gebruik maken van MIP voor de herkenning van moleculen zoals histamine, malachiet groen en L-nicotine.

Een MIP wordt gemaakt door rond een doelmolecule (bv L-nicotine) een unieke pasvorm te creëren. Na het verwijderen van de doelmolecule zal de pasvorm enkel nog de doelmolecule opnieuw kunnen binden. Om de MIP te maken wordt de doelmolecule vermengd met functionele monomeren (MAA) en crosslinker monomeren (EGDM) in een vloeistof. De functionele monomeren zullen verbindingen vormen met de doelmolecule. De monomeren worden vervolgens gepolymeriseerd en zo worden de functionele monoren vastgezet in een welbepaalde positie. Dit polymeer wordt dan verbrijzeld en gezeefd om kleine micro deeltjes te krijgen. Wanneer de doelmolecule verwijderd wordt, verkrijgen we een synthetisch herkenningselement dat de doelmolecule kan herbinden. Om een controle te hebben, wordt een non imprinted polymer (NIP) gecreëerd die op dezelfde wijze wordt gemaakt maar zonder de aanwezigheid van de doelmolecule.

Deze NIP kan de doelmolecule alleen op niet specifieke wijze binden omdat de unieke pasvorm hier niet aanwezig is.

De goedheid van de MIP wordt eerste getest met behulp van *Ultraviolet/Visible* (UV/Vis) spectroscopie. De MIP wordt vermengd met een vloeistof die een gekende concentratie van de doelmolecule bevat. De MIP zal een deel van de doelmolecule binden. De MIPs, en dus ook de gebonden doelmolecules, worden verwijderd uit de vloeistof. De overgebleven doelmoleculen in de vloeistof worden gemeten met UV/Vis spectroscopie. Dit resultaat wordt dan vergeleken met een op voorhand opgemeten basislijn waardoor de gebonden concentratie van de doelmolecule bepaald kan worden. UV/Vis spectroscopie is een goede eerste test om de karakteristieken van de MIP en NIP te achterhalen. UV/Vis spectroscopie kan wel alleen gebruikt worden bij hoge concentraties (milimolaire bereik). Andere sterk gelijkende moleculen worden ook getest op de MIP en NIP. Histidine wordt gebruikt om de selectiviteit van de histamine MIP te testen en cotinine voor de L-nicotine MIP testen.

Eenmaal de MIP geoptimaliseerd is voor de doelmolecule, worden ze in de sensor geplaatst. In dit werk wordt gebruik gemaakt van impedantie spectroscopie en gravimetrische detectie via een kwarts kristal microbalans. De MIPs worden geïmmobiliseerd op een polymeer laag die op de elektrodes aangebracht wordt. De gebruikte polymeer laag is afhankelijk van de gebruikte sensor techniek. Bij impedantie spectroscopie wordt er gebruik gemaakt van het geconjugeerd polymeer OC_1C_{10}-PPV terwijl bij de gravimetrische detectie de kwarts kristallen worden bedekt met PVC.

Impedantie spectroscopie is een zeer gevoelige techniek die veranderingen in de impedantie (elektrische weerstand) meet over een breed frequentie spectrum. De metingen worden uitgevoerd in het lage frequentie bereik want als de doelmolecule bindt met de MIP zullen er capacitieve veranderingen gebeuren aan de herkenningslaag. Met de sensor is het mogelijk om tot 4 verschillende plaatsen te meten. Dit laat toe om op een differentiële manier te meten. Histamine metingen werden uitgevoerd in PBS (*phosphate saline*

buffered) in het nanomolaire bereik. Als de MIP histamine bindt gebeurde er een impedantie stijging die niet werd waargenomen voor de NIP. Histidine toevoegingen toonde noch voor de MIP noch voor NIP veranderingen in de impedantie. Dit bewijst dat de MIP selectief is voor histamine. Na deze succesvolle metingen werd tonijnsap aangevuld met histamine. Ondanks de complexe vloeistof waarin gemeten werd, kan de MIP probleemloos histamine binden terwijl de NIP geen respons toonde. Malachiet groen werd ook succesvol impedimetrisch opgemeten in het nanomolaire bereik.

Gravimetrische detectie maakt gebruik van een kwarts kristal dat op een welbepaalde frequentie zal trillen, de resonantie frequentie. Wanneer de doelmolecule bindt met de MIP, zal de resonantie frequentie lineair dalen door het toegevoegde gewicht op het kwarts kristal. De sensor opstelling werd gebruikt om histamine te meten in gedeïoniseerd water in het micromolaire bereik. De MIP kon meer de 4 maal zoveel histamine binden dan de NIP. Malachiet groen werd ook succesvol gemeten maar wel in het nanomolair bereik wat zeer laag is voor een kwarts kristal microbalans. Deze metingen gebeurden in water met een pH 3. L-nicotine metingen werden uitgevoerd met behulp van een kwarts kristal microbalans met de mogelijkheid om de dissipatie te meten. Dissipatie is een indicatie hoe lang een kristal zal natrillen nadat het niet meer wordt aangedreven. De dissipatie zal sterker veranderen als er zachtere materialen gebonden worden op het kristal. Metingen werden uitgevoerd in zowel PBS als in gedeïoniseerd water. De hoeveelheid L-nicotine die door de MIP gebonden kan worden in gedeïoniseerd water is groter dan in PBS. Dit is door de aanwezigheid van ionen die de binding bemoeilijken. PBS met een lagere concentraties vertoonden dan ook een grote bindingscapaciteit. Wanneer er in PBS gemeten werd, bleek de optimale pH 9 te zijn. De dissipatie veranderingen die bij binding van L-nicotine aan de MIP gebeurden, bleken ook significant groten te zijn in gedeïoniseerd water dan in PBS. De L-nicotine MIP werd ook getest met urine en speeksel dat aangevuld was met L-nicotine. Deze testen toonden aan dat de MIP geen enkel probleem hadden om L-nicotine te binden ondanks dat zij zich in een complexe vloeistof bevonden. Als een laatste test werd het speeksel van een vrijwilliger die

nicotine kauwgom (4mg en 2 mg L-nicotine) and pruimtabak geconsumeerd had, opgevangen en opgemeten. De MIP kon differentiëren tussen de 4mg en 2mg L-nicotine speeksel concentraties. De MIP was ook succesvol in het binden van de L-nicotine die zich in de pruimtabak stalen bevond.

Dit werk heeft bewezen dat MIPs een sterke kandidaat zijn voor toekomstige sensor toepassingen. De MIP kon functioneren in verschillende complexe vloeistoffen zonder verlies van de gevoeligheid. Verder onderzoek zou deze MIP kunnen integreren in andere meer gevoeligere sensors die ook geminiaturiseerd kunnen worden waardoor een draagbaar diagnostische apparaat voor de toekomst mee kan gebouwd worden.

1 Introduction

Advancements in our technological world are only obtained by gathering knowledge. Knowledge can only be gained by observing, measuring and interpreting every aspect of the world around us. This gained knowledge can then be used to eliminate and diminish existing problems. People have some build in ways to observe and feel the world trough, taste, smell, vision, sound and touch. However these all have their limitations and are hard to objectively quantify. To this end, science has created sensors to overcome the limitations of our own. Current sensors are coming close in outperforming any of our own sensors. The advancements in sensor technology allow us to look deeper into the core of a problem and thus get a better understanding of the complexities surrounding all of life. A subgroup of these sensors is the biosensor. What sets them apart from all other sensors is the fact they utilize a biological component in their structures. This gives them unique abilities that could never be achieved with man-made components. Biosensors can be used in a various applications.

1.1 Biosensing

A biosensor is defined by the Physical Chemistry and Analytical Chemistry Divisions of IUPAC as self-contained integrated device, which is capable of providing specific quantitative or semi-quantitative analytical information using a biological recognition element (biochemical receptor) which is retained in direct spatial contact with an electrochemical transduction element (1). A biosensor therefore works according to the same principle as a regular sensor except for the biological component. A biosensor consists out of different components (Figure 1.1). The biological sensing element is the part of the sensor, which recognizes the analyte. This biological recognition layer can consist of various elements like enzymes (2–4), antibodies/antigens (5–7), cells (8–10) and DNA (11–13). The main advantage of using a biological recognition layer is the high specificity to its analyte. This is of course the most important attribute of any biological or

chemical sensor. Another attribute which any sensor should comply to is insensitivity to other components beside the analyte.

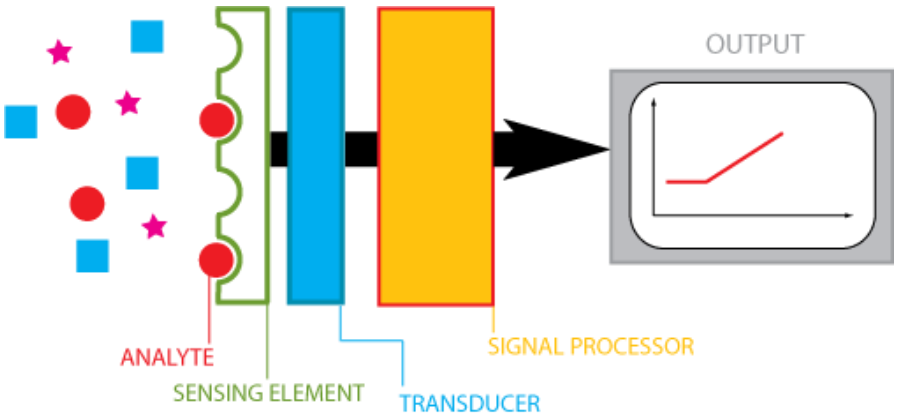

Figure 1.1 – Schematic layout of the components of a biosensor.

The transducer function is to transform the observed physical or chemical change at the biological recognition layer due to the analyte to a measurable signal. Transducers can be optical, electrochemical, piezoelectric or magnetic. The choice of transducer depends on the biological recognition element and the analyte to detect because not all components are suited to be used with each other to achieve the optimal result. The coupling between recognition element and the transducer layer is crucial for the efficiency of the sensor. The link between the recognition element and the transducers can be achieved through several immobilization platforms such as diamond, silicon, organic polymers, gold, etc. The transducer sends the signal to the signal processor, which will transform it to a readable output. One of the greatest advantages is that biosensors can be miniaturized with the aid of modern electronics. Coupled with the specificity and sensitivity of the biological recognition layer this can become a very efficient device.

Most people do not realize that they know biosensors themselves. The most famous is the glucose sensor (Figure 1.2). This sensor is used by patients with diabetes mellitus. In diabetes mellitus type 1 the pancreas of these patients does not produce the hormone insulin, which is responsible to remove excess glucose in the blood. Failure to do so can lead to blurred vision, fatigue, stupor and coma. Long term hyperglycemia can lead to chronic conditions due to damage to the kidney, neurons, cardiovascular system, to the retina and to feet and legs (14). Therefore it is very important for these patients to monitor the blood glucose levels on a regular basis. By applying a small drop of blood to the disposable strip of the glucose sensor, blood glucose levels are determined within a minute. The most important part of this sensor is the enzyme. The first glucose sensors were fitted with glucose oxidase enzyme which metabolizes glucose into D-glucono-δ-lactone. During this conversion oxygen is consumed. This system was coupled to a Clarke electrode which was initially designed to measure oxygen in blood. The consumption of oxygen resulted in a decrease in the measureable oxygen content, which was proportional to the glucose concentration.

Figure 1.2 - Glucose sensor for diabetes patients. (www.accu-chek.com).

Another well known biosensor is the pregnancy test (Figure 1.3). This is used to measure the concentration of the beta subunit of hCG (human

chorionic gonadotropin) in urine. Increased levels of hCG indicate pregnancy and tests can be used the earliest ten days after conception. The read-out is via a colorization method. The presence of hCG induces color changes on a strip via binding to anti-hCG antibodies on colloid gold nanoparticles. This is easy to use for non-trained people and is an excellent example of a biosensor to be used by non-specialist persons due to its simplicity, availability and low cost.

Figure 1.3 - Home pregnancy test. (www.thingamababy.com).

Biosensors in clinical environments are still not a common sight. In order to get biosensors into a competitive market certain criteria are to be met. A high sensitivity towards the analyte in a 'real life' setting is crucial for any success. Biosensors should always strife to achieve a higher sensitivity. A second essential attribute is selectivity. If a biosensor detects not only the analyte but also other similar compounds, the biosensors cannot be trusted as it will give false-positive results. A third attribute is reliability. A successful sensor should be able to measure the same concentration within a certain reliability range. If the results fluctuate strongly the sensor cannot be trusted. This is especially true for biosensors for analytes with a very small concentration. The fourth aspect is device miniaturization. If biosensors want to succeed in becoming a point-of-care device they should be small enough to be handled with ease, the cost should be low if mass distribution is desired and the device should be user friendly so that untrained persons can use it without complex procedures. Depending on the type of biosensor, multiplexing can be desired to handle a large number of samples and to detect multiple target molecules, simultaneously. Reduction of measurement time can also be critical for some biosensors.

Since the development of the first biosensors, the interest in the topic has grown tremendously throughout the years. As can be seen in Figure 1.4 the last 10 years the output on biosensors has grown steadily, indicating that many scientists are working on the subject and they are also succeeding in their efforts to create a biosensor. This growth can be explained by the demand for cheap, fast, reliable and easy to use devices in the healthcare community.

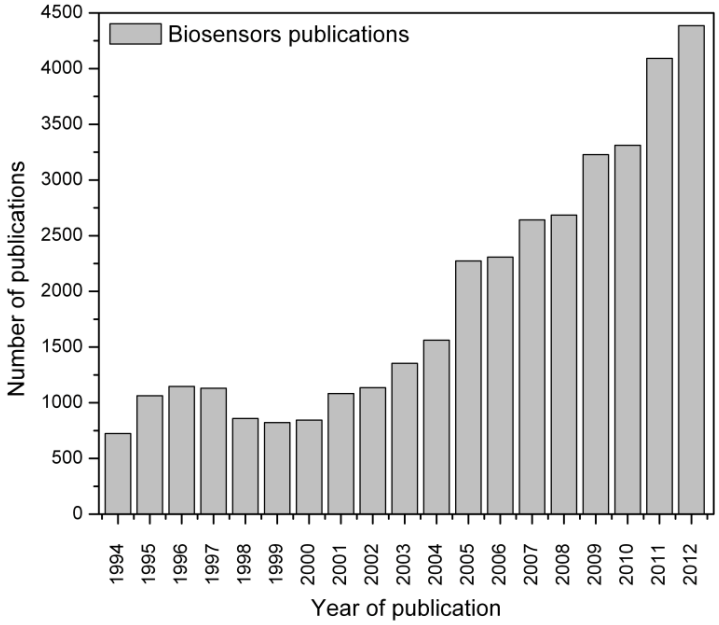

Figure 1.4 - Publications on 'biosensors' per year from science direct (www.sciencedirect.com)

If this evolution keeps on going, a lot of exciting evolutions are to be expected in the future. Small changes in the normal physiological concentrations can be detected using point-of-care devices at the doctor's office or at home. This could provide a service to predict certain diseases, organ failure, etc. Quick scans to test any mutations in DNA can also become reality. It will be possible to assess certain genetic defects early and deal with their consequences to aid the patients.

1.1.1 Sensing with natural receptors

The receptors used in biosensors are chosen specifically because they possess a certain attribute that makes them suitable for the purpose of the biosensor. These traits are all present in the living natural world and all perform many essential functions to sustain life. Many of these receptors can be found on the cellular level. Cellular receptors are proteins that can be found in the membranes of cells and are responsible for communication between cells (Figure 1.5). This communication is essential for all biological processes that are occurring in the body. It is this way our body will react to stimuli from outside sources and from sources inside the body itself. These receptors must be very specific to their corresponding messenger molecules as otherwise cross-binding would disrupt all normal communication and the body will get the wrong signal. The types of communication can be divided in to three different ways, the endocrine pathway for distant signaling, the paracrine pathway for neighboring cells of the same tissue or the autocrine pathway for signaling to itself (15). Upon binding of the messenger molecules, the receptor will induce a cascade of events, which will eventually lead to the cellular response to the original trigger. The common messenger molecules are hormones, neurotransmitters or growth factors. They bind to their respective receptors through means of ionic bonding, van der Waals interactions or hydrophobic interactions (15).

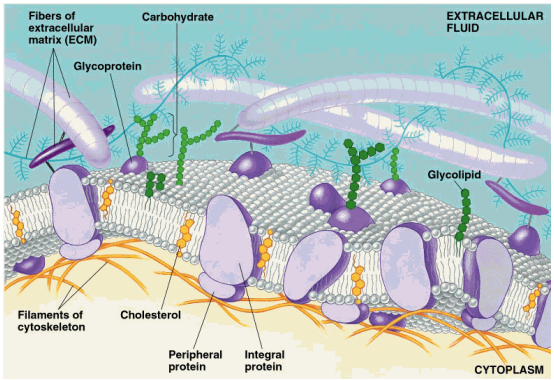

Figure 1.5 - Membrane proteins for communication between cells. (xtalwebary.blogspot.com)

Another natural occurring receptor is an enzyme. Enzymes play a major role in the digestion system as they catalyze metabolic reactions (e.g. catalysis of sucrose into glucose and fructose (Figure 1.6). During metabolism substrates are broken down to their products. However, in the absence of enzymes this chemical reaction would be too slow to be efficient. Enzymes catalyze these reactions considerably faster than without their presence and thus gain sufficient rates to sustain the metabolic needs. Every enzyme can only catalyze one metabolic reaction and is very specific for its substrate. This makes it of course a very good candidate for biosensing purposes. This specificity is accomplished *via* the 'key and lock' principle, in which the geometric shape of the enzyme and the substrate are complementary and no other substrate can fit into the enzyme's 'lock' (16).

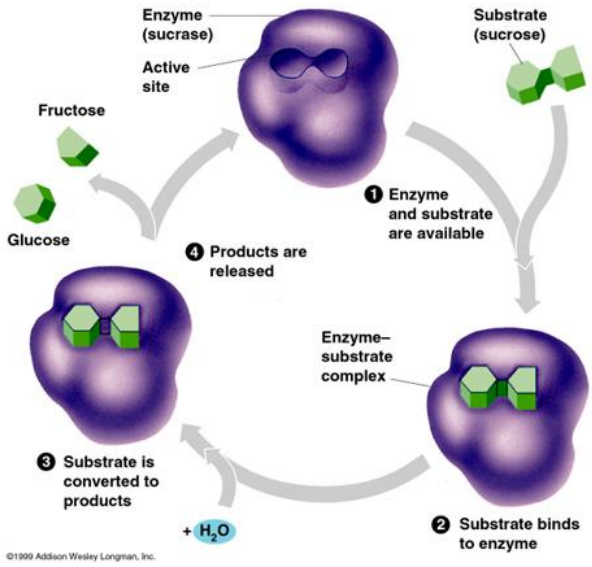

Figure 1.6 - Enzyme catalyzing the substrate's metabolism (labsciencebiology.wordpress.com)

Another important natural receptor is the antibody that can be found in fluids, such as serum, saliva and tears or bound on the membrane of B-cells. Antibodies are part of the immune response when foreign pathogens invade the body and cannot be cleared by the innate immune system. They are well

known for their ability to specifically bind their target. The simplest structure of an antibody (Figure 1.7) is a Y-shape with 2 recognition sites. Each antibody consists of 4 polypeptide chains (2 light - and 2 heavy chains) which are held together by strong and covalent disulfide bonds. All polypeptide chains consist of a constant region and a variable region. The N-terminal sides of the polypeptide chains make up the antigen recognition site. The selectivity of the antigen recognition site can be altered by changing the amino acid sequence. The bonding of the antigen to the recognition site is mediated by weak physiochemical forces (electrostatic interaction, hydrogen bonds, hydrophobic interactions and van der Waals forces) that all together form a strong bond characterized by an affinity constant of 10^6 M^{-1}.

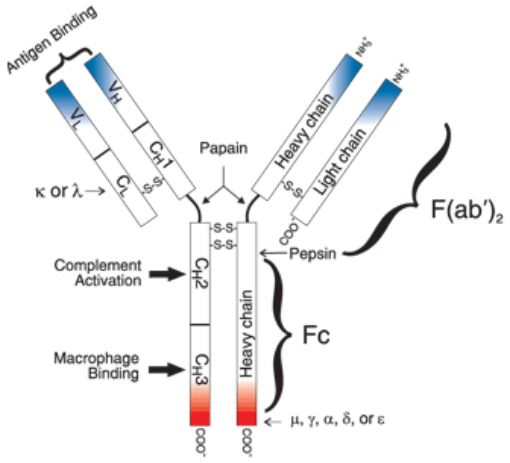

Figure 1.7 - Schematic of an antibody with its different polypeptide chains (www.invitrogen.com).

These antibodies are used extensively in different diagnostic test that are based on the specificity of the antibody. Immunofluorescence uses antibodies with a covalently attached fluorochrome, which emits green light when exposed to UV. This technique is used to detect antigens in tissue and cells. If the green light is visible under a fluorescence microscope the antigen is present. Immunoblotting is applied when specific antigens in a complex

mixture need to be detected. For instance, detection of a target protein in a complex mixture can be achieved. The complex protein samples are mixed with sodium dodecyl sulfate (SDS) and are separated via electrophoresis. Larger proteins travel smaller distances in comparison with lighter ones. After transfer of the proteins to a nitrocellulose membrane, antibodies are added and allowed to react with the proteins. The antibody will bind to the target protein if it is present. After rinsing off the unbound antibodies, a ligand is added in order to conjugate with the antibodies that are bound to the target protein. This ligand generates a colored insoluble product so the protein becomes visible if it is present in the complex mixture. Enzyme-linked immunosorbent assays (ELISA) use antibodies coupled with an enzyme to detect antigens directly or an antibodies/antigen complex. The enzyme (often horseradisch peroxidase) reacts with a colorless fluid which changes color proportional to the amount of enzyme present, which is in turn an indication for the concentration of the antigen (17).
Another natural sensing receptor is deoxyribonucleic acid (DNA) (Figure 1.8). DNA contains the genetic information of every living organism.

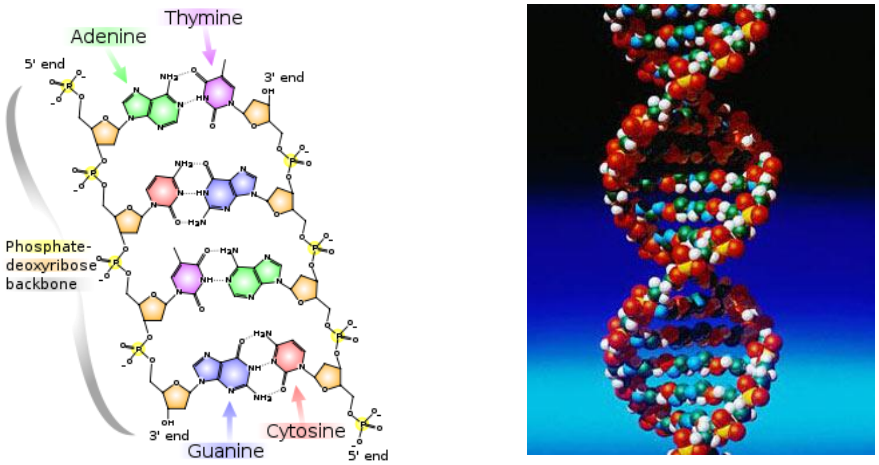

Figure 1.8 - Schematics of the DNA components and helical structure (commons.wikimedia.org).

DNA can be found in the nucleus and mitochondria of every cell and is unique for every organism. The common DNA conformation is a double helix (Figure 1.8) where every strand consists of a backbone with repetitive structure. This phosphate sugar polymer backbone is constructed with alternating phosphate and deoxyribose components. Every sugar is attached to a nucleobase. There are four different nucleobases thymine, adenine, guanine, and cytosine (Figure 1.8). Thymine forms a pair with adenine on the opposing strands while guanine forms a pair with cytosine. These pairs are formed with hydrogen bonding. Thymine and adenosine have 2 hydrogen bonds and guanine and cytosine have 3 hydrogen bonds. This means that a guanine-cytosine bond is stronger than a thymine-adenine bond. This attribute is important in some DNA biosensors to differentiate between complementary and non-complementary DNA. Most DNA sensors require labeling of a DNA strand with radioactive, fluorescent, enzymatic or electroactive labels. A good example of such a sensor is the Affymetrix microarray 'genechip', which uses a fluorescent label (18) to differentiate between complementary and non-complementary DNA strands. Other DNA sensors do not require labeling techniques, such as impedimetric (12) or microgravimetric DNA sensing (19). DNA structures can also be used to construct aptamer structures. Aptamers are formed from DNA or RNA (ribonucleic acid) oligonucleotides and can bind a specific target such as small molecule, cells, proteins, nucleic acids, etc. Their specificity is mostly based upon their form. Aptamers have been successfully used as the receptor in biosensors (20,21).

1.1.2 Biomimetic sensing

Natural receptors have proven their effectiveness in biosensor technology. However, their use has some major practical drawbacks. They only function when certain physiological criteria are met. For example, natural receptors work optimally at 37°C and even small deviations can disrupt their functionality. In addition, control over the pH value of the fluid in which the natural receptors reside is vital as acidic and alkaline fluids will change their sensitivity towards the analyte. Other disadvantages are their limited shelf

life and high production cost. Natural receptors are limited to a certain number of important analytes, especially when it comes to low molecular weight molecules (22).
Molecular Imprinted Polymers (MIPs) can overcome these drawbacks while still being sensitive enough to be used as a recognition element. In general MIPs can be thought of as artificial biomimetic receptors with the same binding and recognition properties as an antibody. The ability of MIPs to specifically bind its target molecule relies on the Key-Lock principle (Figure 1.9) and on covalent or non-covalent interactions

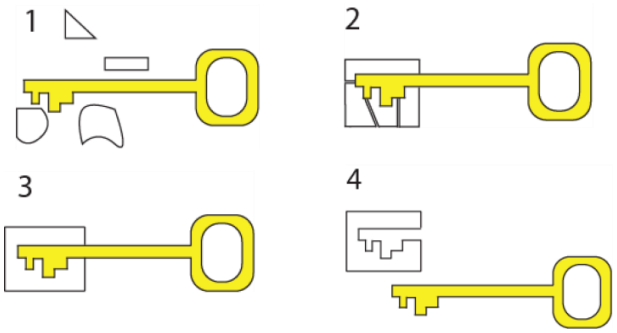

Figure 1.9 - Molecular Imprinted Polymer key-lock detection principle. 1) Key and mold building pieces are mixed. 2) Mold pieces form around the key. 3) Mold pieces are linked together. 4) Key is removed from mold leaving an imprint.

In the first step the key and the mold building pieces are mixed together so they can interact with each other. In the second step the mold pieces bind to the key molecule and subsequently the mold pieces are linked together so the lock is complete. Afterwards the key is removed from the formed lock, which is now specifically formed to fit the key. This principle is achieved through free radical polymerization of functional monomers such as Methacrylic acid (MAA), Acryl Amide (AA), 2-hydroxyethyl methacrylate (2-HEMA) (23) and crosslinking monomers such as ethylene glycol dimethacrylate (EGDM), tetramethylene dimethacrylate (TDMA) and trimethylepropane trimethacrylate (TRIM) (23). In Figure 1.10, in the first

step the chosen functional monomers, the template under investigation and cross linking monomers are dissolved in a porogen (1). This porogen usually is an organic solvent, which will keep everything in solution and will induce porosity in the final material. The monomers bind to the template via covalent or non-covalent interactions such as hydrogen bonding, van der Waals forces, hydrophobic interactions and ionic interactions forming a pre-polymerization complex (2). The mixture is subjected to heat or UV light to start the polymerization process that will polymerize the cross linking monomers together and will fixate the functional monomers in their respective places acquired from the pre-polymerization complex (3). When the polymerization is completed the template is extracted from the MIP (4). This will create many nanocavities, which are now specific to the template molecule (24).

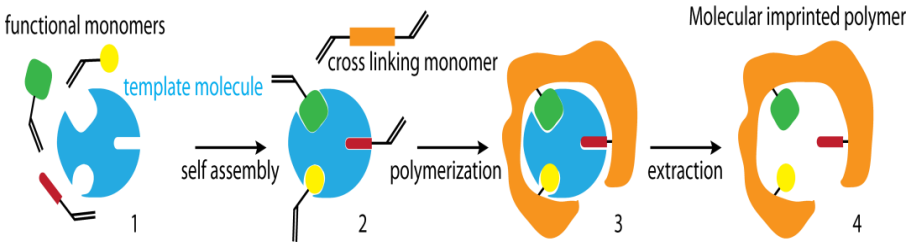

Figure 1.10 - Synthesis of a molecular imprinted polymer. Phase 1, mixing of all components in a porogen. Phase 2, the functional monomers bind to the template molecule. Phase 3, the crosslinking monomers are polymerized. Phase 4, the template is extracted.

The choice of functional monomers depends on the type of binding required. Covalent interaction between the template and the functional monomers is superior in strength and the nanocavities have a uniform distribution in binding strength. The drawback of this method is the removal of the template. Due to the strong binding characteristics the template must be chemically cleaved in order to clear out the nanocavities. This limits the possible templates for a covalent MIP. As a result, this method is rarely used. With non-covalent binding the chemical cleaving is not necessary

because template can be removed by breaking the bonds with polar solvents. The drawback of non-covalent binding is the heterogeneity of the binding strength of the nanocavities. The success of creating a working MIP depends on several factors, such as the ratio of template and functional monomer/ cross linking monomer, temperature of polymerization and polarity of the porogen (25). Stability of the pre-polymerization complex is determined by the porogen. During polymerization the porogen will also determine the porosity of the MIP. The higher the porosity in the MIPs, the easier it is for the template to release from the MIP and for the target molecules to access the nanocavities.

The MIPs are created in a free radical polymerization (23), which is a chain growth reaction consisting of three steps (Figure 1.11). The first step is producing a radical which will start the polymerization. This is accomplished with an initiator (I), which is radicalized through means of heat or UV-light.

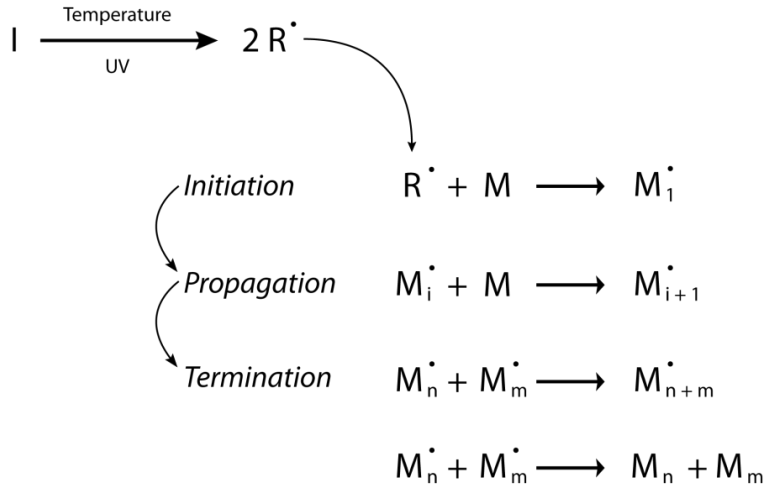

Figure 1.11- Scheme of free radical polymerization steps.

This radicalized initiator ($R^{\bullet}$) will then react with the first monomer (M_1), resulting in a monomer radical, which can now react with the other monomers (M) in the solution to produce a polymer chain or network. This is

the propagation step. The polymerization will be terminated when two chains recombine or by disproportionation of the reaction. Impurities and inhibitors (*e.g.* oxygen) in the mixture can also terminate the polymerization.

There are different ways to prepare MIPs. The most common one is bulk polymerization, which is also the most straigtforward method. Other methods are suspension polymerization (26), precipitation polymerization (27), and electro polymerization (28).

In the *bulk polymerization* all components (functional monomers, cross linking monomers, template and initiator) are mixed together in the porogen of choice. Application of heat or UV-light will start the polymerization process. After polymerization the mixture is solidified in one rigid bulk polymer, which is then grounded and sieved to obtain a bulk MIP size of a few micrometers. Subsequently the template is removed from the MIP via Soxhlet extraction.

Suspension polymerization can be used to obtain uniformly globular MIP particles in the sub micrometer scale (Figure 1.12) (29).

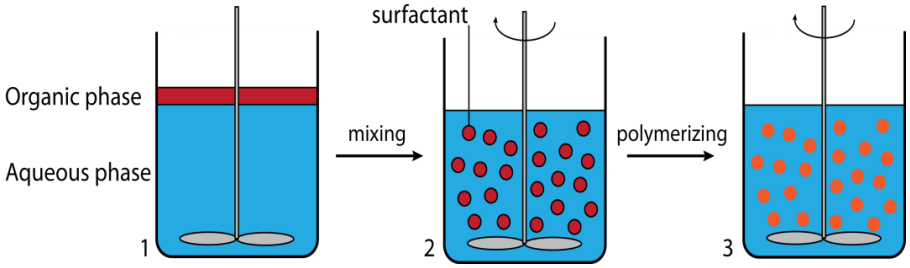

Figure 1.12 - Scheme of suspension polymerization. 1) Two-phase system of an organic and an aqueous phase. 2) After mixing micelles are formed and stabilized with a surfactant. 3) The organic phase is polymerized.

Polymerization occurs in a two-phase system consisting of an aqueous fluid as the dispersion phase and an organic solvent as the hydrophobic subphase (1). All the MIP components reside in the organic solvent. In addition to all

components, which are also present in the bulk polymerization, a surfactant is added in order to form micelles of the organic mixture in the dispersion phase and stabilize them (2). This is crucial as otherwise the formed micelles will disintegrate before polymerization can take place. Polymerization is executed *via* heat or UV-light (3). Apart from the other parameters in bulk polymerization, mixing speed and surfactant concentration are new parameters that can make it more difficult to create a working MIP. The main advantage of suspension polymerization is the homogenous size of the MIP particles (30).

Electro polymerization (Figure 1.13) can be potentially used to create very specific MIP forms. The MIPs are grown directly on the surface. The polymer layer can be grafted on the surface of electrodes (31). Carbazole (32) and Bis(bithiophene) derivates (28) can be used as functional monomers. The thickness of the MIP should be easily controllable. Such a technique could be very useful in biosensors development because MIPs could be directly grown on electrodes and miniaturization can be easily achieved.

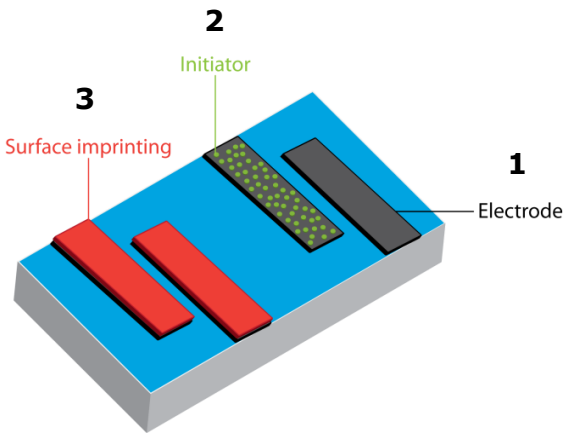

Figure 1.13 - Scheme of surface imprinting principle. 1) Bare electrode, 2) The initiator is coupled to the electrode, 3) Polymerization of the MIPs starts at the initiator on the electrode.

1.1.3 Imprinted polymers applications

The MIP's ability to be tailor-made for a wide variety of molecules while being highly selective makes them versatile to be used in many applications. Imprinted polymers can be synthesized for low-molecular weight molecules (MIP) (33,34), metal ions (35), viruses (36), DNA (37), proteins (38,39) and cells (40). In principle, a MIP can be made for any sort of compound. MIPs and other imprints can be applied in various research fields such as environmental analysis (41), food analysis (42), separation technology (43,44) and biosensing (33). The biggest interest in MIPs usage is separation technology where the MIPs are in the stationary phase of liquid chromatography. High performance liquid chromatography (HPLC) is a popular and effective separation technique that can separate and dilute the analyte to high concentrations. HPLC in combination with MIP is therefore a very useful technique in the detection of drugs, peptides and other substances (45). Because the binding strength between MIP and its template is strong, MIPs can also be used as a controlled drug delivery system (46). MIPs can also be employed as a catalyst. The catalytic MIPs are fabricated with the transition state analog as the template for ester hydrolysis or other processes (47). Another application field are biomimetic sensors. In this application the MIPs are used as the recognition element instead of the more conventional natural receptors. These MIPs can be implemented in various read-out techniques like electrochemical - (48), piezoelectric - (49), optical - (50) and surface Plasmon resonance sensors (51–53). Their strength relies in the fact that they can be utilized under conditions where natural receptors are unable to perform.

1.2 The need for biosensing

Biosensors are a relatively new concept in medical diagnostics, food safety and environmental analysis. They purpose is to provide a fast, reliable, low-cost and easy to use device, which can be employed at the doctor's office, at

home or on site. Most of today's detection techniques and devices are expensive and require trained personnel to operate properly. This can be solved with biosensors. Especially point-of-care devices could improve the efficiency of monitoring of certain disease markers (*e.g.* CRP protein for cardiovascular disorders). An future goal for biosensors is continuous monitoring of metabolites in patients with, potentially coupled a feedback system for the drug release to alleviate the symptoms (54). Such a device could be useful for chronic disorders such as diabetes.
An overview of the template molecules that were used for the creation of MIPs for sensor purposes is presented in the following sections. In addition, the biomedical relevance of these molecules will be discussed.

1.2.1 Histamine

Histamine or 2-(1*H*-imidazol-4-yl)ethanamine (Figure 1.14) is a molecule that functions within the local immune response and can primarily be found in the granules of mast cells that are present in the intestines and other mucous tissue where pathogens can inflict harm upon the body (55).

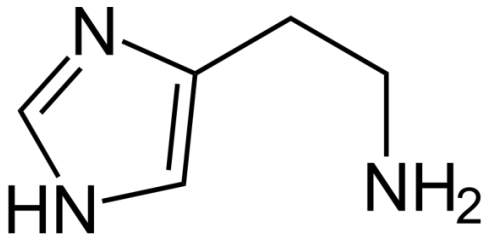

Figure 1.14 - Schematic structure of histamine.

Histamine is also stored within some white blood cells such as basophils (56). Its function is to increase the permeability of capillaries to white blood cells to increase the immune response. Histamine also acts as a neurotransmitter and has a physiological function within the intestine. It has

a molecular weight of 111.15 g/mol and is produced by decarboxylation of the amino acid histidine. Histamine plays a significant role in an allergic event. When an allergen binds to the IgE, which are present on mast cells surface, histamine is released (57). This causes vasodilation and an increase in the permeability of vascular system. These actions cause the most prevalent allergic symptoms, runny nose and watery eyes. Other effects include nasal congestion and sneezing. Histamine release due to degranulation in mast cells lining the inner wall of the intestines is suspected to be a cause for irritable bowel syndrome (IBS).

1.2.1.1 Irritable Bowel Syndrome

The irritable bowel syndroms (IBS) is a prevalent gastro-intestinal disease that is defined as a functional colon disease whereby abdominal pain is associated with defecation or a change in bowel habits with clues to a disturbance defecation and swelling of the abdomen (58). About 30 million people of the American population (10.5%) have symptoms that coincide with IBS (59). The prevalence in Europe differs from country to country: France 20%, The Netherlands 9.0%, Sweden 12.5%, Denmark 6.6% and the United Kingdom 22.0% (60).

1.2.1.2 Symptoms of IBS

The most prominent symptoms in IBS are abdominal pain and troubled bowel movement. Some patients experience these complaints continuously while other experience them periodically. These symptoms are patient related, they can however also change over the course of time. In most patients the abdominal pain is dominant as the main complaint. This abdominal pain is usually cramping, which is intermittant or continuously. Other forms of abdominal pain give a burning or stabbing sensation. Most pain can be felt in the lower left region of the abdomen where the sigmoid, the narrowest part of the small intestine, is located. The pain is caused by spastic contractions closing up the colon. After defecation this pain is diminished because stimuli from the colon remove the cramping stimulus. The stool usually is hard and infrequent (constipation). The cause is an

irregular movement of the colon which slows down the stool passage which causes an excessive uptake of liquid from the stool. It is also possible that the patient experiences alternating periods of constipation and diarrhea. These contractions and hard stool irritate the inside of the intestines causing secretion of extra mucus. Some patients only have diarrhea and no constipation or abdominal pain. This usually results in very frequent defecation of small quantities of slimy material, however, more watery stool is produced by fast passage through the first part of the colon. This fast passage is created by abnormal movement of the colon. Besides the symptoms, patients can also experience non intestine related complaints like reflux of the stomach content, which can lead to inflammation of the esophagus. Other symptoms are nausea, vomiting, and a quick sensation of a full stomach during a meal. Because the presence of stool in the intestines is prolonged, a buildup of bacteria can occur which can cause a bloated feeling and flatulence (61).

1.2.1.3 Causes of IBS

Bowel function is controlled by the enteric nervous system (ENS). The ENS is the neural network that regulates the motility and the stimuli of the bowels. This network can be considered as 'the brain of the bowels' and controls motor and secretion programs, feedback control, reflexes and sensory information processing (62). The central nervous system (CNS) modulates the peripheral intestinal motor and sensory activity. One theory describes that normal gastro-intestinal function results from integration of the intestinal motor, sensory, autonomic and CNS activity. A malfunction in any of these systems could cause the gastro-intestinal symptoms. These systems communicate through bidirectional parallel circuits. This links visceral afferent sensation and intestinal motor function to higher cortical centers that modulate and adjust their activity which enables extrinsic (vision, smell) or enteroceptive (emotions, thoughts) sources to influence the gastro-intestinal sensation, motility and secretion. It appears that physiological and psychological factors can induce pain and other symptoms (63). A new theory suggests that the cause of IBS is related to a dysfunction between

the interaction of the CNS and the ENS (64). The CNS and the ENS can be seen as the ends of an axis. This axis is the connection between visceral intestine sensation and motor function with brain centers that regulate intestine sensation, motility and secretion. Intestine sensation influences the brain and *vice versa*. A disorder in this axis leads to visceral hypersensitivity and abnormal bowel movements, which are two important symptoms in IBS (64).

As IBS is related to change in muscle and nerve function, mast cells are considered as potential candidates in the cause of IBS. Mast cells have many mediators that have inflammatory and immune regulatory effects. Mast cell degranulation and releasing of the mediators is associated with stress, nerve damage, infection and inflammatory conditions. Mast cells are closely located to the ENS which means they have the potential to induce changes in nerve function and visceral sensitivity. This means that mast cells can be an important mediator in the complex interaction between physiological (intestinal damage, inflammation, tissue damage, nerve damage) and psychological factors (stressful events, emotions) (65). In IBS patients there are more mast cells present in the ileum (66) and caecum (65) than in healthy persons. Physical and psychic stress situations induce the release of corticotrophin releasing hormone *via* the hypothalamus. This causes the activation and destabilization of mast cells in the intestinal mucus, which enables the release of tryptase and histamine (67,68). The mediators will increase the motility of the intestine, which can lead to diarrhea. The causal effect of histamine and IBS are not fully understood yet so the capability to measure the concentration of histamine in bowel fluids can be important for further understanding of IBS.

1.2.1.4 Histamine fish poisoning

Scombroid fish poisoning can occur after ingestion of fish with a high concentration of histamine present. This high histamine concentrations can be attributed to high free histidine levels, bacterial histidine decarboxylase and environmental conditions (69). The name scombroid fish poisoning is used because the poisoning was thought only to occur after eating of fish

from the scombroid family, which includes mackerel, tuna and bonitos. Other fish species (bluefish, mahi-mahi, sardines and anchovies) are now also know to induce scombroid fish poisoning (70). Therefore, the more correct name 'histamine fish poisoning' is used, since histamine is the cause of the observed symptoms. These symptons are very similar to an allergic reaction with facial flushing/sweating, burning-peppery taste sensations in mouth and throat, dizziness, nausea, headache, tachycardia, and cold-like symptoms (71). These symptoms may evolve into facial rash, torso or body rash, edema, short-term diarrhea and abdominal cramps. In severe cases, the symptoms include blurred vision, respiratory stress and swelling of the tongue. Because these symptoms resemble an allergic reaction or salmonella poisoning, the incidence of histamine food poisoning is underestimated (69). Histamine is formed in the fish from histidine through aid of the enzyme histidine decarboxylase. This enzyme is produced by enteric bacteria especially *Morganella morganii* (72). These bacteria proliferate at higher temperatures. Therefore the fish should always be stored at very low temperatures. Histamine cannot be destroyed by cooking, making the storage essential for preventing histamine fish poisoning. Histamine dosages can be considered unhealthy when they reach 50 mg of histamine per 100 g of fish (71). Histamine fish poisoning is responsible for 37% of the cases of fish food poisoning (73), making this a significant contributor to illness caused by ingestion of food. Besides histamine, other harmful compounds such as malachite green can be found in fish which pose a threat to human safety.

1.2.2 Malachite green

Malachite green (MG) (4-[(4-dimethylaminophenyl)phenyl-methyl]-*N*,*N*-dimethyl-aniline) (Figure 1.15) is an organic compound which is mostly used as a dye and is part of the triphenylmethane family (74). Malachite green has a molecular weight of 329.4 g/mol and has an intense green color which is produced by a strong absorption band at 631 nm. Besides its intense use as a dye for silk, jute, cotton, wool and leather malachite green is used as an antifungal and antiprotazoal medicine in fish aquaculture (75). It is highly

effective against saprolegnia a fungus that infects fish eggs and is also used as an antiparasitic and antiseptic medicine.

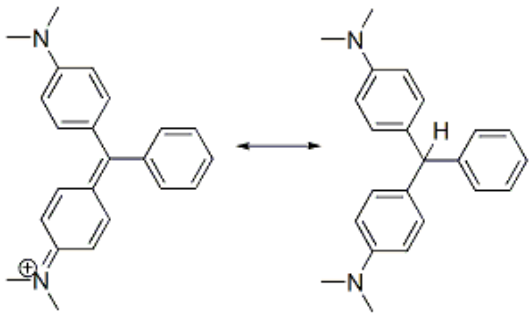

Figure 1.15 - Schematic structure of malachite green (left) and leucomalachite green (right). (safeseafood.ucdavis.edu)

The primary metabolite of malachite green, leucomalachite green (Figure 1.15) can be found in fish that had antifungal treatment. Malachite green has become a controversial compound due to its effects on the immune system, reproductive system and genotoxic and carcinogenic properties after human ingestion (76,77). Although the use of malachite green as antifungal treatment is banned, parts of the world still use it because of its effectiveness, low cost and availability (78). Imported fish could potentially be a hazard to public health. A zero tolerance limit of 0.01 mg/kg (± 30.3 nM) for malachite green and leucomalachite green combined in fish has been established (79).

1.2.3 Nicotine

Nicotine (3-[(2S)-1-methylpyrrolidin-2-yl]pyridine) (Figure 1.16) is an alkaloid that can be found in plants of the nightshade family. Nicotine has a molecular weight of 162.23 g/mol and is an oily, brownish liquid that is miscible with water. Nicotine is present in 2 enantiomeric forms of which L-nicotine is the naturally occurring form.

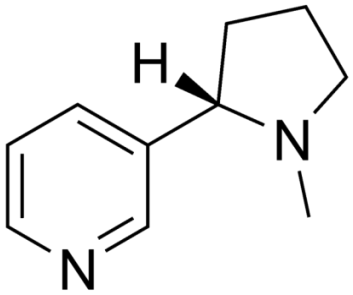

Figure 1.16 - Schematic structure of L-nicotine. (commons.wikimedia.org).

Nicotine is mostly known as the active substance found in tobacco and is seen as one of the most addictive substances, equally or even more so than cocaine and heroin (80). Consumption of nicotine in low doses exerts an effect in the brain by stimulating the mesolimbic or reward system in the brain (81). After intake nicotine will enter the bloodstream and cross the blood-brain barrier in a matter of seconds. When nicotine enters the brain it will bind to the nicotinic acetylcholine receptors present on the neurons. This will result in the release of many neurotransmitters, such as dopamine and glutamate. Dopamine is responsible for the 'happy and relaxed' sensation caused by nicotine intake. Glutamate creates a memory loop between nicotine intake and the happy sensation making this the pathway for addiction (82). So, in small quantities, nicotine acts as a stimulant which relieves depression, reduces anxiety, improves the ability to concentrate, improves long term memory, protects against high blood pressure and protects against weight gain.

Despite these beneficial effects, nicotine intake is a health risk which overshadows any positive response. These negative effects are caused by the byproducts that are also taken into the body while taking in nicotine. Nicotine can be taken up in the body through smoking of cigarettes and cigars, sniffing of tobacco, chewing smokeless tobacco and nicotine gum, electronic cigarettes and nicotine patches. Besides nicotine tobacco smoke contains more than 4000 compounds of which more than 50 are carcinogenic

(83). It has been proven that tobacco consumption causes a higher risk for the development of cancer in the lungs and respiratory tract (84,85) and diseases such as pulmonary disease (86), atherosclerosis (87) and periodontal disease (88). The presence of nicotine can be determined in various samples such as urine, hair, breast milk, plasma and saliva (89). Despite its massive consumption nicotine can still kill by overdose. The LD_{50} (median lethal dose for 50% of subjects) of nicotine is 50 – 60 mg for humans, which translates to a concentration of 61.2 µM in the human blood. The peak L-nicotine concentration in smokers is at 38.2 ng/ml which translates to 0.235 µM.

1.3 Aim of this study

In previous work conducted by the BIOSensor group of the IMO, the proof of concept of a biosensor using MIPs was established for L-nicotine measurements in phosphate saline buffer (PBS) using impedance spectroscopy (48). The sensor was sensitive enough to measure concentrations in the nanomolar range and results were obtained in a fast time taking less than 30 minutes per analysis. Cotinine, a metabolite of nicotine, was used as a control to check for cross reactivity. This proved that MIPs were an excellent candidate for biosensing purposes because they possess the following advantages.

- Fast
- Sensitive
- Selective
- Reliable
- Low cost
- Able to be miniaturized
- Easy to produce
- Label free

These attributes combined with appropriate read out techniques such as impedance spectroscopy (IS) and quartz crystal microbalance (QCM) mean that MIP-based biosensor could replace more expensive and laborious techniques such as ELISA, high performance liquid chromatography (HPLC),

radioimmunoassay, etc. Besides L-nicotine, histamine and malachite green were chosen to test the concept of a MIP sensor. Each MIP has to be tailored to each template by choosing the functional monomer, crosslinking monomer and porogen. When the right components for the MIP are chosen the relative concentrations have to be fine-tuned to get the best results. The polymerization method can also be altered to study whether this will benefit the design of MIP in biosensor applications. The efficiency of a MIP can be tested with UV-Vis spectroscopy because it will give a first indication how much target molecules a MIP can bind and how much a control non imprinted polymer NIP will aspecifically bind. Aspecific binding is caused by the same interactions (non covalent). However, in a NIP the functional monomer are randomly structured there will not be specific sites for the template molecule (key – lock principle). These MIPs will then be tested for their efficiency in more sensitive read out techniques. UV-Vis has sensitivity in the milimolar range while more sensitive read out techniques can achieve sensitivities in the micromolar range (quarz crytal microbalance - sensor) and in the nanomolar range (impedimetric spectroscopy). Another aspect which needs to be addressed in biosensor research is the sensitivity, specificity and reliability of the MIP biosensor during measurements in "body fluids" or "environmental samples" as this is the final goal of any biosensor. Relevant "body fluids" or "environmental samples" should be chosen for each template. In a first stage these "body fluids" or "environmental samples" should be tested after they are spiked with the corresponding template to see if the MIP is still able to bind the target molecule in a complex matrix and give a detectable response. If the MIP bionsensor is able to adequately respond to a spiked "body fluids" or "environmental samples", non spiked "body fluids" or "environmental samples" should be obtained for analysis. If the MIP biosensor is able to measure the target molecule in a sensitive enough way in the physiological concentration range, the MIP biosensor has achieved the goal. To achieve this success, considerable thought should be put in the way the sensor is constructed and which materials should be used to improve the detection for each read-out technique. The aim of this work is to develop functional MIPs which can be integrated in multiple sensing techniques for the detection of the target molecule. Specifically the QCM was

used to optimize the detection of histamine, malachite green and L-nicotine so the relevant physiological concentration range could be measured while being present in "body fluids" such as saliva or "environmental samples" such as tuna brine.

2 Materials and Methods

In this section, the various techniques, devices and materials that are used to create and operate the MIP biosensor are explained. When synthesizing MIPs the efficiency is tested using batch-rebinding experiments based on UV-Vis spectroscopy. The MIPs that show promise in their efficiency as biosensor receptor are integrated into the sensor setups. Construction of the biosensor starts with choosing the correct immobilization platform. This depends on the read out technique to be used. After choosing the correct substrates electrodes are applied to the substrate. The MIPs are immobilized to the electrodes *via* a transducer layer. The choice of transducer is again dependent on the read out technique. If the MIPs are immobilized on the transducer layer the MIP biomimetic sensor is ready to be used. Measurements take place in aqueous fluids under static or flowing conditions with a stable temperature.

2.1 Materials

2.1.1 MIPs

Molecular imprinted polymers consist of multiple components which need to be fine tuned to achieve a working synthetic receptor. The characteristics of MIPs are not always the same because of the use of different components and processes employed to create the MIP. When using MIPs for filtration purposes, the difference between a MIP and a NIP does not need to be very pronounced, since besides the selectivity an additional important factor is the quantity of molecules a MIP can bind. When developing a MIP for biosensor purposes, the emphasis lies more on the ability of the MIP to bind more target than the NIP does (selectivity). A second factor in MIPs for sensor purposes is also the amount it can bind. This factor is less crucial for MIPs for separation or filtration purposes. The choice of components used and their ratios will determine these characteristics. The choice of the polymerization method will also affect these characteristics.

Bulk MIPs were created for histamine and L-nicotine. The general protocol for making a bulk MIP is straightforward. All the components are dissolved in a porogen together with the radical initiator. The components used to create a bulk MIP are (23):

- Functional monomer
- Crosslinking monomer
- Initiator
- Porogen
- Template

This mixture is degassed to remove oxygen as this can interfere with the polymerization. Subsequently, the mixture is subjected to heat or UV-light in order to initiate the polymerization. This polymerization can take several hours after which a monolith is formed. Subsequently, this monolith is crushed and sieved to obtain the desired particle size. These particles are washed to remove the template molecule from the MIP particles. A non imprinted polymer (NIP) is made in the exact same way as the MIP, however, without the presence of a template. This NIP serves as a control.

2.1.1.1 Histamine

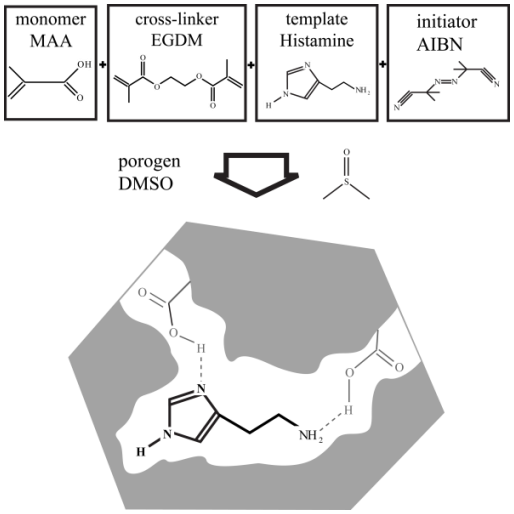

Figure 2.1 – Schematic picture of the imprinted histamine MIP and its components.

The histamine MIP (Figure 2.1) was obtained with a mixture of methacrylic acid (MAA) (17.8 mmol), ethylene glycol dimethacrylate (EGDM) (36 mmol), azobisisobutyronitrile (AIBN) (0.66 mmol) and the template molecule histamine (8.99 mmol). This mixture was degassed for 5 minutes with N_2 to remove oxygen. For polymerization the solution was sealed and kept in a thermostatic oil bath at 65°C for 12 h. After polymerization the bulk polymer was grounded with a mechanical mortar for 24 h and sieved through a 25 µm sieve. Only particles with a smaller size than 25 µm were used. Next, the histamine was removed from the MIP powders by Soxhlet extraction with methanol (48 h), followed by a mixture of acetic acid/acetonitrile (1/1) (48 h) and finally again with methanol (12 h). The extracted MIP powders were dried in vacuum for 12 h. A non-imprinted polymer (NIP) was synthesized in the same manner with all the components except for the presence of histamine. This results in a randomized polymer structure without specific binding sites. This NIP will serve as a control to test the selectivity of the MIP structure. Because of the randomization this NIP can also be used to eliminate aspecific binding of the MIP when measuring in a differential way.

2.1.1.2 Malachite green

Malachite green MIPs were created *via* suspension polymerization. As described in Chapter 1, this polymerization method creates spherical particles instead of the random shapes acquired after bulk polymerization. The procedure consisted of a fixed amount of malachite green (0.216 mmol), which was mixed with the functional monomer MAA and crosslinker EGDM. Subsequently, all components were dissolved in a well-defined amount of chloroform, which served as the porogen. This mixture of monomer, cross-linker and porogen was added to a fixed amount of water (4 mL) containing Poly vinyl alchohol (PVA) (0.02 g), which was used as a surfactant. After addition of the initiator AIBN (0.055 g) a uniform distribution of PVA stabilized micelles was achieved using a homogenizer. These micelles contain the pre-polymerization complex. Subsequently, the suspension was flushed with nitrogen for 2 minutes to remove oxygen and was placed in an oven at 65 °C for 2 hours. To remove the template after polymerization, the reaction mixtures containing the MIP and NIP beads were placed in solid phase extraction (SPE) cartridges and were flushed repeatedly for one hour alternating with methanol and an aqueous solution of acetic acid of 7 M. After extraction of the malachite green, the MIP beads were air dried at room temperature. A NIP was created with the same protocol, however, without malachite green present.

2.1.1.3 L-nicotine

L-nicotine MIPs were also made by bulk polymerization (Figure 2.2). The protocol is the same as used with the histamine bulk MIP except that the components are different. In addition, multiple L-nicotine MIPs were tested for their efficiency. These MIPs were made with the same monomers, while the used porogen was varied. Changing the porogen will alter the porosity and polar properties of the MIP and therefore also the efficiency of the MIP. A typical L-nicotine MIP was made with a mixture of MAA (12.5 mmol), EGDM (25.2 mmol) and AIBN (0.66 mmol) dissolved in 7 mL porogen, *e.g.* hexane, together with the template molecule L-nicotine (6.41 mmol).

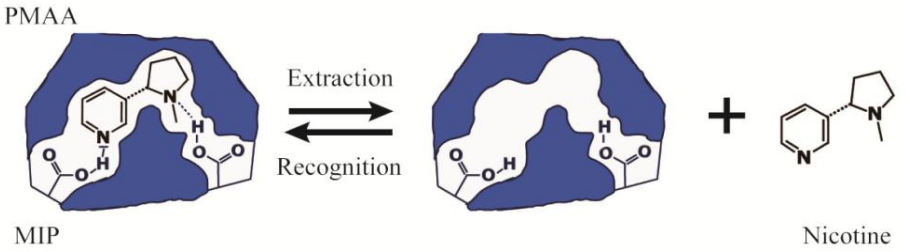

Figure 2.2 - Scheme of the L-nicotine MIP binding principle.

The mixture was degassed for 10 min with N_2. In the following step, the solution was polymerized with an ultraviolet source (360 nm) at room temperature for 24 hours. The resulting monoliths were mechanically crushed and sieved to particles sizes lower than 25 µm. The L-nicotine was extracted from the polymer by a continuous extraction of the MIP powder with methanol, followed by a mixture of acetic acid/acetonintrile (1/1) and ending again with methanol. A NIP was also created using the same procedure, however, without the presence of L-nicotine.

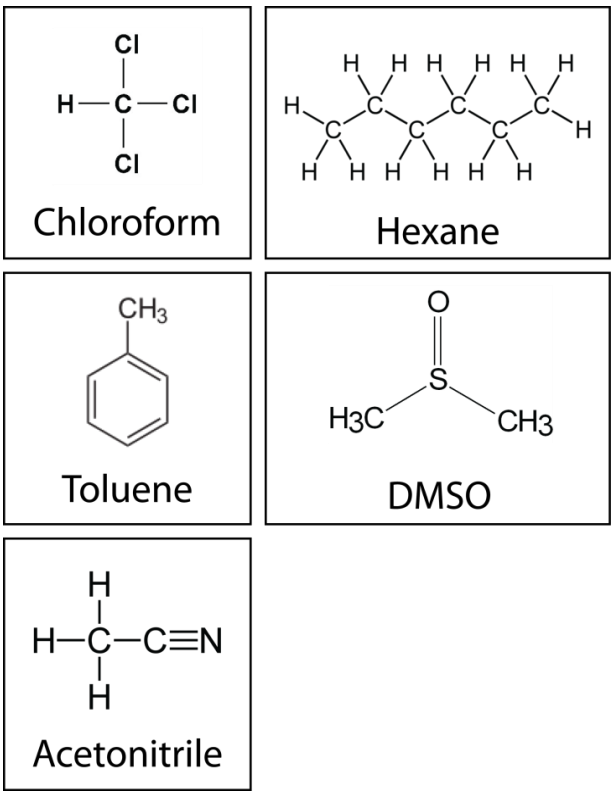

Figure 2.3 – Overview of porogens used for the synthesis of L-nicotine MIPs.

Using the same procedure L-nicotine MIPs with other porogens were prepared. The solvents used are visualized in Figure 2.3. For each of the MIPs a corresponding NIP was also synthesized.

2.1.2 Transducer layer

MIPs are the key part in the design of the MIP-biosensor. In order to use MIPs in a sensor design, they must be immobilized onto the electrodes of the sensor. A direct connection would be preferable, however this is not yet easy to achieve. To circumvent this issue a transducer layer is required, which connects the receptor and the electrodes. The choice of transducer material is determined by the read out technique employed.

For impedance spectroscopy, a conjugated polymer is used, because besides immobilization of the MIP this transducer also needs to conduct electricity to be able to detect small electrical changes upon binding of the target to the MIP. For this purpose OC_1C_{10}-PPV (Figure 2.4) has been chosen. This Poly(p-phenylene vinylene) (PPV) derivative is synthesized *via* the sulphinyl precursor route (90). The polymer acts as a p-type semiconductor with a bandgap of 2.1 eV.

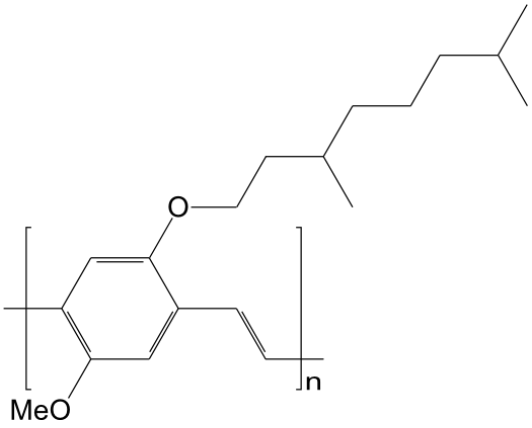

Figure 2.4 – Molecular structure of OC_1C_{10}-PPV. (carbon.physics.ncsu.edu).

This polymer can be dissolved in chlorobenzene. Once dissolved the mixture can be spincoated on flat surfaces in a straightforward manner. In this way it is possible to form a thin film on top of the electrodes.
For quartz crystal microbalance (QCM) measurements the transducer layer does not have to posses conductive properties. Polyvinyl chloride (PVC) is used as a thin film on the upper electrode of the quartz crystal. This polymer is readily available and low-cost, making it more practical as QCM adhesive than OC_1C_{10}-PPV.

2.1.3 Electrodes

For impedance spectroscopy measurements aluminum (Al) electrodes on a glass substrate was used. Aluminum can be deposited on the substrate *via*

physical vapor deposition (PVD). Using a mask, the electrodes can be evaporated into specific patterns. In this work the electrodes were used in a coplanar setup. On each substrate 4 electrode pairs were evaporated, which allows for differential measurements (Figure 2.5).

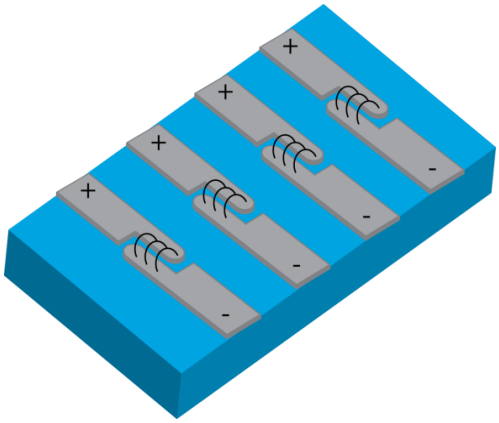

Figure 2.5 - Scheme of coplanar electrode configuration on a glass substrate with electric field lines between neighboring electrode pairs.

This coplanar method reduces the influence of the electrolyte in comparison with more conventional top-bottom electrode configurations as the field lines do not pass through the whole electrolyte, thereby reducing interfering effects by conduction changes in the electrolyte.

For QCM measurements 5 MHz crystals were bought from Maxtek Inc., Cypress, USA and Lot-Oriel, manufacturer Q - Sense, Gothenburg, Sweden. The former are 1 inch diameter crystals (Figure 2.6) while the latter are ½ inch diameter discs. Both crystals have an upper and lower electrode made out of gold. Between the quartz and the gold is a very thin chrome layer to ensure better bonding between quartz and gold. Both crystals are optimized for use in liquids and have a sensitivity of about 1 ng/cm² in liquid.

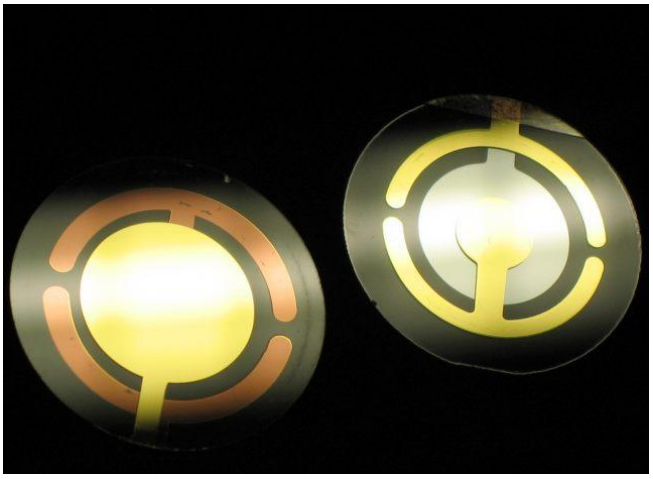

Figure 2.6 - 5 MHz quartz crystal, front side (left) and backside (right). (kisseva.web.elte.hu).

The front side electrode (Figure 2.6) has a larger surface are as compared to the backside. This is to ensure that it is possible to create homogenous layers on the surface. The homogeneity of the layer is important because the center of the crystal is more sensitive than the edges. The reproducibility of measurements can only be assured if homogenous layers can be created.

2.1.4 MIP sensor setups

The above sections describe the various components of the sensor setups. Now that all the parts have been described, it is of interest to look at the building of the actual sensing devices. In the first part the design of the impedance sensor will be described. The second part will describe the quartz crystal microbalance setup.

2.1.4.1 Impedance spectroscopy

Glass substrates were cut to the appropriate size of 20 mm x 12 mm with a diamond tipped glass cutter from microscope slides. The substrates were wiped with a dust free cloth. In order to evaporate Al electrodes successfully, the surfaces must be clean as otherwise residing particles can endanger the

integrity of the Al layer. The following protocol was used for all glass substrates.

- Ultrasonic bath in a soap cleaning solution for 30 min.
- Rinsing with deionized water to remove soap remains.
- Ultrasonic bath in acetone for 15 min.
- Immersing in isopropanol (120 °C).
- Drying with N_2.

Subsequently, the substrates were placed into a mask holder with the appropriate electrode structure. They were moved into a glovebox with a N_2 environment with O_2 and H_2O concentrations below 1 ppm. This was to protect the sensor from degradation. After evaporation in the glovebox, electrodes with a thickness of 70 nm were obtained (Figure 2.7 – step 1). The OC_1C_{10}-PPV was dissolved in chlorobenzene (0.7 wt%) and spincoated on the substrate with the electrodes (Figure 2.7 – step 2). The used spincoating protocol is as follows:

- Step 1: 10 seconds with speed 300 rpm and acceleration 300 rpm/s.
- Step 2: 10 seconds with speed 2500 rpm and acceleration 500 rpm/s.
- Step 3: 60 seconds with speed 300 rpm and acceleration 300 rpm/s

Step 2 in the spincoating process is crucial for determining the actual thickness of the polymer layer. Spincoating the glass substrate with the OC_1C_{10}-PPV transducer with this protocol yields layers with a thickness of ± 120 nm. The next step was to immobilize the MIP or NIP particles on the electrodes surface. A poly(dimethylsiloxane) (PDMS) stamp was used to transfer the MIP particles to the surface of the transducer. The substrate was placed on a hotplate at 120°C for 15 min, which is above the glass-transition temperature (T_g) of OC_1C_{10}-PPV. This will cause the MIP particles to sink into the polymer layer. After cooling of the samples the substrates were rinsed with isopropanol, removing any MIP particles that did not stick

to the OC_1C_{10}-PPV layer (Figure 2.7 – step 3). The sensor chip was then dried with N_2.

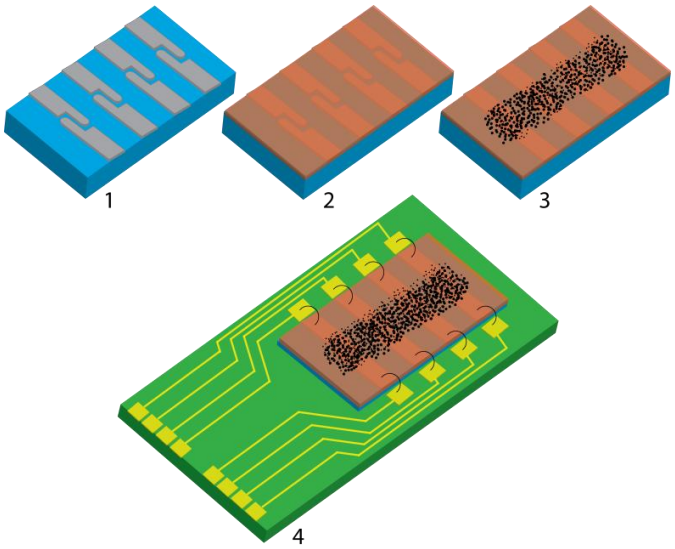

Figure 2.7 – Work flow for the preparation of the construction process of a impedance MIP biosensor. 1) Glass substrate with 4 coplanar electrode couples 2) spincoating of the OC_1C_{10}-PPV transducer layer, 3) Stamping of MIPs, 4) Integration in sensor chip carrier with wire bonding.

The sensor chip was transferred to a chip carrier and was wirebonded to the contacts (Figure 2.7 – step 4). By using a Teflon hood and a PDMS O-ring, a watertight fluid chamber was created (Figure 2.8). This chamber was filled with phosphate-buffered saline (PBS) in which the measurement were performed. This "addition setup" also allows for easy additions of target molecules or control components during the measurements.

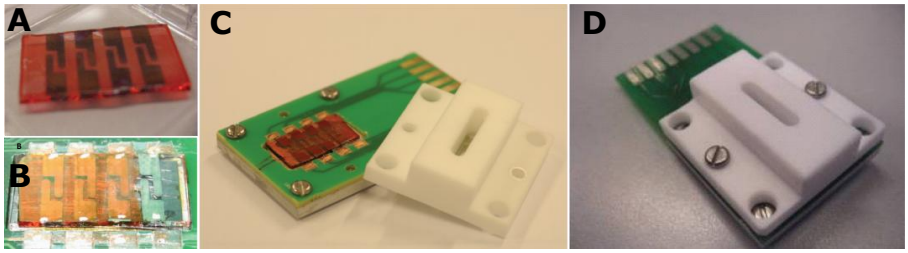

Figure 2.8 - Impedimetric MIP sensor. A) Glass substrate with 4 coplanar electrode couples with the OC_1C_{10}-PPV transducer layer, B) Stamping of MIPs and integration in sensor chip carrier with wire bonding, C) Chip carrier with integrated sensor chip and teflon hood, D) Fully assembled Impedimetric MIP sensor.

The PBS was prepared by dissolving 151 g NaCl (2.58 mol), 19.4 g Na_2HPO_4 (0.122 mol) and 4.2 g KH_2PO_4 (0.0308 mol) in 2 liters of deionized water to obtain a 10x PBS, which was used as a stock solution. Subsequently, the pH was adjusted with NaOH or HCl to the desired amount.

The 4 channel MIP impedance spectroscopy sensor is now ready to be used. The main advantage of this MIP biosensor setup is the ability to measure multiple MIP receptors and NIP controls at the same time under the same conditions.

2.1.4.2 Quartz crystal microbalance.

5 MHz quartz crystals were purchased from Maxtek Inc., Cypress, USA and Lot-Oriel, manufacturer Q - Sense, Gothenburg, Sweden (Figure 2.9). The cleaning was in both cases as follows:

- Ultrasonic bath in tetrahydrofuran (THF) for 15 min.
- UV-Ozone treatment for 15 min.
- Rinsing in $H_2O_2/NH_4+/H_2O$ (1/1/5) solution at 70 °C for 10 min
- Rinsing with deionized water
- UV-Ozone treatment for 15 min.

Once cleaned the QCM crystals were spincoated with PVC in a THF solution (0.35 wt%).

- Step 1: 10 seconds with speed 300 rpm and acceleration 300 rpm/s
- Step 2: 30 seconds with speed 5000 rpm and acceleration 900 rpm/s
- Step 3: 10 seconds with speed 300 rpm and acceleration 300 rpm/s

This protocol will produce samples with a homogenous PVC layer with a thickness of ± 60 nm. The transducer layer with QCM crystals is thinner than the transducer with the impedance spectroscopy samples. This is because the QCM sensitive area is limited to ± 250 nm above the crystal thus the thinner the adhesive layer, the more sensitive the QCM sensor will be. The MIPs or NIPs were attached to the surface in the same manner as with the impedance spectroscopy samples. When the MIPs or NIPs are immobilized, the MIP QCM sensor is ready for use.

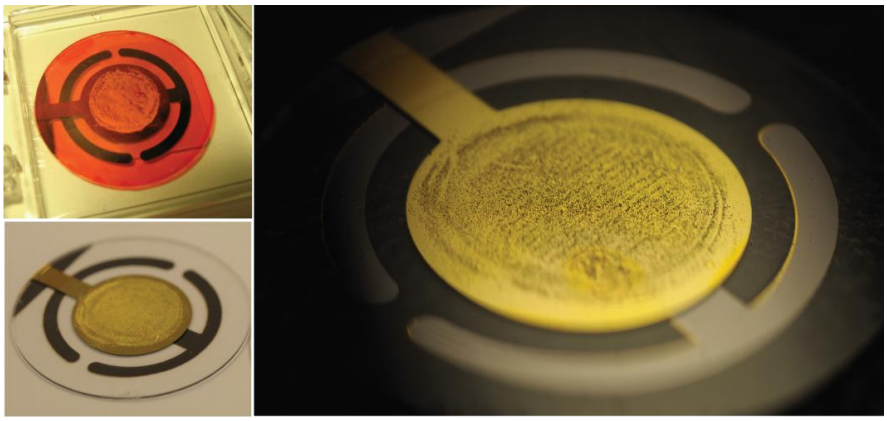

Figure 2.9 - QCM crystals; upper left corner with an OC_1C_{10}-PPV adhesive layer and the others with PVC transducer layer.

2.2 Techniques

2.2.1 UV-Vis spectroscopy for batch rebinding experiments

A first screening of the synthesized MIPs is necessary before they can be used in sensor-based read out techniques. Batch rebinding tests are an easy way to evaluate the efficiency of the MIP and the control NIP (91–93). Parameters that are investigated are the amount of target that they are able to bind, the amount of aspecific binding that takes place and evaluation of cross selectivity with analogues of the target. Batch rebinding test are performed with an UV/VIS spectroscopy device. The device will emit light in the ultraviolet (UV) and in the visible (VIS) range of the electromagnetic spectrum. Each target will absorb light at a specific wavelength. This absorbance is proportional to the concentration of the target present. Thus a fixed amount of MIP or NIP is mixed with a know concentration of the target or analogue in a selected fluid. This mixture is left on the shaker until equilibrium is obtained. A certain amount of the target molecule will bind to the MIP or NIP, this is the bound concentration C_b. The MIPs or NIPs are filtered from the mixture and the remaining free concentration in the mixture is measured using the UV/VIS device. The remaining, free concentration is called C_f. With this information the amount of bound target per gram of MIP or NIP can be calculated (S_b). These measurements are performed for a range of target concentrations and a binding isotherm can be plotted (Figure 2.10).

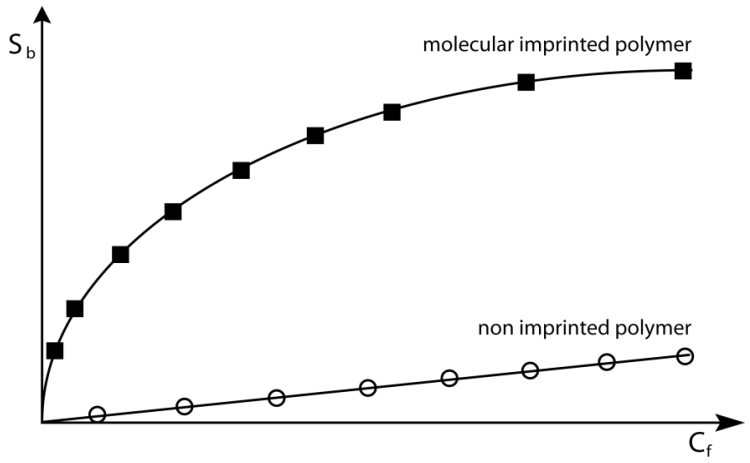

Figure 2.10 - Schematic binding isotherms for MIP and NIP and the target molecule.

The S_b is plotted as a function of C_f. This plot is indicative for the amount of target or analogue that is bound by the MIP or NIP. Another useful data representation is the Scatchard plot (Figure 2.11). In this model S_b/C_f is plotted as a function of S_b. This representation method gives insight in the heterogenic distribution of the binding sites. A straight line is this plot corresponds to a MIP or NIP with a homogenous distribution of binding sites with one affinity constant (K) and it can be described with the Langmuir isotherm, Equation (2.1). N equals the total amount of binding sites present.

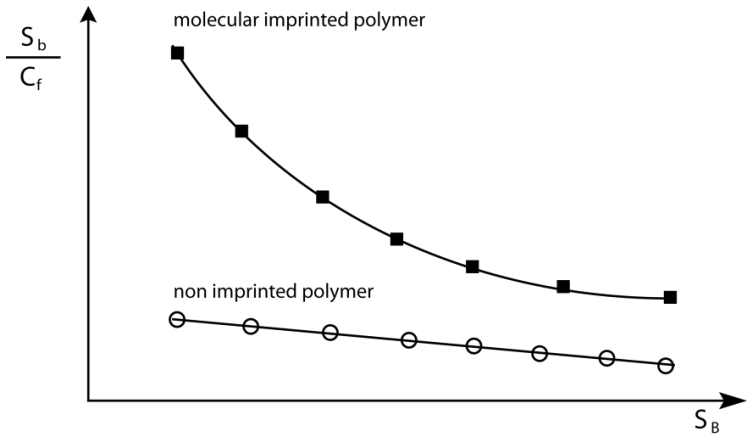

Figure 2.11 - Schematic Scatchard plot for MIP and NIP.

$$S_b/C_f = -KS_b + NK \quad (2.1)$$

When a non-linear relationship is observed a heterogenic distribution of binding sites is present. This can be attributed to different organizational binding sites with different amount of functional monomers and different composition of the binding site cavity. The Freundlich isotherm (92) (Equation 2.2) can be used in a case of a heterogeneous distribution.

$$S_b = A \cdot C_f^{\nu} \quad (2.2)$$

S_b is the amount of target bound per gram of MIP (or NIP). A is the Freundlich constant and correlates to a higher affinity for the target. ν is the Freundlich heterogeneity parameter, which is between 0 and 1. A smaller number indicates a more heterogeneous distribution of binding sites. By fitting the Freundlich model in the binding isotherm, the parameters can be used in a affinity distribution equation (equation 2.3).

$$N = \frac{Asin(\pi\nu)}{\pi}(K_{min}^{-\nu} - K_{max}^{-\nu}) \quad (2.3)$$

With this equation it is possible to calculate the total number of binding sites (N) within a range of affinity constants (K_{min} to K_{max}) (Figure 2.12).

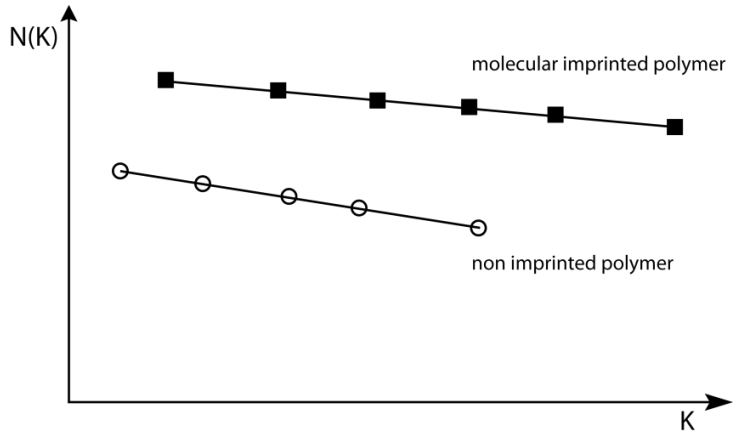

Figure 2.12 - Affinity distribution in a heterogeneous MIP and NIP for their target molecules.

All these isotherms make it possible to evaluate and compare different types of MIPs and NIPs and their efficiency to bind their target and to check for cross reactivity. The straightforward nature of the batch rebinding measurements grants the ability to characterize the MIPs in fluids with different characteristics. The technique also has some downsides. First of all, the concentrations used for these measurements must be relatively high (mM) and cannot be used to evaluate the detection abilities of the MIP in physiological concentrations. A second drawback is the fact that with batch rebinding it is impossible to detect the target molecules in "real life" fluids with a complex matrix because the background noise is too high to be able to identify the absorption peak of the target molecule. Despite these drawbacks it is a very valuable method for a first screening of MIP characteristics.

2.2.2 Electrochemical impedance spectroscopy

Electrochemical impedance spectroscopy (EIS) is a useful tool in biosensing because of its sensitivity and fast read out properties. The potential of EIS has already been proven in other biosensors, for example using aptamers (20,21), DNA (11,12) and antigen-antibody interactions (7,94,95). Impedance is a frequency dependent resistance (R). Resistance is a measure to quantify how much electrical current is resisted by the circuit elements. Resistance follows Ohms law.

$$R = \frac{V}{I} \tag{2.4}$$

The problem with Ohms law is the fact that it is only applicable with an ideal resistor. The resistor must follow Ohms law for every voltage and every current level. The resistor value is independent of the frequency. An alternating current (AC) and voltage signals are in phase when going through a resistor. Complex circuit containing capacitors and inductors do not fall under these restrictions so Ohms law cannot be used. Complex circuits use impedance. Similar to resistance, impedance is a measure of how an electrical circuit will resist the electrical current. Capacitors and inductors are frequency dependent and there is phase difference between the AC voltage and the resulting AC current. Electrochemical impedance is usually measured by applying an AC potential to an electrochemical cell and measure the resulting current. When a sinusoidal excitation potential is applied, an AC current with the same frequency and harmonic attributes will be induced, the amplitude however will be different and there will be a phase shift (Figure 2.13).

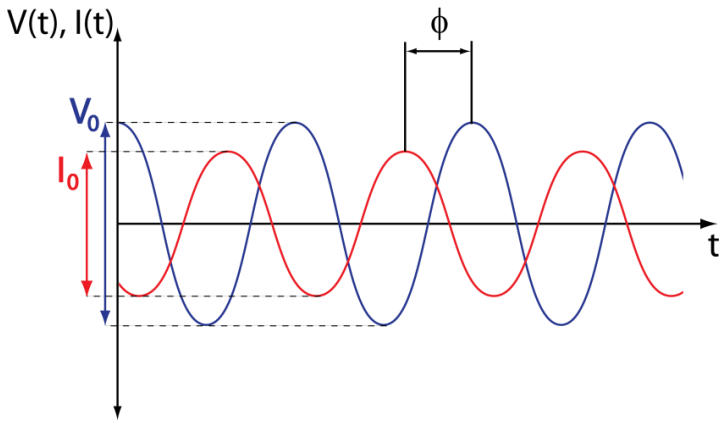

Figure 2.13 – Schematic time dependence of AC voltage and AC current from impedance spectroscopy with phase angle.

Impedance is measured using an excitation voltage signal V(t) and the response is the current signal I(t), which is shifted in time causing the phase shift (ϕ).

$$V(t) = V_0 e^{i\omega t} \tag{2.5}$$

$$I(t) = I_0 e^{i(\omega t - \phi)} \tag{2.6}$$

Describing the curves of Figure 2.13 yields equation 2.5 and 2.6 for V(t) and I(t) respectively. The Impedance (Z) in function of ω can now be calculated.

$$Z = \frac{V(t)}{I(t)} = Z_0 e^{-i\phi} = Z_0(cos\phi + \mathrm{i}\ \mathrm{sin}\phi) \tag{2.7}$$

As is seen in equation 2.7, the impedance Z can be expressed as a modulus Z_0 and a phase shift ϕ**.** It also shows that impedance consists of a real part and an imaginary part.

$$Re(Z) = Z_0 cos\phi \text{ and } \mathrm{Im(Z)} = \mathrm{Z_0 sin\phi} \quad (2.8)$$

There are several ways to represent the complex impedance data. One of the easiest ways is via a bode plot (Figure 2.14). The impedance data is plotted with the log(10) of the frequency on the x-axis and both log(10) of the modulus Z_0 and the phase shift ϕ.

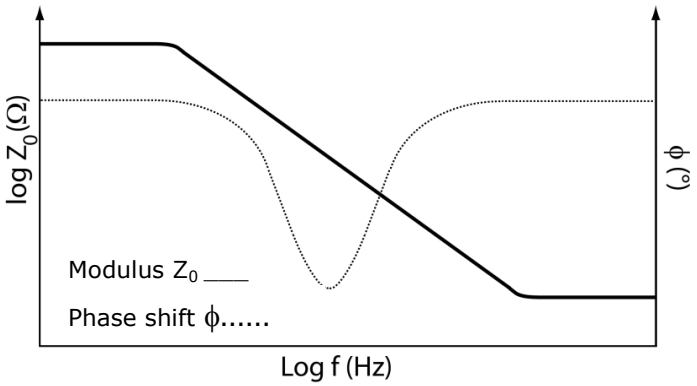

Figure 2.14 - Example of a Bode plot representation.

Another data representation method is the Nyquist plot. From equation 2.7 it is clear that impedance can be written as a complex number. In equation 2.8 the real and imaginary parts are presented. When the real part (x-axis) is plotted against the negative of the imaginary part (y-axis) a Nyquist plot is formed (Figure 2.15).

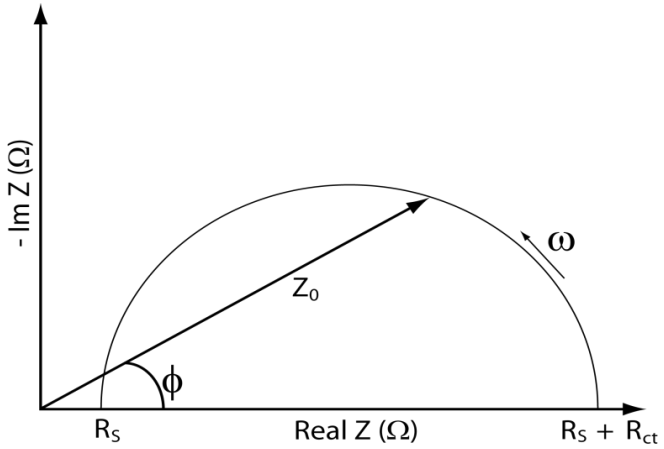

Figure 2.15 - Schematic example of a Nyquist plot.

Each point on the curve is the impedance at a fixed frequency. On the right side are the lower frequencies, whereas on the left side the higher frequencies are presented. On a Nyquist plot the impedance can be represented by a vector, of which the length is the modulus Z_0 and the angle is phase shift ϕ. A Nyquist plot can have many different shapes, which is dependent on the circuit that is being measured. Therefore; the Nyquist plot is a valuable tool for equivalent circuit fitting. Electrochemical impedance data can be plotted with a Nyquist plot and a suitable equivalent circuit is fitted with a set of the most logical components. This is used to make a model of the sensor in order to better understand the changes in the components, which are occurring during measurements. A sensor consists of many different components in various configurations and each component has a different influence on the impedance data. In the following table the different components and their influence on impedance are presented.

Table 2-1 - Components used for equivalent electrical fitting.

Component	Impedance	Circuit Element
R	$Z_R=R$	Resistor
L	$Z_L=i\omega L$	Inductor
C	$Z_C=(i\omega c)^{-1}$	Capacitor
CPE	$Z_{CPE}=(Q_0)^{-1}(i\omega c)^{-n}$	Constant phase element
W	$Z_W=(Y_0)^{-1}(i\omega c)^{-1/2}$	Warburg component

One of the mostly used equivalent electrical circuits is the Randles cell (see Figure 2.16).

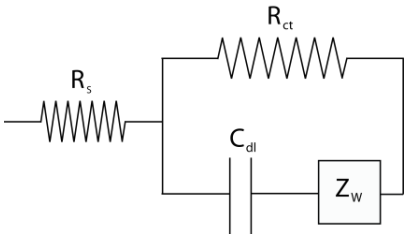

Figure 2.16 - Randles cell circuit consisting of R_s (solution resistance), R_{ct} (charge transfer resistance), Z_w (Warburg component) and C_{dl} (double layer capacitance).

The Randles cell models the impedance of an interface and is a starting point for many other, more complex equivalent circuits of biosensors (96). The interface is the boundary between the solution and the sensor, which is the area of importance because the receptors bind their target at this interface. The R_S component is the resistance of the solution, C_{dl} is the capacitance of the double layer, Z_w is the Warburg component which takes into account unrestricted diffusion to large planer electrodes and R_{ct} is the charge transfer resistance. The double layer capacitance exists on the electrode surface when it is put into an electrolyte solution. It is at this electrode/electrolyte interface that metallic conduction is translated into ionic conduction (Figure 2.17). The transition zone comprises a non-uniform distribution of charges

and acts as a capacitor. Because the distance between charges is in the nanometer range, the capacitive effects can be substantial.

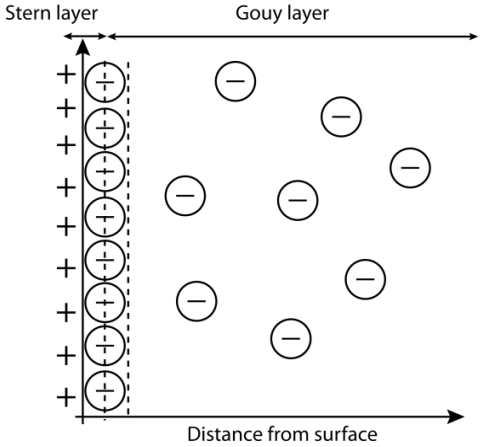

Figure 2.17 - Stern's model of a diffuse double layer.

This phenomenon was described by Stern, who combined the theory of Helmholtz and the Gouy-Chapman theory. The Helmholtz model was a simple double layer, while the Gouy-Chapman model describes a diffuse double layer (96). The charge of the ions forming the double layer depends on the bias voltage (a positive bias voltage will attract negatively charged counter ions and *vice versa*) of the electrodes. The R_{ct} describes how readily the transition between ionic conduction and metallic conductance occurs. At higher frequencies the resistance of the electrolyte solution will contribute more to the overall impedance, while in the lower frequency range the double layer capacitance and charge transfer resistance contribute more. This means that for detection, binding effects happening at the interface are preferably measured at lower frequencies. The Bode plot (Figure 2.14) and the Nyquist plot (Figure 2.15) are examples of the impedance spectrum of a Randles cell.

Other ways of displaying impedance data can be done as a function of time or dose at a fixed frequency. Especially the latter is a good way of displaying the concentration range and sensitivity of a biosensor. The impedance data

can also be visualized for one specific frequency. Before data can be presented in this way, the sensor must be tested for the most sensitive frequency. This frequency can change depending on the sensor design being utilized.

The device used for impedance spectroscopy was an Iviumstat electrochemical analyzer from Ivium technologies B.V. (Eindhoven, The Netherlands) with a frequency range from 10 µHz to 2 kHz. The measurements were performed with an AC voltage of 50 mV and zero bias. The frequency range was usually restricted (100 Hz to 100 kHz) to decrease the time of one measurement cycle. The impedance analyzer is connected to a multiplexer, which allows to measure up to four electrode pairs. All measurements were performed in a temperature controlled incubator oven at 37°C (Figure 2.18).

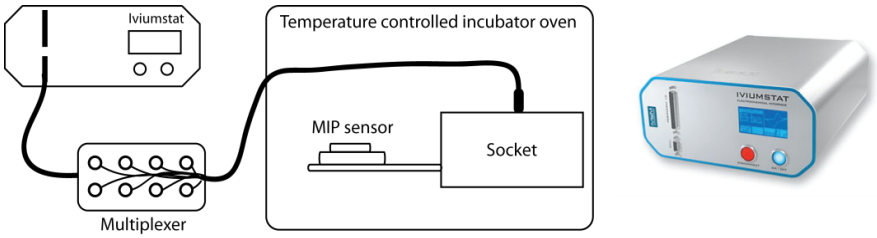

Figure 2.18 - Scheme of impedance spectroscopy measurement setup and the Iviumstat analyzer. (www.ivium.nl).

2.2.3 Quartz crystal microbalance

A second detection method is the quartz crystal microbalance (QCM). Quartz consists of one Si^{4+} ions surrounded by a tetrahedron of O^{2-} and has piezoelectric properties. When force is applied to the crystal, an electric signal is produced (Figure 2.19).

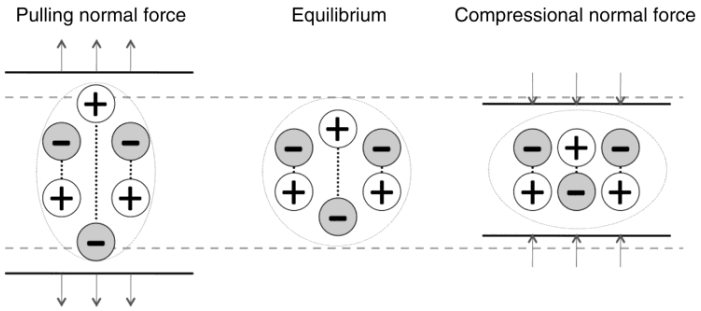

Figure 2.19 - Piezoelectric effect of quartz with applied force. (ult.rsmjournals.com).

When no force is applied, the positive and negative centers coincide resulting in no polarization. When force is applied, the centers shift apart and a net polarization is achieved. On the other hand, when an electrical signal is driven through the crystal, it will mechanically change. When an oscillating voltage is applied to the crystal, the crystal will also mechanically oscillate. The frequency of this oscillation depends on the volume of the crystal and other materials coated onto the crystal. In QCM devices quartz crystal used are AT-cut crystals (Figure 2.20).

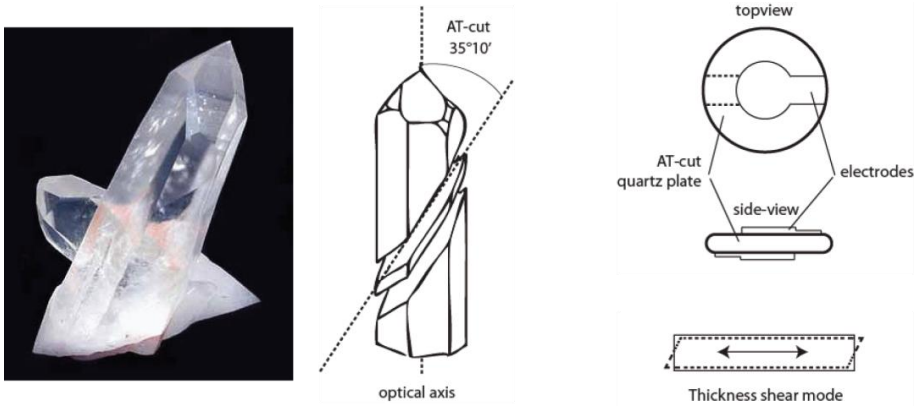

Figure 2.20 - Quartz crystal (left side), scheme of an AT-cut crystal and its operation mode (right side). (www.tau.ac.il).

The angle at which the crystals are cut determines the way they oscillate. AT-cut crystals under an oscillating voltage will oscillate in thickness shear mode and the eigenfrequency is very stable at room temperature. The thickness of the cut crystal will determine the resonance frequency. Thicker cut crystals have a lower resonance frequency. QCM crystals are coated with gold electrodes in order to transfer the oscillating voltage. To improve the adhesion between gold and quartz a thin layer of chrome or titanium is deposited on the quartz. When additional mass is added to the crystals their resonance frequency will change in a proportional way with the added mass. This was described by Sauerbrey in 1959 in the Sauerbrey equation (97).

$$\Delta f = \frac{-2f_0^2}{A\sqrt{\rho_q \mu_q}} \Delta m = \frac{-\Delta m}{m_0} \cdot f_0 \qquad (2.9)$$

With

f_0	=	Resonance frequency of the crystal (Hz)
Δf	=	Frequency change (Hz)
Δm	=	Mass change (g)
ρ_q	=	Density of the quartz crystal (2.648 g/m³)
μ_q	=	The shear modulus of a quartz AT-cut crystal (2.947·g/cm·s²)
A	=	Piezo electric active crystal area (m²)

The sensitivity of the QCM is in the range from ng/cm² to µg/cm² making this a sensitive and versatile research tool. Initially QCM was used for film thickness monitoring. However, the technique quickly found its way in other areas of interest, such as biotechnology (98), biosensing (99), coatings (100) and surface functionalization (101).

The QCM first used in this study a PLO-10 phase lock oscillator (Figure 2.21) from Maxtek Inc (Cypress, United States). The crystals were standard AT-cut, 5 MHz, Ti/Au polished with an active oscillation region of 34.19 mm². This PLO-10 is a voltage driven oscillator, which measures the crystal current

and adjusts the frequency until there is no phase difference between the voltage and the current. The PLO is connected to a frequency counter and a voltmeter to measures the crystal's resistance.

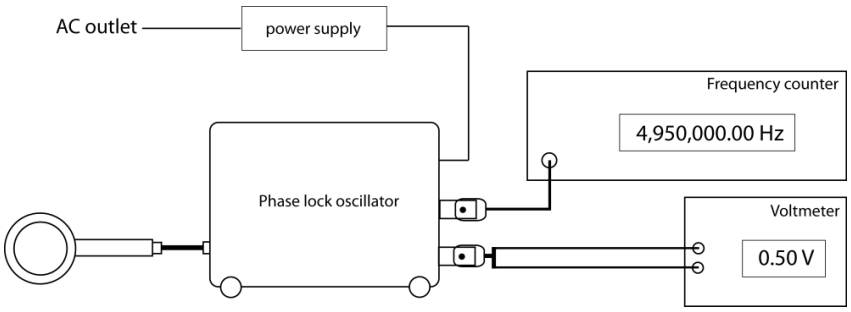

Figure 2.21 - Scheme of the PLO-10 measurement setup.

Another used QCM was the Q-sense E4 system from Lot-Oriel (Figure 2.22), manufacturer Q-sense, Gothenburg, Sweden. This Q-sense also uses AT-cut 5 MHz crystals and has the ability to measure up to 4 crystals at the same time and has a build in temperature control unit (10°C – 50°C).

Figure 2.22 - Q-sense E4 quartz crystal microbalance and dissipation. (www.q-sense.com).

The main difference with the Q-sense E4 is the ability to measure dissipation. Each quartz crystal has a quality factor (Q) (equation 2.10).

$$Q = {f_0}/{w} \tag{2.10}$$

f_0 is the resonance frequency and w is the full width of the resonance curve at half of its maximum. The quality factor is a dimensionless parameter that indicates how much energy is lost per cycle relative to the stored energy. The higher Q the less energy is lost. The inverse of Q equals the dissipation or lost energy per cycle divided by the total energy in the system.

$$D = {1}/{Q} \tag{2.11}$$

Because the Q-sense E4 is able to measure the dissipation, it must function differently from the PLO-10. The Q-sense excites the crystal for a brief moment. After the excitation the sensor oscillation will start to decay in an exponential way. During this period the frequency and the dissipation are monitored. Added mass will cause a resonance frequency shift. If the added mass is rigid, the dissipation will not change. However if the added mass is soft the dissipation will increase as it will dampen the oscillation (Figure 2.23).

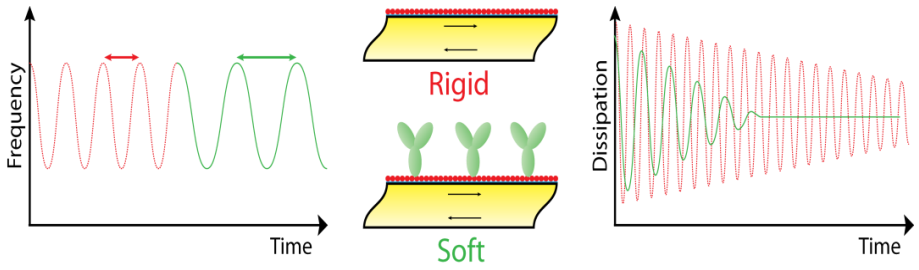

Figure 2.23 - Resonance frequency change and dissipation change due to added mass. (www.q-sense.com).

The combination of frequency and dissipation monitoring gives more information on the changes occurring at the electrode surface than the PLO-

10, which is only sensitive to mass changes. This is especially useful when working with soft materials, which will induce bigger changes upon binding to the surface. It is also very useful for studies in which swelling and shrinking of layers such as polymers or particles is considered.

3 MIP-based sensor platforms for the detection of histamine in the nano- and micromolar range in aqueous media

3.1 Introduction

In this work MIPs are integrated into two different biosensor setups. The first setup is based on impedance spectroscopy and makes it possible to detect targets in the nanomolar range (5,11,48). The other setup is based on the principle of quartz crystal microbalance (QCM) and is useful to detect targets in the micromolar range. In this way the binding events of the MIPs can be monitored over a large concentration range. Furthermore, a medically relevant target is selected, *i.e.* histamine (Figure 3.1), which plays a crucial role in allergic reactions. For example, histamine detection is of interests for research into the Irritable Bowel Syndrome (IBS) since a high concentration of histamine in the intestine can be linked to IBS (68).

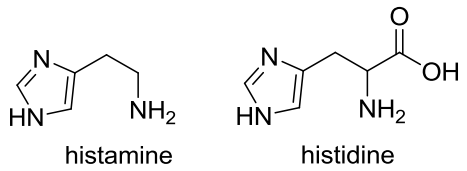

Figure 3.1 – Molecular structures of histamine and histidine. (chemistry.about.com)

In this chapter, a well-functioning biosensor is constructed for the sensitive and specific detection of histamine over a wide concentration range *in vitro* in an aqueous solution. In contrast, a comparable molecule, *i.e.* histidine (Figure 3.1), does not give a significant response. Since the detection of histamine is important for food science and biomedical testing, the developed sensor platforms may find use in a variety of applications. For example, typical histamine concentrations in human plasma range from

approximately 1 to 15 nM (102) The actual histamine concentration can be indicative of certain diseases, *e.g.* the histamine concentration in group of women with breast cancer was 8.23 ± 3.4 nM, whereas the healthy control group only has a histamine concentration of 5.92 ± 3.1 nM in the plasma (103). Hence, concentration detection in the nanomolar range is of significant importance. Another possible application for a histamine biosensor is the verification of the freshness of food samples. Spoiled foods contain higher histamine levels due to the degradations of proteins (104). In this type of applications, relevant histamine concentrations are much higher. For example, fish poisoning can occur if spoiled fish contains more than 50 mg of histamine per 100 g of fish (0.45 µmol/g) (69). Already several expensive techniques exist to detect histamine. The most common methods make use of high-pressure liquid chromatography (HPLC), gas chromatography (GC) or Enzyme-Linked Immuno Sorbent Assay (ELISA) (105,106). Whereas these techniques need extensive sample preparation procedures and are laborious to execute, the biosensor system described here is not only capable of detecting histamine with high sensitivity and selectivity, it does not require complex sample preparation. In the current work, a new bulk polymerized MIP has been developed and optimised for use in biosensors, which can bind histamine with a high affinity and selectivity in aqueous solutions.

3.2 Materials and methods

3.2.1 Reagents

Ethylene glycol dimethacrylate (EGDM), methacrylic acid (MAA) and dimethylsulfoxide (DMSO) were purchased from Acros Organics (Geel, Belgium). Prior to polymerisation, the stabilizers in the MAA and EGDM were removed by filtration over alumina. Azobisisobutyronitrile (AIBN) was purchased from Fluka (Diegem, Belgium). The target molecule histamine was obtained from Sigma-Aldrich (Diegem, Belgium). The analogous molecule, histidine was obtained from Fluka and was used to test the specificity of the MIPs. All solvents were of analytical grade and purchased

from Acros Organics (Geel, Belgium). They were used without further purification. The PPV derivative, OC_1C_{10}-PPV was used as the immobilization layer for the impedance based biosensor (see section 2.1.2). Polyvinyl Chloride (PVC) was used as the immobilisation layer for the MIP and NIP in the QCM measurements (section 2.1.2). Water used for the dilution range of histamine and histidine for the QCM measurements was demineralised with a Sartorius Arium 611 filtering system (18.2 MΩ□cm) and degassed using a MD4 diaphragm vacuum pump from Vacuubrand. A homemade phosphate buffered saline (PBS) solution was used for the impedance spectroscopy measurements instead of deionized water.

3.2.2 Equipment

Optical absorption measurements for batch rebinding experiments were performed with a Varian Cary 500 UV-Vis-NIR spectrophotometer. The morphology of the sensor surface was investigated using optical microscopy with a Zeiss Axiovert 40 MAT and using scanning electron microscopy (SEM) with a FEI Quanta 200 FEG. Microscope images were processed using the image analysis program ImageJ 1.37v (Wayne Rasband from the Research Services Branch, National Institute of Mental Health, Bethesda, Maryland, USA). The quartz crystal microbalance (QCM) measurements were performed using a PLO-10 phase lock oscillator (see section 2.1.4.2). The pump used during the QCM experiments was a NE-500 syringe pump from Prosense B.V. Impedance spectroscopy was performed using an Iviumstat electrochemical analyzer from Ivium Technologies B.V (see section 2.1.4.1).

3.2.3 MIP synthesis

The MIP synthesis was optimized to obtain MIPs with a high affinity and selectivity for histamine detection in biomimetic sensors. The six most suitable MIP compositions are presented in Table 3-1. These six MIPs were created using the protocol described in section 2.1.1.1 except with varying functional monomer (MAA)/ crosslinking monomer (EGDM) ratios as presented in Table 3-1. The protocol in section 2.1.1.1. describes the amounts used for the MIP which was for the remainder of the experiments.

Table 3-1 - Relative molar composition of selected MIPs with the corresponding amount of binding sites.

MIP	Histamine	MAA	EGDM	N_{tot} (µmol/g)[a]
MIP1	1	0.5	1	219
MIP2	1	1	2	270
MIP3	1	2	4	524
MIP4	1	3	6	84
MIP5	1	1	4	84
MIP6	1	2	8	98

[a] The total number of binding sites within the range of affinity constants from 1 to 100 mM^{-1}, as obtained after fitting with Freundlich isotherms.

3.2.4 Sensing systems

3.2.4.1 QCM

For the actual measurements, the quartz crystals were placed in the crystal holder, which is on one side connected to the syringe pump and on the other side to an addition reservoir. Each measurement started with a base volume of 10 mL of demineralised water in the addition reservoir. Subsequently, this water was pumped through the crystal holder with a flow rate of 1 mL/min. Measurements were performed at room temperature. When the signal stabilized, the flow was stopped and the desired amount of histamine or histidine was added to the addition reservoir. This mixture was stirred for 20 seconds with a magnetic stirrer. After 20 seconds, the stirrer was stopped and the pumping was resumed at the same flow rate. Upon binding to the MIP or NIP the frequency dropped in accordance with the bound mass. After each measurement, the addition reservoir and the crystals were adequately rinsed to remove any remaining target molecules. Increasing concentrations of histamine and histidine were measured with both the MIP and the NIP covered crystals in the concentration range 1 µM to 100 µM with 10 µM increments.

3.2.4.2 Impedance spectroscopy

The impedimetric sensor was build using 4 coplanar aluminium contacts (giving a total of 8 electrodes) with a thickness of 70 nm and an interspace of 0.6 mm. Measurements were performed in a controlled temperature environment at 37 °C using an addition setup, which consists of a 500 µL reservoir placed upon the printed circuit board (PCB). For each sensing spot, spectra were measured sequentially at a low-frequency range from 1Hz to 1 kHz with zero bios voltage and an oscillating voltage of 50 mV. The concentration of histamine was increased in a 0 to 12 nM range. First a histamine concentration range of 9 to 31 nM was prepared in 12 equal steps. Constant volumes of 25 µl of these concentrations were sequentially added to the PBS, resulting in the desired 1 nM increments. The histidine concentrations were increased by repeated addition of 50 mL of a 29 nM solution, resulting in unequal steps of 5.8 nM, 9.7 nM and 12.4 nM. Time-resolved analysis of the impedance spectra occurred also at a low frequency, *i.e.* 213 Hz. At low frequencies, the sensor is more sensitive for surface interactions between the MIP binding sites, the target molecules and the electrolyte (48). It can be assumed that upon binding, electrical changes occur at that location, which alter the capacitive strength of the double layer interface (107).

3.3 Results and discussion

3.3.1 Batch rebinding experiments

To study the binding characteristics of all prepared MIPs and NIPs, batch rebinding experiments have been performed. To this end, the MIP or NIP powder (20 mg) was added to 5 mL of various concentrations of histamine in aqueous solutions. The resulting suspensions were shaken during 4 h on a rocking table at room temperature. After filtration the free concentration (C_f) of histamine has been measured using UV-Vis spectroscopy. Subsequently, the amount of histamine bound per gram MIP has been calculated (S_b) and binding isotherms and corresponding affinity distributions for the imprinted

and non-imprinted polymers towards histamine have been made. These affinity distributions are based on the Freundlich model, which is known to give an excellent description of the binding characteristics in MIPs as a result of the presence of a heterogeneous distribution of binding sites (25,48,108,109). Using the Freundlich model, the total number of binding sites, N_{tot}, within the range of affinity constants K_i = 1 to 100 mM^{-1} can be calculated (Table 3-1) (25). This number is a measure for the binding capacity of the individual MIP materials.

From these batch rebinding experiments it becomes evident that MIP3 has the best performance for integration into biosensors. MIP 3 has a relative molar composition of 1/2/4 for histamine/MAA/EGDM respectively. This ratio is the optimal because of a good balance between functional monomers (MAA) and crosslinker (EGDM) which results in binding spots with a high affinity for histamine. An imbalance between functional monomer and crosslinker causes inferior binding affinities. Therefore, MIP3 and its corresponding NIP counterpart have been selected for the biosensor experiments. The binding isotherms and affinity distributions of MIP3 are shown in Figure 3.2. For simplicity, they will be denoted as "MIP" and "NIP" in the remainder of this chapter. The results confirm the higher binding affinity of histamine for MIP compared to the corresponding NIP. Within the region between 1 and 100 mM^{-1} the amount of binding sites for histamine is 524 µmol/g for MIP and 137 µmol/g for the corresponding NIP. This indicates that in the used integration range, the MIP has about four times more binding sites for histamine as the corresponding NIP.

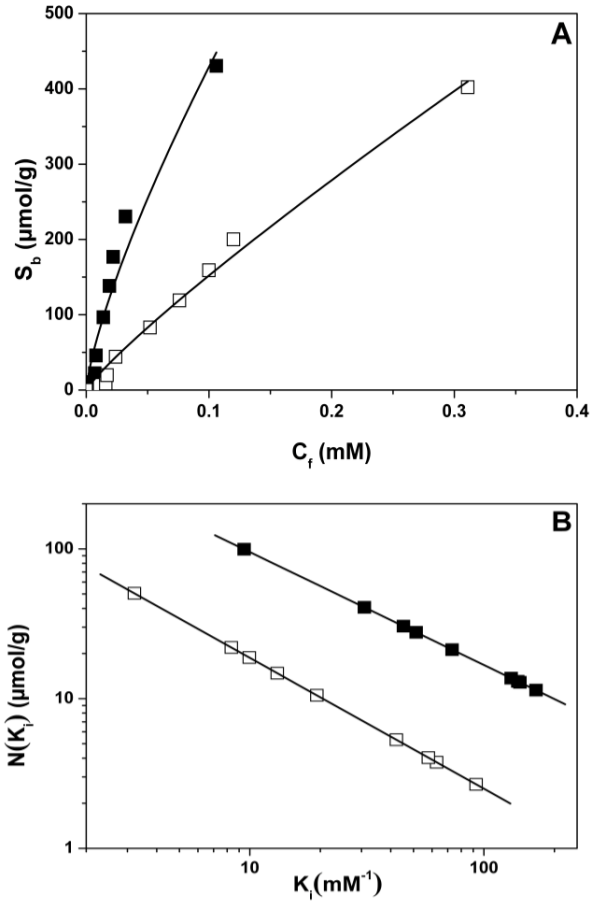

Figure 3.2 - Binding isotherms for MIP (solid squares) and corresponding NIP (open squares) exposed to histamine (A) and resulting affinity distributions after fitting with Freundlich isotherms (B).

One can also estimate an overall binding constant for the MIP and NIP by assuming that every binding site present has the same affinity for histamine by using a Langmuir isotherm. This assumption is obviously incorrect, it can however still provide a rough comparison of the MIP and NIP materials. In this way, binding constants for the MIP and NIP are found of 6.4 mM^{-1} and 1.2 mM^{-1}, respectively. This indicates that, as expected, the MIP binds histamine significantly better than the NIP. This specific chemical recognition of histamine is to a large degree the result of the presence of directional hydrogen bonds in the cavities of the MIPs.

For comparison, the same MIP and NIP have also been exposed to various concentrations of histidine. Histidine has a molecular structure (mw 155.19 g/mol), which is very similar to that of histamine. Hence, it can be safely assumed that if the sensor can successfully differentiate between histamine and histidine, a satisfactory specificity is achieved and that the sensor will exhibit no response to less similar molecules. From an analysis of the binding isotherms and affinity distributions it becomes evident that the amounts of histidine bound to the MIP and NIP are more or less equal and significantly lower as compared to the histamine binding characteristics. For the region between 1 and 100 mM^{-1} the amount of binding sites for histidine is 20 µmol/g for MIP and 13 µmol/g for the corresponding NIP, as compared to 524 µmol/g for the amount of histamine binding sites on the same MIP. The low binding of histidine originates from aspecific interactions with the MIP and NIP (Figure 3.1).

3.3.2 Impedance spectroscopy

Since it is evident that the optimized MIP can bind histamine in a selective manner, the MIP and NIP have been integrated into two different sensor setups (impedimetric and microgravimetric). In the first setup, the chemical recognition occurring at the MIP and NIP covered surfaces is directly translated into an electrical signal using impedance spectroscopy. For the impedance measurements, the MIP and NIP are immobilized using the conjugated polymer OC_1C_{10}-PPV, to minimize interfering resistance at the interface due to the adhesion layer. For a good comparison of the MIP and the NIP sensor data, the immobilised amounts of the MIP and NIP on the sensor surface must be of the same order of magnitude. Hence, optical microscopy and SEM were utilized to study the MIP and NIP covered surfaces (Figure 3.3).

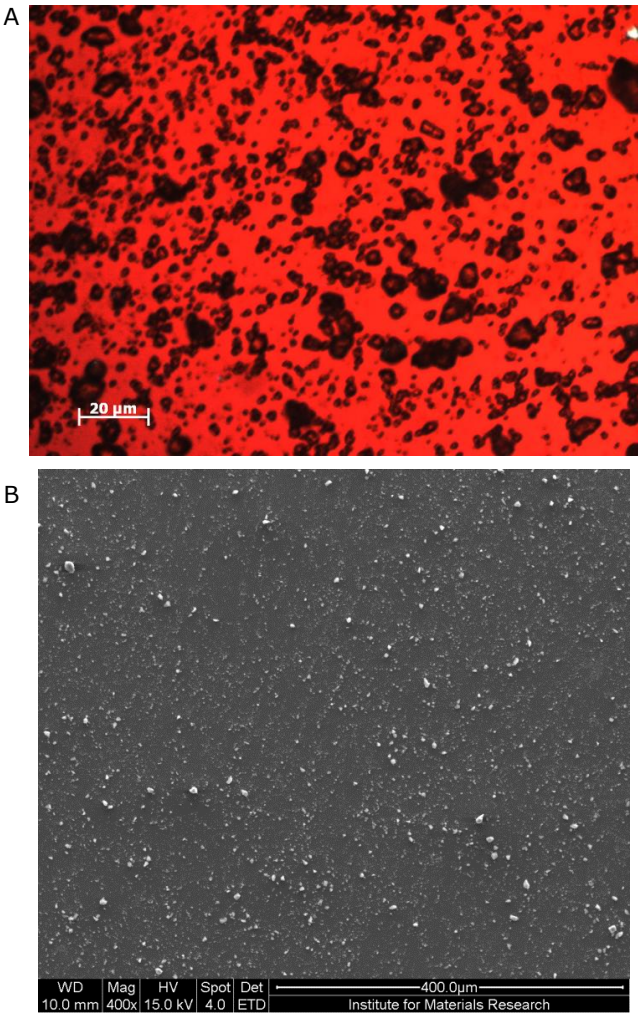

Figure 3.3 - A) Optical micrograph of the MIP covered electrode surface with the MIP particles (black) visible against the conjugated polymer background (red); B) SEM image of a small section of MIP covered surface with the MIP particles (white) visible against the conjugated polymer background (gray).

The analysis of the optical data indicates that the surface coverage is 38.6 % for the MIP and 38.2 % for the NIP, with some minor differences in the size and quantity of the particles. This indicates that indeed a comparable surface

coverage is observed. An analysis of the SEM images provides less accurate data, since the contrast does not allow for a full differentiation between the particles and the conjugated polymer. As a result, a lower coverage is found of 16.8 % for the MIP and 14.8 % for the NIP. Although it can be assumed that the actual coverage is substantially higher, these images confirm the similarity between the MIP and the NIP covered surfaces. For the actual measurements, the sensor cell is filled with PBS and is kept at 37 °C to simulate a biological environment. After a stabilization period of 15 minutes, increasing concentrations of histamine have been added in a stepwise manner. Subsequently, the impedance is measured and a clear dose-response curve is obtained in the 0 - 12 nM concentration range at a frequency of 213 Hz (Figure 3.4). From Figure 3.4, it is evident that the dose-response curve is not linear. This is a result of the fact that MIPs typically contain a heterogeneous distribution of different binding sites, with a concomitant large variety in binding constants [33]. As a result, the dose response curve for a MIP-based sensor is expected to resemble a typical binding-isotherm, with an initially linear rise, followed by gradual saturation. This is in agreement with the experimental results from the batch rebinding experiments. It should be noted that all impedance data are normalized relative to their initial impedance value, prior to addition of the target molecule. The resulting value is referred to as the relative impedance signal. A response value is obtained 20 minutes after addition of the target molecule by averaging five data points. The stability of the measured impedance signal is excellent and as a result, the noise level is very low.

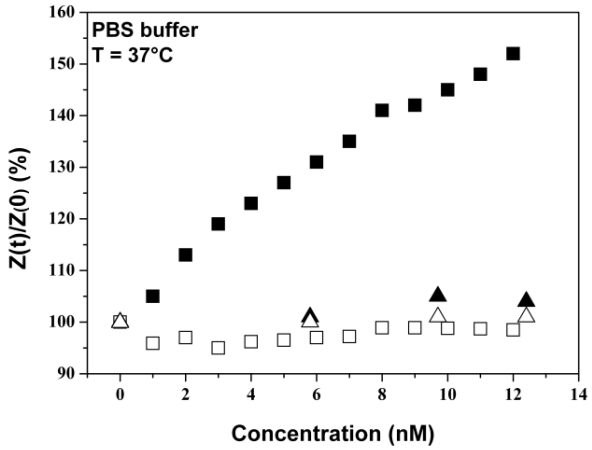

Figure 3.4 - Dose response curve of MIP and NIP channels in response to addition of histamine and histidine obtained with impedance measurements. (MIP exposed to histamine: solid squares; MIP exposed to histidine: solid triangles; NIP exposed to histamine: open squares; NIP exposed to histidine: open triagles).

At 213 Hz the MIP-sensor shows a 45 % response to a concentration of 10 nM histamine. At higher concentrations, the sensor obviously will reach its saturation level. Due to the low signal to noise ratio of the measurements, the limit of detection is well below 1 nM. The NIP channel, which measures non-specific binding of histamine molecules to the sensor surface, shows no sensitivity towards histamine. In addition, the specificity is tested with the analogous molecule histidine. At 213 Hz both the MIP and NIP channel show no response to histidine concentrations in the same nanomolar range. This confirms that the sensor is highly selective for histamine and does not respond to other molecules, even if they have a widely similar structure. The capability of the sensor to measure in the nanomolar range is relevant for medical applications, in which deviations in the histamine concentration of a few nanomolar can be indicative of a disease (section 3.1). Furthermore, it is noteworthy that our impedimetric sensor performs considerably better than a previously reported impedimetric

device with which a histamine detection limit of 5 nM was achieved under optimized flow conditions of a comparatively large sample volume of 1ml 0.5 M HEPES buffer [28].

3.3.3 Quartz crystal microbalance

The surface coverage on the quartz crystals, as obtained from optical microscopy, was 27.1% and 28.7% for the MIP and NIP particles, respectively. Although the visual distribution of the particles at the PVC surface as observed with microscopy was identical to the distribution on the impedimetric electrodes, the actual coverage values are somewhat lower than observed for the OC_1C_{10}-PPV immobilization. This can be explained by the higher hardness and lower thickness of the PVC adhesion layer as compared to OC_1C_{10}-PPV, which apparently is less favourable for entrapment process. It is important that the surface coverage of the MIP and NIP on each crystal is widely similar, since otherwise the QCM results would be difficult to compare. After integration of the MIP and NIP covered crystals in the sensor setup, the crystals have been exposed to a series of different concentrations (1 µM- 100 µM) of histamine and histidine. This resulted in typical dose-response curves (Figure 3.5). Frequency shifts have been obtained after stabilization of the frequency before addition of the next concentration.

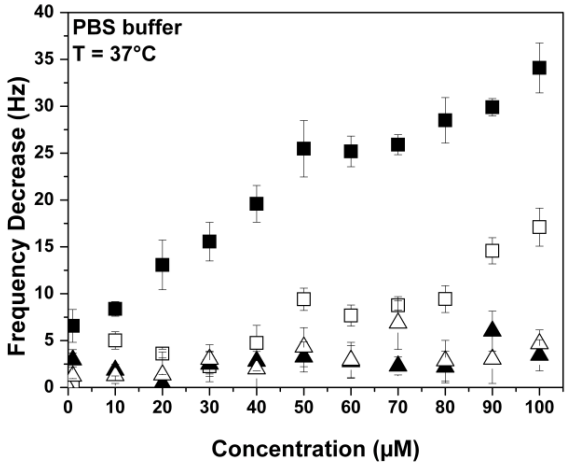

Figure 3.5 - QCM dose- response curves for MIP and NIP exposed to increasing concentrations of histamine and histidine (MIP exposed to histamine: solid squares; MIP exposed to histidine: solid triangles; NIP exposed to histamine: open squares; NIP exposed to histidine: open triangles).

As can be seen in Figure 3.5, the observed frequency shifts for the MIP exposed to histamine are significantly higher than for the NIP exposed to histamine as well as for the MIP and NIP exposed to histidine. For the MIP a concentration of 1 µM histamine causes a frequency shift of 6.6 Hz, which rises until the highest measured concentration of 100 µM causing a frequency shift of 34. Hz. The shape of the dose-response curve is similar as observed for the impedimetric experiments. In contrast, for both the MIP and the NIP exposed to histidine the frequency remains widely constant (minimum 0.4 Hz and maximum 6.9 Hz) over the entire concentration range. As expected, there are no specific binding sites for histidine and only aspecific binding is observed. This confirms the previous observations on the excellent specificity of the MIP-based sensor. Due to aspecific binding, the NIP exposed to histamine exhibits a similar behaviour, with a slightly higher frequency shift for the larger concentrations. This rise can be attributed to

the significantly higher concentrations used in these experiments, as compared to the impedimetric measurements. In addition, this frequency shift associated with aspecific binding is slightly more pronounced than that observed for histidine because of the fact that the MIP synthesis has been optimised for the specific binding of histamine. Hence, the NIP synthesized from the same optimised mixture of monomers, cross-linkers and porogen (without the presence of a template), can be expected to have also a somewhat higher amount of aspecific binding sites for histamine.

For a correct comparison, the corresponding mass change has been calculated for each frequency shift. It is found that the binding of 6.11 ng of target molecules corresponds to frequency decrease of 1 Hz. The thus obtained mass change of the sensor has been compared to the total mass that passed the sensor while flowing, for that given concentration, giving an estimate of the percentage of molecules that bind to either the MIP or NIP. From these calculations it is apparent that histamine binds about 14 times better to the MIP based sensor surface than histidine does. Histamine binds also almost five times better to the MIP based sensor surface as compared to the NIP. This is in agreement with the batch rebinding experiments, which demonstrated that the MIP has about four times as many binding sites for histamine as compared to the NIP. The concentration range for the QCM based sensor in the micromolar range is well suited for food sample measurements.

3.3.4 Histamine detection in fish-brine samples

As mentioned in the introduction, histamine is commonly found in food samples. In seafood products, high levels of histamine can be associated with food spoilage and can lead to severe health problems. Generally it is found that seafood containing histamine levels of 50 ppm or more are of unacceptable quality (110). It is therefore important to be able to differentiate between acceptable histamine concentrations and levels above 50 ppm. To demonstrate the viability of our MIP based sensor for such measurements, impedance measurements have been performed on the packing fluids collected from canned tuna. To this end, the collected fluid has

been first filtered with a series of filters, with a smallest mesh size of 45 µm. The fluid has subsequently been split into two parts and one part of the fluid was spiked with histamine to a concentration of 50 ppm (which corresponds to ± 450 µM histamine), while the other part remained unaltered. Since the histamine concentration in the spiked samples is well above the suitable detection range of our sensor, this stock fluid of 50 ppm histamine was diluted with PBS to the desired histamine concentration, *i.e.* 50, 100, 150, 200, 250 ppb.

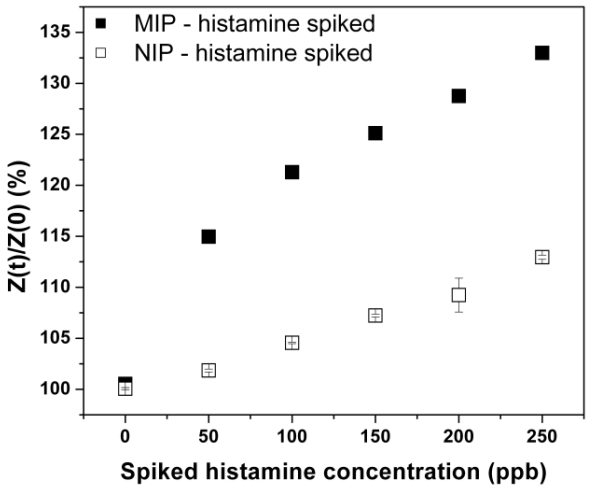

Figure 3.6 – Response of the MIP-based sensor to various concentrations of histamine in spiked samples of canned tuna liquid.

Upon exposing the sensor to these diluted solutions, it becomes evident that the measurements with the spiked tuna samples exhibit a considerable larger response than the unaltered sample. For example, for the tune fluid sample spiked with 250 ppm histamine, an increase in the impedance is found of 33.0 ± 0.3%, while after addition, of the non-spiked sample only an increase is found of 12.8 ± 0.1 %, which is probably associated with differences in the composition of the fluid in the measurement cell due to the tuna fluid addition. The NIP exhibits only a minor increase in response, which

is a result of aspecific adsorption. In Figure 3.6 the effect of the spiked brine tuna samples is presented for the MIP and the NIP. It is immediately clear that the MIP is able to bind much more histamine from the complex tuna brine mixture than the NIP. Even at 50 ppb the MIP has a response of 15.0 ± 0.7 % while the NIP has a response of 1.9 ± 0.1 %. Both the MIP and the NIP signal keep on rising with increasing histamine concentrations.

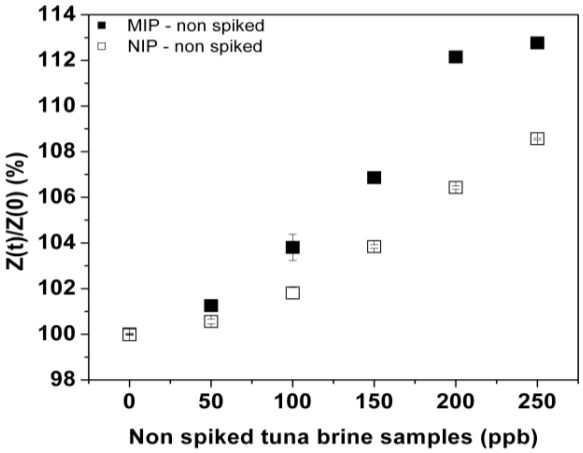

Figure 3.7 - Response of the MIP-based sensor to various non-spiked volumes (equal to the volumes in the histamine spiked measurements) of canned tuna liquid.

In Figure 3.7 the same measurements were performed with tuna brine, however without the presence of spiked histamine. The same dilutions as the spiked tuna brine were used to serve as the samples to be measured. The impedance signal response is significantly lower than the measurements performed with spiked tuna brine for both the MIP and NIP (Figure 3.6). In Figure 3.7 the MIP does show a greater response to the non spiked tuna brine samples than the NIP, indicating that some histamine is already present in the tuna brine.

For a true representation of the specific binding events, the NIP signal is subtracted from the MIP signal. The results are presented in Figure 3.8.

Upon spiking with 50 ppm a large increase in the differential sensor signal is visible. However, spiking with higher concentrations leads to a gradual saturation of the sensor. Notwithstanding, it is clearly demonstrated that the sensor performs well with an actual sample. This proof of principle indicates that it is possible to measure histamine concentrations of 50 ppb, and possibly much lower, in filtered food samples using the MIP based sensor setup.

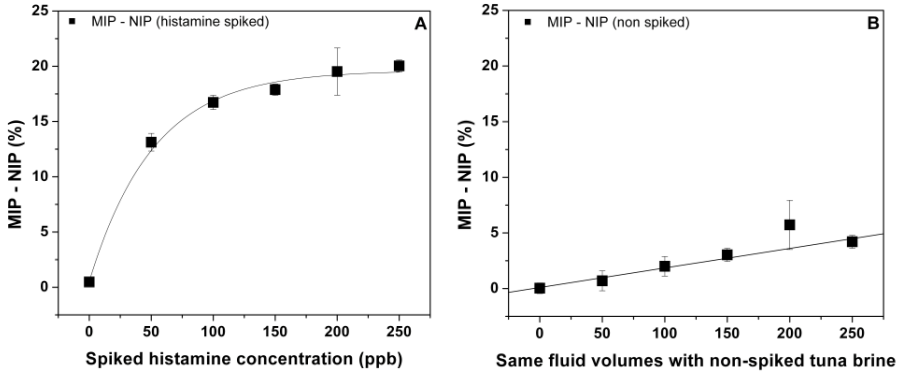

Figure 3.8 - Response of the MIP-based sensor to various concentrations of histamine in spiked samples of canned tuna liquid (A) and to the same fluid volumes with non-spiked tuna brine (B).

3.1 Conclusion

MIPs with high affinity and specificity towards histamine have been developed for sensor applications. Executing batch rebinding experiments to characterize the target binding phenomena has proven to be a suitable way to screen the MIPs and the corresponding NIPs. In this manner, it is possible to predict, which MIP is most useful for integration into the biosensor systems. The optimised MIP binds significantly more histamine as compared to the corresponding NIP. The limited binding on the NIP is governed by aspecific interactions between histamine and the polymer matrix. In contrast, the binding isotherms for the MIP and corresponding NIP towards

the analogous molecule histidine show even less aspecific binding. Both the optimised MIP and the corresponding NIP have been successfully integrated as synthetic recognition elements for the detection of histamine into two sensing platforms, *i.e.* QCM and impedimetric detection. Whereas QCM can be successfully used to detect histamine in the micromolar range, impedance based measurements make it possible to detect the target in the nanomolar range. Using the analogous molecule histidine, it is demonstrated that both sensor platforms have a high specificity for the detection of histamine. In conclusion, it has been demonstrated that using our MIP based sensor platforms, histamine can be readily detected over a large concentration range from 1 nM to 100 µM in a sensitive and selective manner. This opens the way for many other novel MIP based sensor applications. As a first proof of principle, the measurement of histamine in the liquid of canned tuna is demonstrated using the MIP-based sensor for food safety analysis.

4 MIP Beads for the Detection of Malachite Green

4.1 Introduction

In this work also, an alternative MIP morphology, consisting of beads synthesized *via* a suspension polymerization, is optimized for sensor applications (29). Although the use of a suspension polymerization to obtain MIP particles for chromatographic applications is established (111), the optimization of such particles for sensor applications and their subsequent integration into a prototype sensor has to our best knowledge not yet been reported. It can be expected that the use of MIP beads provides a considerable level of control over particle size and homogeneity of the binding characteristics and, hence, the reproducibility of the sensor. This is a result of the fact that a suspension polymerization typically produces homogeneous and spherically shaped particles (see section 4.3.1), which will be able to cover the sensor surface more densely and reproducibly. In addition, the imprinting effect is more uniformly distributed in a suspension polymerization because the polymerization is better controlled within every MIP bead. This is of considerable importance since there is only a limited amount of MIP present on the sensor surface. After optimization of the MIP synthesis, the most suitable MIP beads have been incorporated into our sensor platform. Subsequently, the sensor surface coverage has been studied and the sensor has been tested using the quartz crystal microbalance (QCM) and impedimetric detection as the electronic readout techniques.

In addition to the new MIP morphology on the sensor surface, a target molecule of special interest, *i.e.* the dye malachite green (MG), was selected for the optimizations. Considerable interest exists in the quantitative analysis of dye-molecules in environmental and food samples. For example, in many parts of the world, dyes belonging to the triphenylmethane family, such as MG, are being used as an inexpensive method to control fungal attacks and

infections in aquaculture. However, this class of dyes is linked to carcinogenesis and respiratory toxicity (78,112). As a result, it is extremely desirable to monitor the concentration of these dyes in water and fish, which provides an interesting potential sensor application area. Currently, state of the art MG detection is performed with HPLC and liquid chromatography tandem mass spectroscopy (LC-MS-MS), with a detection limit of 1 µg/kg (3.04 nmol/kg) and 0.2 µg/kg (0.61 nmol/kg) respectively (113). However, a sensor alternative with a similar limit of detection would allow for a faster and lower cost detection, which, for example, would enhance the possibilities to screen large amounts of food samples. In literature only two MG sensors are presented. The first MG sensor is based on fluorimetric detection, which is an indirect sensing technique and therefore less reliable and less reproducible (114). The second sensor is not specific towards MG in 'real life' samples and requires expensive Raman equipment (115). Therefore, it is desirable to have a direct and specific detection of MG combined with a straightforward and versatile sensor design. To this end, MG binding receptors are needed. Although in the literature many low-cost biomass materials have been tested as adsorbents for MG in the environment, such materials do not have sufficient specificity (116–119). To bind MG in a more specific way, MIPs are a class of artificial receptors with considerable potential (120,121). For example, literature reports exist on the use of MG MIPs as a packing material for Solid Phase Extraction (SPE), which is used in combination with HPLC to monitor fish samples and pond water (122–124). However, this procedure is laborious and a direct detection would be favorable. To achieve this, we present a MIP based MG-sensor, which is able to bind MG in a sensitive and selective manner. To this end, the MIP synthesis has been optimized to achieve not only an optimal MG binding in aqueous media, but also to obtain a suitable MIP morphology in the form of beads for good sensor coverage.

4.2 Experimental

4.2.1 General

Ethylene glycol dimethacrylate (EGDM) and methacrylic acid (MAA) were purchased from Acros. Prior to polymerization, the stabilizers in the MAA and EGDM were removed by filtration over alumina. Azobisisobutyronitrile (AIBN) was purchased from Fluka. The target molecule Malachite green oxalate and the polyvinyl alcohol (PVA) were obtained from Aldrich. All solvents were of analytical grade and purchased from Acros and used without further purification. Water for the batch rebinding experiments was collected from a fish aquarium and was filtered to remove small particles.

For the MIP synthesis an IKA T-10 basic ULTRA-TURRAX homogenizer was used to create micelles. For template removal a solid phase extraction (SPE) setup from Biotage was used. This setup included a VacMaster-10 sample processing manifold, which was connected to a vacuum pump *via* a VacMaster trap kit. Small SPE columns were placed on top of the VacMaster-10 and filled with the MIP/NIP powder allowing a straightforward extraction of the residual MG from the powders.

UV-Vis absorption measurements for batch rebinding experiments were performed with a Varian Cary 500 UV-Vis-NIR spectrophotometer. The morphology of the sensor surface was investigated using optical microscopy with a Zeiss Axiovert 40 MAT. Microscope images were processed using the image analysis program ImageJ 1.37v (Wayne Rasband from the Research Services Branch, National Institute of Mental Health, Bethesda, Maryland, USA). The quartz crystal microbalance (QCM) measurements were performed using a Q-sense E4. The crystals were standard AT-cut, 5 MHz, Cr/Au polished. The pump used during the QCM experiments was a peristaltic IPC-N pump from Ismatec. Impedance spectroscopy was performed using an Iviumstat electrochemical analyzer from Ivium Technologies B.V.

Polyvinyl Chloride (PVC) was used as the immobilization layer (see section 2.1.2) for the MIP and NIP in the QCM measurements. Water used for the dilution range of MG for the QCM measurements was deionized with a

Sartorius arium 611 (18.2 MΩ□cm) and degassed using a MD4 diaphragm vacuum pump from Vacuubrand. HCl was used to bring the resulting concentrations to pH value pH 3.0. The PPV derivative, OC_1C_{10}-PPV was used as the immobilization layer for the impedance based biosensor (see section 2.1.2). A homemade phosphate buffered saline (PBS) solution was used for the impedance spectroscopy measurements.

4.2.2 MIP Synthesis

Eighteen different MIPs were synthesized with different compositions. In addition, using the same procedure (in the absence of the template molecule), the corresponding non-imprinted reference polymers (NIPs) were prepared. In a typical procedure a fixed amount of MG (0.216 mmol) was mixed with the functional monomer MAA and crosslinker EGDM in a specific molar ratio (*see* Table 4-1). Subsequently, all components were dissolved in well-defined amount chloroform (0.5, 1, 2 ml), which served as the porogen.

Table 4-1 - Composition of the reaction mixtures of the prepared MIPs and NIPs. The amount of MG is 0.216 mmol. ([a] No MG is added for the NIP synthesis).

Relative molar composition MG[a]/MAA/EGDM	Porogen 0.5 mL $CHCl_3$	Porogen 1 mL $CHCl_3$	Porogen 2 mL $CHCl_3$
1/2/4	MIP 1	MIP 8	MIP 15
1/4/8	MIP 2	MIP 9	MIP 12
1/8/16	MIP 3	MIP 10	MIP 13
1/2/8	MIP 4	MIP 6	MIP 17
1/4/16	MIP 5	MIP 7	MIP 16
1/8/32	MIP 18	MIP 11	MIP 14

This mixture of the monomer, cross-linker and porogen was added to a fixed amount of water (4 mL) containing polyvinyl alcohol (PVA) (0.02 g), which was used as a surfactant. After addition of the initiator AIBN (0.055 g) a uniform distribution of PVA stabilized micelles containing the pre-

polymerization complex was achieved using a homogenizer. Subsequently, the suspension was flushed with nitrogen for 2 minutes to remove the oxygen and was placed in an oven at 65 °C for two hours. To remove the template after the polymerization, the reaction mixtures containing the MIP and NIP beads were placed in SPE cartridges and were flushed repeatedly for one hour alternating with methanol and an aqueous solution of acetic acid of 7 M**.** After extraction of the MG, the MIP beads were air dried at room temperature.

4.2.3 Sensing Systems

All QCM measurements were performed with the QCM-D setup. The QCM crystals were prepared as described in section (2.1.4.2).
For the actual measurements, the crystals were placed in a holder, which was on one side connected to the pump and on the other side to a reservoir. Each measurement started with water with a pH value of pH 3.0. This water was then pumped through the crystal holder, which was temperature stabilized at 22°C with a flow rate of 100 µL/min. When the signal stabilized, the flow was stopped and the reservoir was switched with a new one containing the first concentration of MG in water. In order to make sure that no air bubbles would get into the system the flow was reversed for 3 seconds, after which the pumping was resumed at the same flow rate. After 10 minutes the flow was stopped and after stabilization of 10 min a measurement was performed. This procedure was repeated for all MG concentrations. In this manner, increasing concentrations of MG were measured with both the MIP and the NIP covered crystals in the concentration range 100 nM to 1000 nM with 100 nM increments.
The impedimetric sensor was constructed as described in section 2.1.4.1. For each sensing spot, spectra were measured sequentially at a low-frequency range from 1 Hz to 1 kHz with zero bios voltage and an oscillating voltage of 50 mV. The concentration of MG was increased in a 0 to 200 nM range. Time-resolved analysis of the impedance spectra occurred also at a low frequency, *i.e.* 213 Hz. It was previously found that at such a low frequency

the sensor is more sensitive for surface interactions between the MIP binding sites, the target molecules and the electrolyte (48).

4.3 Results and Discussion

4.3.1 Synthesis and morphology

The main aim of this work is to obtain a reproducible and high capacity MIP based sensor. To achieve this, the MIP morphology has been adapted to allow for a more optimal sensor coverage. A suspension polymerization is very suitable to prepare uniformly sized MIP beads, which are expected to be suitable for this purpose. These MIPs should also be able to detect MG in aqueous environments with high affinity. To obtain a suitable MIP, the polymerization reaction was optimized by changing the amount of porogen as well as the feed ratio of template, monomer and cross-linker. To this end, eighteen different MIPs were synthesized with different compositions. In addition, using the same procedure (in the absence of the template molecule), the corresponding non-imprinted reference polymers (NIPs) were prepared. Details on the amount of porogen as well as the feed ratio of template, monomer and cross-linker can be found in the experimental section (*see* Table 4-1). As a first assessment of the polymerization result, light microscopy images were taken (Figure 4.1). It is evident from the light microscopy images that most of the prepared MIPs form a collection of beads of different sizes varying from 5 µm to 40 µm. However, MIPs 12, 15 and 17 did not show a bead-like appearance and clustered together. This is due to the disproportional amount of porogen in comparison to the amount of monomers used. In a suspension polymerization, there is a balance between all components resulting in a spherical morphology or lack thereof, as is the case for the formulations 12, 15 and 17. As a result, these MIPs are unsuitable for improved sensing applications, since a similar sensor coverage as the crushed monoliths can be anticipated.

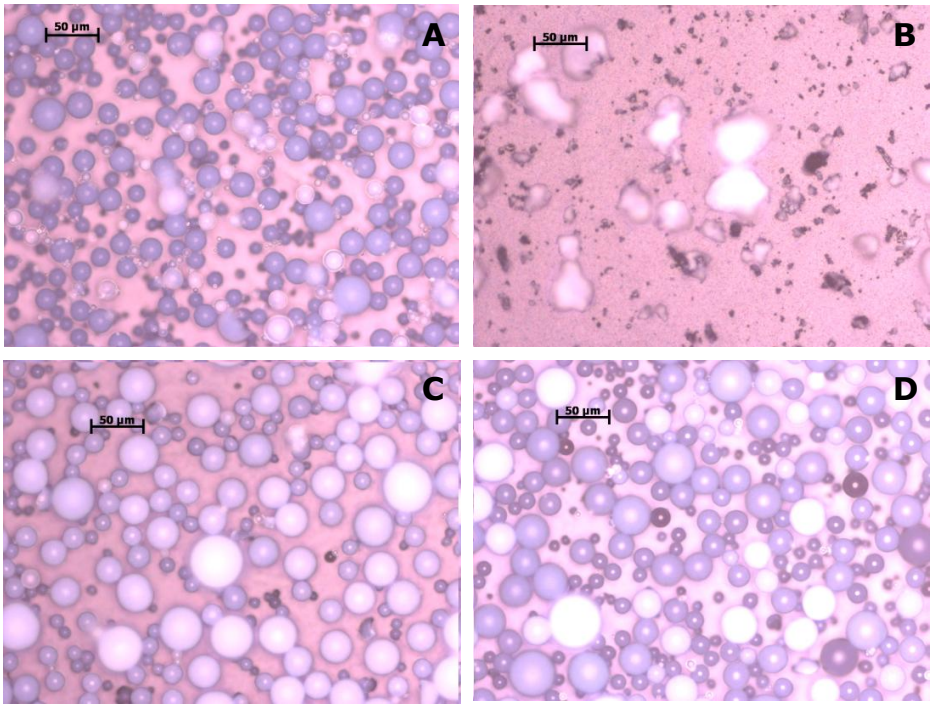

Figure 4.1 – Optical micrographs of representative MIP beads (A: MIP 1; B: MIP 15; C: MIP 10; D: MIP 3).

4.3.2 Batch rebinding experiments

The MIP synthesis has been optimized in terms of morphology and also to bind MG as selectively as possible. To asses the binding behavior of all prepared MIPs and NIPs, batch rebinding experiments were performed on the MIPs and NIPs with a satisfactory spherical shape. For this purpose, MIP or NIP powder (20 mg) was added to 10 mL of various concentrations of MG in aqueous solutions (0.05 mM, 0.10 mM, 0.15 mM, 0.20 mM, 0.25 mM, 0.30 mM, 0.35 mM, 0.4 mM). Two types of water were used for the batch rebinding experiments, *i.e.* standard deionized water and water from a fish tank. The latter was only purified by filtration to obtain a clear solution. The fish tank water was selected to test if other unknown compounds would

interfere with the MIP rebinding. However, from the resulting binding isotherms no differences were observed in the binding behavior between the two types of water utilized, which demonstrates that the MIPs are functional as synthetic receptors for use in environmental monitoring.

After addition of the MIP beads to the water, the resulting suspensions were shaken during 2 h on a rocking table at room temperature. After filtration, the free concentration (C_f) of MG was measured using UV-Vis spectroscopy. Subsequently, the amount of MG bound per gram MIP was calculated (S_b). With these data binding isotherms and the corresponding Scatchard plots for the imprinted and non-imprinted polymers towards MG were constructed. All obtained Scatchard plots display a curved trend indicating the presence of binding site heterogeneity, which is typical for MIPs. This was also reflected by the fact that the data could be modeled with a bi-Langmuir isotherm by means of two linear fits, each representing a total number of binding sites, N, and a corresponding binding constant, Ka (125). The steepest line corresponds to the high affinity binding sites in the MIP and the more horizontal line with the low affinity binding sites. In contrast to this, the NIP data can be fitted with a single linear fit, since the NIP only exhibits low affinity aspecific binding. For each MIP/NIP the values for the binding constants Ka and the corresponding amount of binding sites N are presented in Table 4-2. It is noteworthy that the values for the low affinity binding sites of the MIP are in the same order of magnitude as the NIP values. This confirms that the low affinity binding sites of the MIP bind the target molecule in an aspecific manner. The batch rebinding results presented in Table 4-2 display several clear trends. For example, it can be seen that for most MIPs, *e.g.* comparing MIP 2 with MIP 5, MIP 3 with MIP 18 or MIP 10 with 11, increasing the amount of EGDM will make the MIP structure more rigid and will contribute to a reduction of the number of binding sites (lower N value). However, the remaining binding sites will be more specific towards their target (higher Ka value). The only exceptions on this observation are found for MIPs prepared with only two equivalents MAA (comparing MIP 1 with MIP 4 and MIP 8 with MIP 6). Apparently, due to the low amount of MAA in these MIPs, the pre-polymerization complex is not optimal and the introduction of more EGDM further destabilizes the binding sites. As this

indicates that the use of not enough MAA leads to unsatisfactory results, it should be noted that the use of a larger amount of MAA in the MIP mixture can also be unfavorable, since it is more likely to result in a MIP with more binding sites (higher N value), which are, however, less specific (lower Ka value).

Table 4-2- Binding constants (Ka) and amount of corresponding binding sites (N) for each MIP and NIP calculated from the corresponding scatchard plots.

	MIP Ka (M^{-1}) (high affinity)	MIP N (µmol/g) (high affinity)	MIP Ka (M^{-1}) (low affinity)	MIP N (µmol/g) (low affinity)	NIP Ka (M^{-1})	NIP N (µmol/g)
1	7.90	73	0.75	131	0.45	73
2	6.10	64	0.79	83	0.21	82
3	3.23	73	0.15	150	0.05	103
4	2.50	71	0.54	82	1.55	59
5	23.38	42	0.30	75	0.15	68
6	3.17	64	0.35	89	3.19	60
7	6.60	67	0.71	68	2.66	61
8	6.10	51	0.54	81	3.94	64
9	3.32	69	0.46	92	0.73	76
10	3.21	73	0.14	152	0.06	119
11	11.00	48	0.71	68	0.24	61
13	0.98	73	0.03	102	13.28	61
14	4.88	50	0.26	96	0.41	65
16	3.23	64	0.48	80	2.82	66
18	16.84	35	0.09	85	0.15	48

To avoid this effect, the maximum amount of MAA was limited to eight equivalents as compared to MG. Finally, a porous MIP structure, *i.e.* an increase in the amount of porogen, potentially can contribute to a better availability of the binding sites for the target molecules. However, it was observed that in these experiments high amounts of porogen lead to a destruction of the spherical morphology of the MIP. Fortunately, satisfactory results were obtained with lower porogen amounts. In addition, from the data it can be seen that there is no significant difference between the binding properties of the MIP prepared with 0.5 mL $CHCl_3$ and 1 mL $CHCl_3$. The binding behavior of the NIPs will provide evidence of the aspecific binding effects, which occur for a specific polymerization mixture. Therefore, it is important to compare the binding behavior of the MIP with the corresponding NIP to conclude which MIP is most suitable to be integrated into the sensor platform. An ideal MIP for sensor integration should have high Ka and N values as compared to the corresponding NIP, indicating that most of binding occurs in a specific manner. From the batch rebinding experiments it becomes evident that more than one MIP/NIP combination satisfies this requirement. A further selection was based on the actual magnitude of the non-specific binding, *i.e.* the value of Ka in the NIP. The lowest values were observed for MIP 3 and MIP 10, which otherwise also have virtually identical binding characteristics. Hence, it was decided to utilize one of these two MIPs, *i.e.* MIP 10 and its corresponding NIP counterpart, for all further sensor experiments in aqueous media. In the remainder of this chapter they will be referred to as MIP and NIP. The binding isotherms and Scatchard plots of this MIP and NIP are shown in Figure 4.2 and Figure 4.3. As indicated in Table 4-2, the overall binding constant for the MIP and NIP can be readily calculated using the bi-Langmuir isotherm. This isotherm, which divides the available binding sites into low and high affinity, provides a good comparison of the MIP and NIP systems. This way, the binding constant for the high affinity binding sites in the MIP is found to be 3.21 M^{-1} and the binding constant for the NIP is found to be 0.06 M^{-1}. The low affinity binding sites in the MIP have a comparable binding

constant of 0.14 M^{-1}. This indicates that the MIP binds MG significantly better than the NIP, especially in the low concentration range.

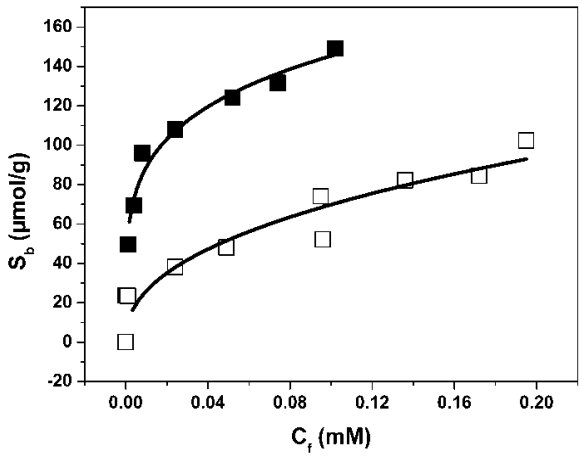

Figure 4.2 - Binding isotherm of MG to MIP 10 (solid squares) and NIP (open squares).

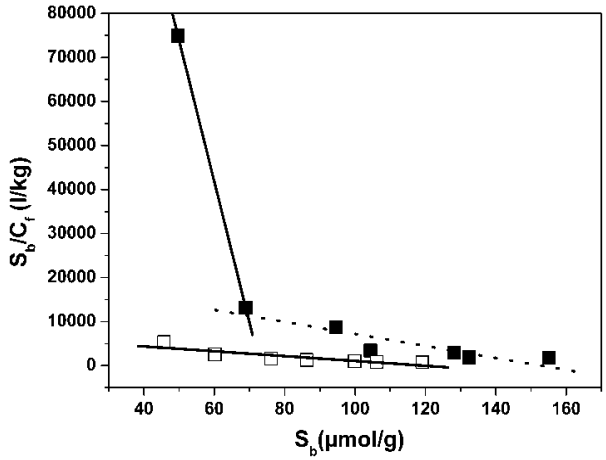

Figure 4.3 - Scatchard plot where MIP 10 data is fitted with two lines, one representing the high affinity binding sites (solid) and one low affinity binding sites (dotted). The NIP is fitted with one line (solid).

The affinity distributions in Figure 4.4 are based on the Freundlich model, which describes the MIP and NIP as a pool of heterogenic binding sites (25,33,48,108).

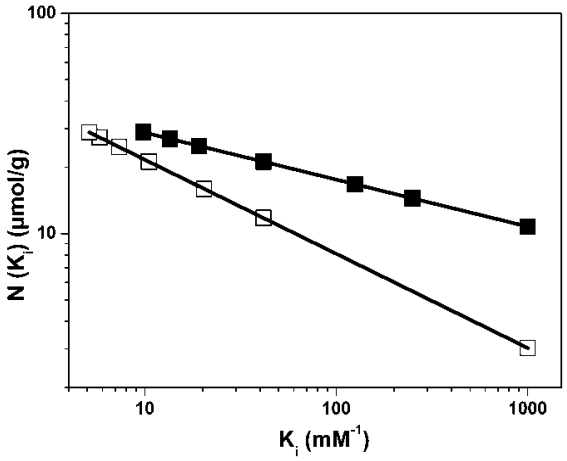

Figure 4.4 - Affinity distribtutions of MIP 10 (solid squares) and its corresponding NIP (open squares) after fitting with a Freundlich isotherm.

Compared to the bi-Langmuir model, which only divides the binding sites in low and in high affinity, this is a more global approach. From the affinity distribution it becomes clear that the MIP has many more binding sites with a high Ka available compared to the corresponding NIP. This is an ideal situation for the detection of low concentrations of MG in sensor applications. After all, it can be expected that at low concentrations of MG, most of the MG will first bind to those binding sites with the highest Ka. Since these sites are abundant in the MIP, this will ultimately result in a low limit of detection. At higher concentrations, also the sites with lower Ka values will start contributing (non-specific binding) and the difference between MIP and NIP disappears. This is reflected by the fact that in the affinity distribution of MIP and NIP approach each other.

4.3.3 QCM Detection of MG

For the QCM measurements, the quartz crystals were first coated with an adhesive polymer layer after which the MIPs and NIPs were fixated onto this layer by matrix entrapment. Subsequently, the resultant surface coverage was assessed using light microscopy. The surface coverage obtained, was 30% and 34% for the MIP and NIP crystals, respectively. While these coverages are comparable to the previously reported surface coverage of grinded and sieved bulk MIPs (33,48), repeated experiments resulted in very little spreading of the surface coverage. In addition, it is noteworthy that due the suspension polymerization each MIP bead has the same binding behavior for MG. This is not the case for a grinded and sieved bulk MIPs, which can exhibit large variations in the binding properties between different particles. Furthermore, the size distribution of the MIPs in a suspension polymerization is narrower compared to the sieved bulk particles. All these factors contribute to the uniformity and reproducibility of the sensor surface coverage. Scanning electron microscopy (SEM) images of the sensor surface and cross section confirm the uniform character (Figure 4.5).

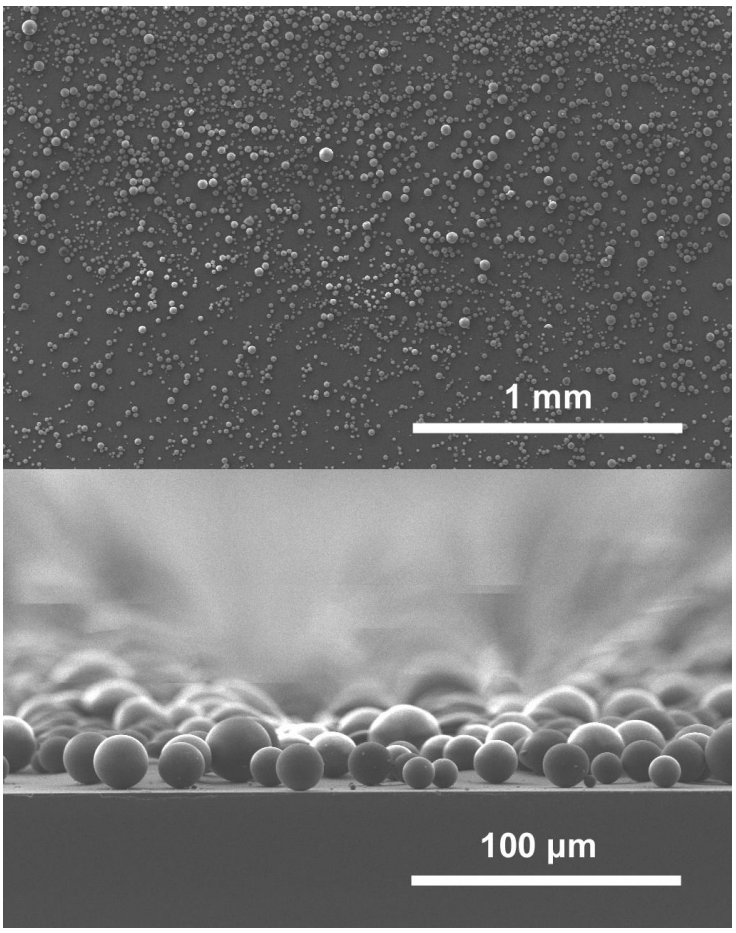

Figure 4.5 - SEM images of the sensor surface (top) and corresponding cross section (bottom).

After matrix entrapment, the MIP and NIP covered crystals were placed in the sensor setup and exposed to a series of different concentrations (100 nM – 1000 nM) MG in water at pH value of pH 3.0. As an extra control, samples solely covered with PVC were used. The measurements resulted in typical dose-response curves for MIP and NIP (Figure 4.6 A). Since the NIP only exhibits non-specific binding, the NIP sensor response can be utilized as a reference, which can be subtracted from the MIP sensor response. The resulting MIP-NIP response therefore corresponds to the specific binding of

MG (Figure 4.6 B). Each data point is obtained when the frequency is stabilized after MG addition.

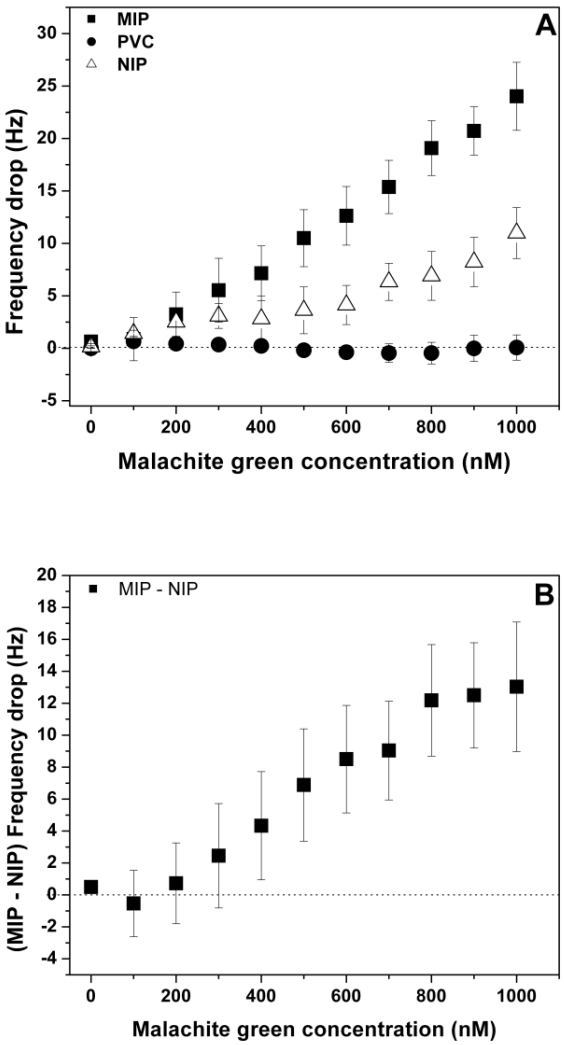

Figure 4.6 – A) QCM dose response curves for both MIP and NIP exposed to increasing concentrations of MG in water (MIP: solid squares; NIP open triangles; PVC surface: solid dots); B) Difference between the MIP and the NIP exposed to increasing concentrations of MG.

It is noteworthy that the QCM measurements were executed in an acidic environment with a pH value of pH 3.0 to suppress the aspecific binding of MG to the MIP. A similar strategy is often used in chromatographic separation in which MIPs are employed as the solid phase material (126,127). Due to the low pH value, it can be anticipated that hydrogen bonding between MG and the polymer matrix is disturbed. Such hydrogen bonding is a major source of non-specific bonding and, as a result, a lower Ka of aspecific binding sites can be expected. This hypothesis has been first tested by performing a batch rebinding experiment with a pH value of pH 3.0. After fitting the Scatchard plots with the bi- Langmuir isotherm, for the MIP a Ka of 3.01 M^{-1} and for the NIP a Ka of 0.01 mM^{-1} are found. From this measurement it is evident that the affinity constant for the NIP, which was already quite low at 0.06 M^{-1} with a pH value of pH 7.0 is dramatically reduced, virtually eliminating the aspecific binding. In contrast, the binding at the specific sites is only minimally affected by the pH value change, *i.e.* a Ka of 3.21 M^{-1} is observed at pH value of pH 7.0 *versus* a Ka of 3.01 M^{-1} at pH value of pH 3.0. As can be seen in Figure 4.6, the observed frequency shifts for the MIP exposed to MG are significantly larger than those observed for the NIP exposed to MG. In the concentration range of 200 nM - 800 nM the MIP binds almost exclusively in a specific manner, as is evident from the low NIP response in this concentration range. At higher concentrations the NIP response increases, indicating that aspecific binding starts occurring. This observation is corroborated by the batch rebinding experiments. From the difference between MIP and NIP it becomes clear that using our current setup, a dynamic range of 200 nM to 1000 nM is possible for the QCM sensor.

4.3.4 Impedance-based detection of MG

To detect MG binding at concentrations below 200 nM, impedance measurements have been performed. It has been previously demonstrated that impedance measurements with MIP based sensors perform well at lower concentration ranges than QCM measurements (33). Binding experiments were performed in PBS with a pH value of pH 7.0, since measurements at a pH value of pH 3.0 are not compatible with the impedance sensor

configuration. The immobilization procedure of the MIP/NIP beads in the MDMO-PPV results in the same sensor coverage as was observed for the QCM sensors. It is clearly visible from Figure 4.7a that MG binds better to the MIP in a concentration range from 0nM to 200nM. Although we did not establish a limit of detection, the measurements clearly demonstrate that this will be well below 50 nM.

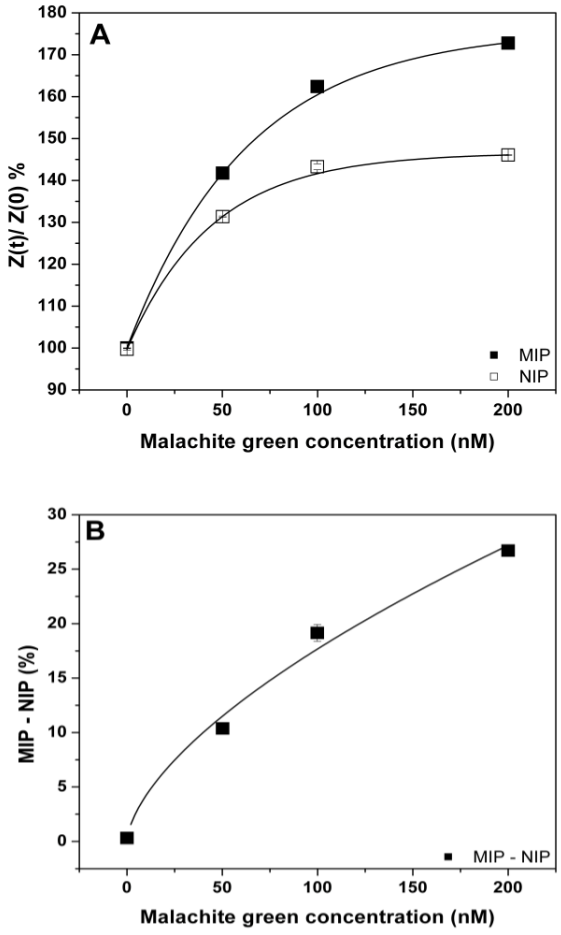

Figure 4.7 – A) Dose response curves for the impedance meausuments of both the MIP and NIP exposed to increasing concentrations of MG (MIP: solid squares; NIP: open squares. B) Difference between the MIP and NIP exposed to increasing concentrations of MG.

From the impedance measurements it is found that the MIP-channel shows a 73 % response at a concentration of 200 nM MG. At higher concentrations the sensor will reach its saturation level. The NIP channel, which measures non-specific binding of MG molecules to the sensor surface, shows a response of 46 % to a concentration of 200 nM. The amount of aspecific binding in these experiments is larger than was found for the QCM measurements as a result of the fact that the impedance measurements had to be performed at a higher pH value. To visualize only the specific binding, also in this case the MIP response can be subtracted from the NIP response (Figure 4.7b). From this graph it is clear that impedance sensor extends the available concentration range for measurements considerably, allowing an additional dynamic measuring range from 0 nM to 200 nM.

4.1 Conclusion

A series of MIPs with high affinity towards MG has been synthesized for sensor applications. Special attention has been paid to obtain MIPs with a spherical morphology. For sensor operations, also the binding behavior of the MIPs as compared to the NIPs is very important. Therefore, each MIP/NIP couple has been screened with batch rebinding experiments and the most suitable MIP/NIP combination has subsequently been incorporated into two sensing platforms, *i.e.* QCM and impedimetric detection. It has been demonstrated that QCM can detect MG in the range of 200 nM to 1000 nM, whereas impedimetric detection allows for the detection of MG in a range of 0 nM to 200nM. The limit of detection is expected to be in the same order of magnitude as currently used more laborious analytical liquid chromatography procedures to measure the MG concentration in food samples. It can be anticipated that further optimization of the spherical MIP morphology with respect to size and composition, will lead to additional improvements in the binding characteristics, thus further lowering the limit of detection. As a result of the optimized morphology, a better and more uniform imprint effect has been observed for the obtained polymer beads. In addition, the application of the MIP beads on the surface using matrix entrapment, as compared to the immobilization of crushed monoliths, considerably improves

the reproducibility of the sensor manufacturing and operation. In conclusion, it has been demonstrated that using spherical MIPs, a more stable and reproducible MIP based sensor can be obtained, which can be utilized to detect MG over a wide concentration range.

5 Detection of L-nicotine with dissipation mode quartz crystal microbalance using molecular imprinted polymers

5.1 Introduction

In this work a quartz crystal microbalance (QCM) setup was used for the detection of L-nicotine to evaluate its performance in comparison with L-nicotine MIPs measured earlier with impedance spectroscopy by Thoelen *et al*. (48). The advantage of the QCM sensing platform is that it can be used in a variety of ways, be it fast sensing or a way to test the characteristics of the MIP. QCM applies the piezoelectric ability of quartz to sense an increase or decrease of mass on the surface of the quartz crystal. This mass change will cause the resonance frequency to change in a proportional way. This relationship is described in the Sauerbrey equation (97). With the QCM-D setup it is also possible to measure the dissipation (128–131). Changes in dissipation relate to the loss of energy of quartz crystal after addition of mass. The MIP particles are immobilized on the crystal via a transducer layer, which consists of polyvinyl chloride (PVC). Measurements are performed in demineralised water and phosphate buffer saline (PBS). The fluid environment in which the measurements are performed will influence the ability of the MIP to capture the molecule and finally influence the efficiency of the sensor. This is important when using "body liquids" and "environmental samples", because an optimal medium to measure in is required. In this work, the effect of the pH value and ionic strength on molecular recognition is investigated.

5.2 Materials and methods

5.2.1 Reagents

The imprinted polymer was synthesized using ethylene glycol dimethacrylate (EGDM) as the cross-linker, methacrylic acid (MAA) as functional monomer and hexane as the porogen. Prior to polymerization, the stabilizers in the MAA and EGDM were removed. For the initiator, azobisisobutyronile (AIBN) was used. All chemicals used in the polymerization were of analytical grade and were obtained from various commercial sources. The target molecule L-nicotine, $C_{10}H_{14}N_2$ (MW: 162.23 DA) was obtained from Acros. A similar molecule, L-cotinine, $C_{10}H_{12}N_2O$ (MW: 172.22 Da), which was obtained from Sigma-Aldrich, was used to test the specificity. Cotinine is a by-product of the human metabolism of L-nicotine. PVC was purchased from Sigma-Aldrich. The MIP and the NIP were prepared as described in section 2.1.1.3.

5.2.2 Equipment

The binding constants and quality of the molecularly imprinted polymer were evaluated with UV-Vis spectroscopy using a NanoDrop 2000c UV-Vis NIR spectrophotometer from Thermo Scientific, Waltham, Massachusetts (Figure 5.1). The advantage of the UV-Vis spectrophotometer in comparison with other UV-Vis spectrophotometers the sample amount is greatly reduced to a few µl. This is very helpful when sample volume is limited.

Figure 5.1 NanoDrop 2000c UV-Vis NIR spectrophotometer. (www.bioresearchonline.com)

The morphology of the sensor surface was studied by optical microscopy with a Zeiss axiovert 40 MAT. Microscope images were processed using the

image analysis program ImageJ 1.37v (Wayne Rasband from the Research Services Branch, National Institute of Mental Health, Bethesda, Maryland, USA). Quartz crystals (5 MHz) with Cr/Au electrodes were purchased from Lot-Oriel. The QCM (Q-sense E4) was also purchased from Lot-Oriel. A flow setup was connected to a peristaltic pump (IPC-N) from Ismatec.

5.2.3 Sensing system

The QCM crystals were prepared as described in section 2.1.4.2. The surface coverage was assessed with light microscopy and the images were processed with the aid of ImageJ. An average surface coverage of 19.4% for the MIP and 20.2% for the NIP was found (Figure 5.2). This is consistent with the surface coverage reported by Thoelen et al. (48). QCM measurements were performed as follows. First of all, the system was left to stabilize in the fluid (deionized water or PBS) in which the performance of the MIP was to be tested. The stabilization was performed at a temperature of 22°C with a flow rate of 200 µl/min. After the signal was stable different concentrations were consecutively introduced to the flow system without rinsing in between samples. This results in a dose-response curve for the frequency and dissipation of the QCM-D system. The frequency noise was on average 0.835 Hz and the dissipation noise was on average 0.426×10^{-6}.

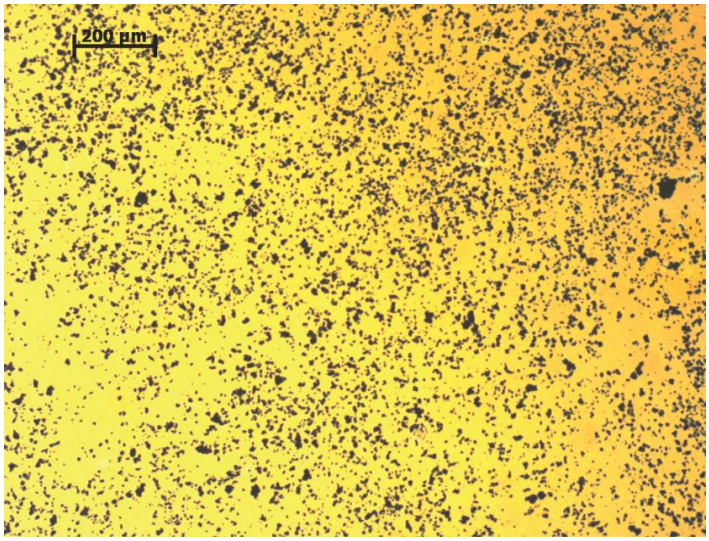

Figure 5.2 - Optical microscopy image illustrating the surface coverage of MIPs (black areas) on a PVC-covered quartz crystal (light area).

5.3 Results and discussion

5.3.1 Batch rebinding experiments

To characterize the binding characteristics for the MIP and NIP in deionized water and PBS with varying pH values, batch rebinding experiments were performed. To achieve this, 20 mg of MIP or NIP was added to 5 ml of water (or PBS) with different pH values and different L-nicotine concentrations. These mixtures were shaken for 3 hours on a rocking table at room temperature. Afterwards the mixtures were filtered using syringe filters (1 µM) in order to remove the MIP and NIP particles. The concentration of L-nicotine left over in the fluid (C_f) is measured *via* UV-Vis spectroscopy. With this information the amount of L-nicotine bound per gram (S_b) of MIP/NIP can be calculated and binding isotherms for MIP and NIP for deionized water and PBS can be made. From these experiments it is apparent that in deionized water the MIP binds L-nicotine very well in comparison with the NIP (Figure 5.3). Fits in Figures 65 – 67 are achieved with Freundlich

isotherms (section 2.2.1). The difference in binding capacity proves that this MIP/NIP is a very good candidate for use in sensing applications as the difference at low concentrations between MIP and NIP is significant. It is also clear that a difference in pH value range pH 5 and pH 9 does not affect the binding ability of the MIP or NIP significantly.

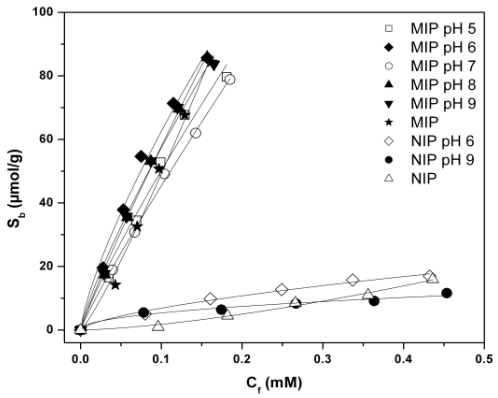

Figure 5.3 - UV-Vis spectroscopy of L-nicotine in demi water at varying pH values for MIP and NIP (pH value was altered with NaOH or HCl except for the MIP and NIP without pH notation).

Table 5-1 Fitting parameters and calculated total amount of binding sites and average affinity constant for MIPs and NIP in deionized water with varying pH values.

	R^2	A	v	N (µmol/g)	K (mM)-1
MIP pH 5	0.97	362.60	0.86	48.58	5.68
MIP pH 6	0.98	360.26	0.76	76.03	6.59
MIP pH 7	0.99	363.89	0.90	33.84	5.32
MIP pH 8	0.99	460.15	0.90	44.30	5.34
MIP pH 9	0.99	376.77	0.82	63.63	6.04
NIP pH 5	0.98	30.32	0.64	8.24	7.92
NIP pH 9	0.91	15.66	0.47	4.37	10.60

The Fits from Figure 5.3 are presented in Table 5-1. The fits presented again clearly show the difference between MIP and NIP. The main difference between MIP and NIP is the amount of binding places (N) available.

In PBS the amount of bound L-nicotine is significantly reduced in comparison to deionized water (Figure 5.4).

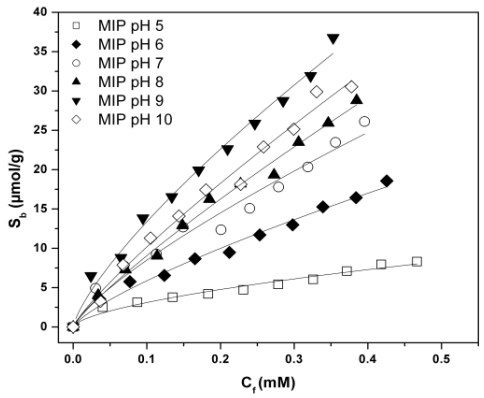

Figure 5.4 - UV-Vis spectroscopy of L-nicotine in PBS with varying pH values for MIP.

This is probably a result of the presence of ions in PBS. In PBS the pH value plays a more important role in the binding ability. This is due to protonation and deprotonation of L-nicotine and the functional monomer MAA respectively (132,133). A more acidic PBS gives the least amount of binding. PBS at pH value of pH 5 binds as much L-nicotine as the NIP does at pH value pH 10. The more basic the PBS is, the higher the amount of bound L-nicotine until it reaches its optimal pH value of pH 9. Similar results with NIP in deionized water were observed where the NIP does not bind much L-nicotine and the effect of pH value on the amount of bound L-nicotine is significantly diminished (Figure 5.5).

Table 5-2 Fitting parameters and calculated total amount of binding sites (N) and average affinity constant (K) for MIP in PBS with varying pH values.

	R^2	A	v	N (µmol/g)	Kn (mM)-1
MIP pH 5	0.96	12.80	0.61	3.59	8.31
MIP pH 6	0.98	34.29	0.77	7.10	6.54
MIP pH 7	0.96	50.13	0.77	10.22	6.49
MIP pH 8	0.99	63.19	0.84	9.31	5.81
MIP pH 9	0.99	76.52	0.76	16.31	6.62
MIP pH 10	0.98	71.10	0.84	10.41	5.80

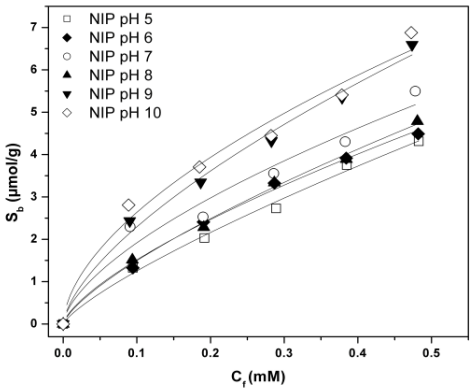

Figure 5.5 - UV-Vis spectroscopy of L-nicotine in PBS water at varying pH values for NIP.

Table 5-3 Fitting parameters and calculated total amount of binding sites (N) and average affinity constant (K) for NIP in PBS with varying pH.

	R^2	A	v	N (µmol/g)	Kn (mM)-1
NIP pH 5	0.99	7.67	0.79	1.47	6.32
NIP pH 6	0.99	7.64	0.70	1.88	7.21
NIP pH 7	0.92	8.27	0.64	2.27	8.03
NIP pH 8	0.99	8.07	0.73	1.85	6.89
NIP pH 9	0.98	10.37	0.65	2.77	7.78
NIP pH 10	0.95	9.97	0.58	2.87	8.81

The Fits for the MIP and NIP measured in PBS are presented in Table 5-2 and Table 5-3. From these fits it also clear that the main difference between MIP and NIP are the available binding sites (N).

The experimental results from Figure 5.4 suggest that in PBS, the most L-nicotine MIP binding occurs at pH value of pH 9. A theoretical model was used to verify the optimal pH value for L-nicotine binding to the MIP (133). The theoretical model was calculated for a pH value range of 1 to 14 using the prevalence of protonated and unprotonated states of the functional monomer MAA (pK_A 6.5) and the prevalence of the diprotonated, monoprotonated and unprotonated states of L-nicotine (pK_A 3.5 for Diprotonated and monoprotonated states and pK_A 8.5 for monoprotonated and unprotonated states (134)). The formula used for the calculation is the Henderson-Hasselbalch equation (equation 6.1).

$$pKa = pH + \log(\frac{[HA]}{[A^-]}) \quad 6\text{-}1$$

The concentration of A^- can be calculated using the pH equation as $[H^+]$ equals $[A^-]$.

$$pH = -\log([H^+]) \quad 6\text{-}2$$

Once $[A^-]$ is known, [HA] can be calculated using equation 6-1 and then the ratios of [HA] and $[A^-]$ can be calculated. Knowing the prevalence of the states of L-nicotine and MAA enables the calculation of the probability of all binding complexes which are formed via hydrogen bonding. In Figure 5.6 the probability of L-nicotine binding to the MIP per pH value is presented. The theoretical model suggests that the optimal pH value for binding is between pH 7.5 and pH 8. This theoretical result differs slightly from the optimal pH value measured using UV-Vis spectroscopy. Both results do suggest that L-nicotine binding to the MIP is favorable in the neutral to basic part of the pH value range.

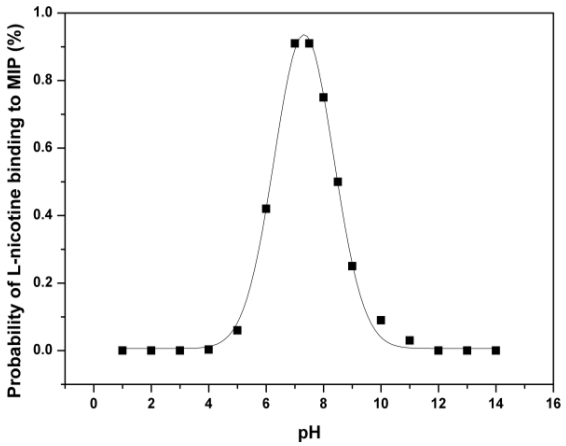

Figure 5.6 - The theoretical probability of L-nicotine binding to the MIP at different pH values assuming the pK_a values of 3.5 and 8.5.

5.3.2 QCM in water

As mentioned before, the actual sensing system is a QCM-D, which works on the principle that an increase of mass on the sensor surface will induce a shift in the resonance frequency, which is proportional to the added mass. In addition, dissipation shifts or loss of energy can be measured. This damping of the oscillating crystal can thus also indicate changes at the sensing surface. The frequency and dissipation changes are measured simultaneously in function of time. In Figure 5.7, an example is shown of a typical frequency and dissipation shift due to binding of L-nicotine to MIP and NIP. It is clearly demonstrated that the MIP has a larger frequency and dissipation shift due to a greater binding capacity of L-nicotine than the NIP. Although the relationship between added mass and frequency shifts is according to the Sauerbrey equation a linear relationship, the non-linear relation between addition of soft material and dissipation shifts can be used as a sensing method.

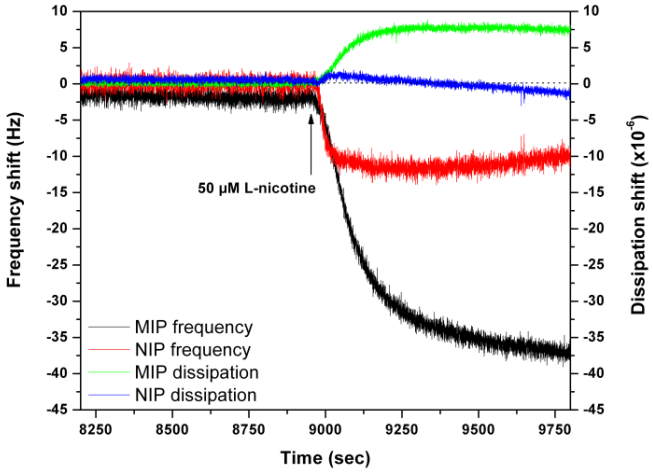

Figure 5.7 - Frequency and dissipation shift vs time for 50 µM L-nicotine addition measured in deionized water.

The relationship between frequency shift and dissipation shift are shown in Figure 5.8. For the MIP, the dissipation shift has a linear relationship with the frequency shift, indicating that the relationship between added mass and dissipation change is also linear. This relationship is not present for the NIP, which could indicate that, as anticipated, the binding of L-nicotine to the NIP happens in a different way and is not just a difference in binding capacity.

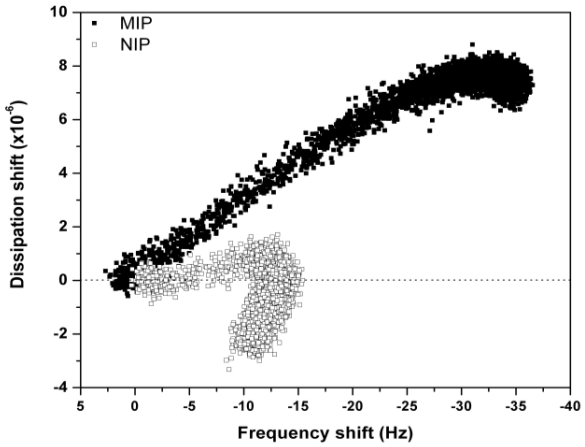

Figure 5.8 - The relationship between frequency and dissipation for an addition of 50 μM L-nicotine measured in deionized water (data show from addition of L-nicotine and 750 s later).

Another advantage of the use of MIPs is the reversibility of L-nicotine binding, which is useful for repeated uses of the same sensor. This reversibility is shown in Figure 5.9.

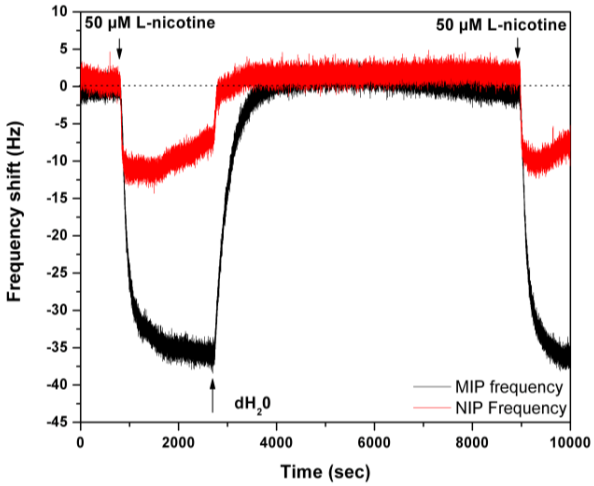

Figure 5.9 - MIP and NIP frequency response shifts illustrating the reusability of the sensor by consecutive additions of L-nicotine with an intermediate washing step.

In Figure 5.9 it can be seen that the frequency drops after the first 50 µM addition of L-nicotine and then rises during the washing step with demineralized water. During the second addition of 50 µM L-nicotine, the frequency drops once again by the same amplitude thereby confirming the reproducibility and reusability of the sensor. This happens for both the MIP and the NIP with a distinct difference in the changed amplitude.

The prepared MIP and NIP crystals were exposed to different L-nicotine concentrations in deionized water (12.5 – 150 µM). The pH value of the deionized water was unaltered because the UV-Vis spectroscopy showed that changing the pH value did not affect the binding capacity of the MIP. In Figure 5.10 it is clear from the frequency change that the MIP binds much more L-nicotine than the NIP.

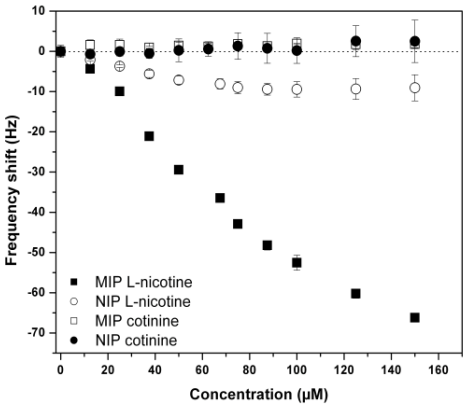

Figure 5.10 - QCM-based dose response curve of the frequency change for L-nicotine and cotinine with L-nicotine MIP and NIPs in water.

On average over all concentrations, the MIP binds almost five times better than the NIP. At higher concentrations the response of the MIP is lower, meaning that the MIP is becoming saturated. This is also apparent from the NIP as the only frequency shift occurs at lower concentrations, whereas at higher concentrations there is no further response. As a control reference for specificity testing, cotinine is also measured under the same concentrations

and conditions (Figure 5.10). It is evident that neither MIP nor NIP binds any cotinine. As can be seen Figure 5.11, also the dissipation changes indicate that the MIP binds L-nicotine more than the NIP.

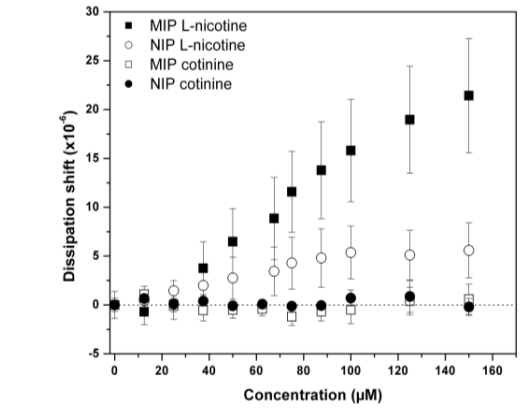

Figure 5.11 - QCM-based dose response curve of the dissipation change observed with L-nicotine and cotinine in water.

The difference between the dissipation of MIP and NIP is less obvious in comparison to the frequency shift. The Difference in dissipation effect between MIP and NIP on average is only 2.13 times larger for the MIP. Notwithstanding, also from these results it is evident that cotinine does not bind to the MIP or NIP (Figure 5.11).

5.3.3 QCM in PBS

From the UV-Vis spectroscopy results in PBS it is empirically clear that binding of L-nicotine to the MIP is optimal at pH value of pH 9 and that ions present in the fluid inhibit interactions between the MIP and L-nicotine. To see how much this ionic content influences the binding, L-nicotine concentrations were measured in different PBS dilutions (1x -, 0.5x - and 0.1x PBS). Each PBS buffer at a different concentration was adjusted to the optimal pH value of pH 9 with the aid of NaOH. For these measurements, a

higher concentration range was chosen (100 – 500 µM) to give a clear view on the difference of recognition between the buffers.

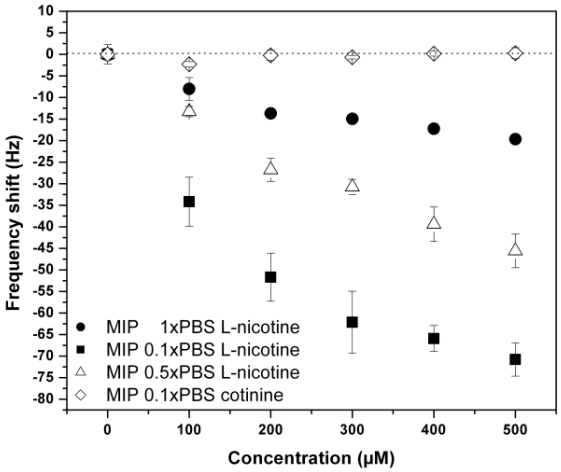

Figure 5.12 - QCM-based dose response curve (MIPs) of the frequency change for L-nicotine in PBS at pH value of pH 9 with varying ionic strengths. As a control, also data for cotinine in 0.1xPBS at pH value of pH 9 are presented, showing that the MIPs have no affinity for this competitor molecule.

The frequency response between the differential diluted buffers with the MIP is very distinct (Figure 5.12). The 0.1x PBS has the best response due to the lowest ionic strength followed by 0.5x PBS and 1x PBS the latter giving the least response. The same trend is also observed for the NIP samples, However the response is much lower in comparison with the MIP (Figure 5.13). Taking into account both the MIP and NIP, recognition in 0.1x PBS is 3.3 times more effective than 1x PBS and 1.71 times better than 0.5x PBS. Also for these experiments, cotinine was used as a control reference for specificity testing with the same conditions and concentrations. As can be seen in both Figure 5.12 and Figure 5.13, neither the MIP nor the NIP show any binding affinity to cotinine.

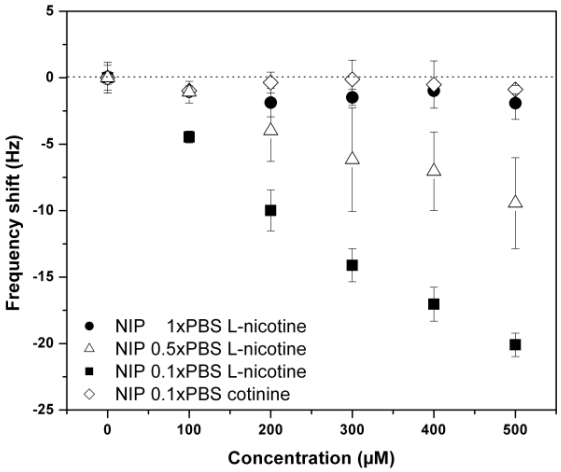

Figure 5.13 - QCM-based dose response curve (NIPs) of the frequency change for L-nicotine in PBS at pH value of pH 9 with varying ionic strengths. As a control, affinity for cotinine in 0.1xPBS at pH value of pH 9 is presented and indistinguishable for a zero response.

The dissipation has the same trend as the frequency response except that the difference between 0.1x and 0.5x PBS is less pronounced with the NIP samples (Figure 5.14 and Figure 5.15). Looking at the differential signal of MIP and NIP, recognition in 0.1x PBS is 4.5 times better than 1x PBS and 2.07 times better than 0.5x PBS. The dissipation does not change with the addition of cotinine (Figure 5.14 and Figure 5.15) thereby proving the specificity of the MIPs for L-nicotine. From these results it is evident that the optimal fluid for measuring the recognition of L-nicotine is 0.1x PBS at a pH value of pH 9. In order the compare the results with recognition in deionized water, the same L-nicotine concentration range was measured in 0.1x PBS at pH value of pH 9. For the same concentrations of L-nicotine the frequency response in deionized water (Figure 5.10) on average is 2.1 times bigger than in 0.1x PBS at pH value of pH 9 (Figure 5.16). This lowered response is again due to the presence of ions in the PBS. On the other hand, there is no difference in the dissipation response as water (Figure 5.11) causes almost the same response (96 %) as 0.1x PBS at pH value of pH 9 (Figure 5.17).

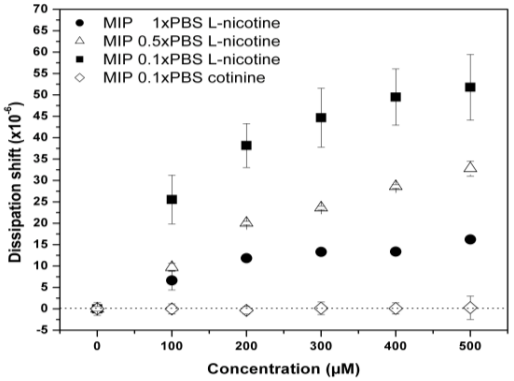

Figure 5.14 - QCM-based dose response curve (MIPs) of the dissipation change for L-nicotin in PBS at pH value of pH 9 with varying ionic strengths. As a control, affinity data for cotinine in 0.1xPBS at pH value of pH 9 is presented and has no binding affinity with the MIP.

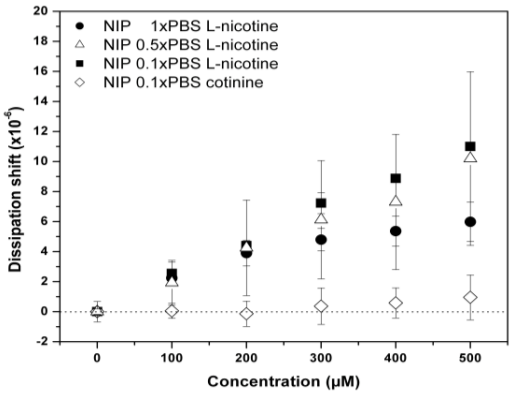

Figure 5.15 - QCM-based dose response curve (NIPs) of the dissipation change for l-nicotine in PBS at pH value of pH 9 with varying ionic strengths. Cotinine measured in 0.1xPBS at pH value of pH 9 does not show any significant binding affinity to the NIP.

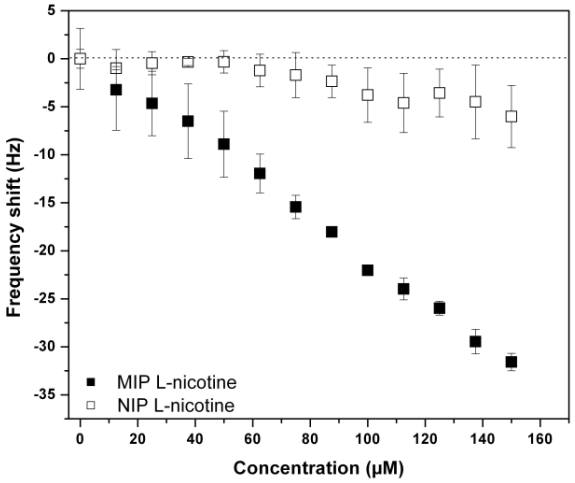

Figure 5.16 - QCM-based dose response curve of the frequency change for l-nicotine in 0.1x PBS at pH value of pH 9.

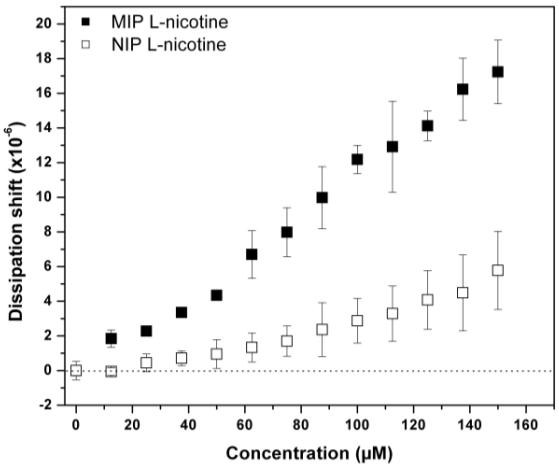

Figure 5.17 - QCM-based dose response curve of the dissipation change for l-nicotine in 0.1x PBS at pH value of pH 9.

5.4 Conclusion

MIPs for the detection of L-nicotine were successfully developed *via* bulk polymerization. UV-Vis spectroscopy proved the effectiveness of the MIP/NIP in deionized water and showed that the pH value has little to no effect on recognition. UV-Vis spectroscopy was also utilized to examine the effect of pH value in 1x PBS buffer. In PBS the pH value plays a much larger role in the binding capacity of the MIP. It was shown that a pH value of pH 9 was optimal for maximum binding in 1x PBS. QCM-D proved to be a fast, sensitive, specific and reproducible sensing platform. The best performance was achieved in deionized water. As seen in both the frequency and dissipation change the sensor was the most sensitive in the 12,5 – 50 µM concentration of L-nicotine region. At higher concentrations the sensor began to be saturated. The underlying principle behind the dissipation changes due to L-nicotine binding to the MIP is unknown, however, it has been empirically demonstrated that dissipation changes are a reliable detection method. Cotinine was used as a control for the specificity of the MIP. It showed no response in the frequency nor in the dissipation. QCM-D was also used to test the influence of the ionic strength of PBS. Here it was found that a higher ionic strength is detrimental for the binding of L-nicotine. The optimal buffer fluid to use as a medium for measuring was 0.1x PBS at pH value of pH 9. The reason for using 0.1x PBS is the need for a good medium to perform measurements on "real life" samples without losing the buffering capabilities and maintaining a high sensitivity for L-nicotine.

6 MIP-based QCM-D sensor platform for the detection of L-nicotine in saliva and urine samples

6.1 Introduction

In this work, a MIP was created for the detection of L-nicotine in aqueous media including urine and saliva. L-nicotine is the major addictive substance found in tobacco and is taken up in the human body through smoking, chewing or sniffing tobacco, consuming nicotine gums and tablets, nicotine patches and inhalers (135). Besides L-nicotine, tobacco smoke contains more than 4000 compounds of which more than 50 are carcinogenic (83). It has been proven that tobacco consumption causes a higher risk for the development of cancer in the lungs and respiratory tract (84,85) and diseases such as pulmonary disease (86), atherosclerosis (87), and periodontal disease (88). The presence of L-nicotine can be determined in various samples such as urine, hair, breast milk, plasma, and saliva (89). The detection of L-nicotine is preferably done in a non-invasive way with easily obtained samples. Saliva is simply collected from test persons and, shortly after consumption of products containing L-nicotine, the concentration of L-nicotine is higher than the cotinine concentration [38]. It is important to measure the L-nicotine concentrations in their natural matrix as this will give the most accurate result. Detection in saliva has been established with several methods such as liquid-phase microextraction and high performance liquid chromatography coupled with UV-Vis detection (89). The analysis of L-nicotine and its oxidation products in nicotine chewing gum has been reported with molecularly imprinted solid phase extraction, however, these tests were not yet performed in saliva (136). The detection techniques used so far are complex, time consuming, and require trained personal, which makes them disadvantageous. Quartz crystal microbalance-Dissipation (QCM-D) provides a fast, easy and reliable testing platform for the use of MIPs in in combination with body fluids. MIPs are immobilized on

the quartz crystal via a polyvinyl chloride (PVC) adhesion layer. When L-nicotine binds to the MIP, the eigenfrequency of the quartz crystals will shift according to the added mass as described by the Sauerbrey equation (97). Binding of the template can also cause shifts in the dissipation of the functionalized quartz crystal. This shift is measured after every excitation and is an indication for the loss of vibrational energy. These changes are due to conformational and viscoelastic changes at the surface and can serve also as an additional read-out technique (49,128). In previous work, the binding capacities of the MIP were already studied in L-nicotine spiked deionized water (dH2O) and PBS using the QCM-D setup, showing specific binding of the target in both fluids (49). In this contribution, the MIPs' efficiency to bind L-nicotine in more complex fluids was tested with saliva- and urine samples. As a start, the saliva and urine samples were spiked with L-nicotine and subsequently diluted with dH2O or PBS. For further validation of the sensor, a test person was instructed to chew nicotine chewing gums with a concentration of 2 or 4 mg L-nicotine to obtain saliva samples with different concentrations. As a second trial, a test person was instructed to consume smokeless tobacco. These saliva samples were tested with the MIP sensor to investigate whether the L-nicotine can be detected in these matrices. The various tests demonstrate the practicality, specificity, and sensitivity of the MIP-based QCM-D sensor platform for these analytical tasks.

6.2 Materials and methods

6.2.1 Reagents

The molecularly imprinted polymer was synthesized using ethylene glycol dimethacrylate (EGDM) as the cross-linker, methacrylic acid (MAA) as functional monomer and hexane as the porogen. Prior to polymerization, the stabilizers in the MAA and EGDM were removed by passing through an alumina column. For the initiator, azobisisobutyronile (AIBN) was used. All chemicals employed in the polymerization were of analytical grade and obtained from various commercial sources. The PVC adhesive was purchased

from Sigma-Aldrich NV/SA, Bornem, Belgium. The target molecule L-nicotine, $C_{10}H_{14}N_2$ (MW: 162.23 Da) was obtained from Acros Organics, Geel, Belgium. The nicotine chewing gums (Nicorette®, Johnson & Johnson NV, Beerse, Belgium) were used in concentrations of 2 mg and 4 mg L-nicotine per tablet while also nicotine-free 'taste samples' of the Nicorette® gums were employed for reference purposes. The smokeless tobacco was SKOAL® Wintergreen Longcut, Stamford, Connecticut USA.

6.2.2 Equipment

The morphology of the sensor surface was studied by optical microscopy with a Zeiss Axiovert 40 MAT (Carl Zeiss, Jena, Germany). Microscope images were processed using the image analysis program ImageJ 1.37v (Wayne Rasband the National Institute of Health, Bethesda, USA). Quartz crystals (5 MHz) with Cr/Au electrodes were purchased from LOT-Oriel (Darmstadt, Germany). The QCM system (Q-sense E4) was also purchased from Lot-Oriel, (manufacturer Q-Sense, Gothenburg, Sweden). A flow setup was established with a peristaltic pump (IPC-N) from Ismatec.

6.2.3 MIP synthesis

For the preparation of the L-nicotine MIP, a mixture of MAA (12.5 mmol), EGDM (25.5 mmol) and AIBN (0.66 mmol) was dissolved in 7 ml hexane together with the template molecule L-nicotine (6.41 mmol). To exclude oxygen in the mixture, it was degassed for 10 min with N_2. Subsequently for polymerization, the solution was sealed and kept in a thermostatic water bath at 60°C (72 h). After polymerization, the solid MIP was grounded with a mechanical mortar (24 h) and passed through a 25 µm sieve. Only particles with a size smaller than 25 µm were used. Subsequently, the L-nicotine was extracted from the MIP powder by extensive washing with methanol (48 h), followed by a mixture of acetic acid/acetonitrile (1/1) (48 h) and finally again with methanol (12 h) using a continuous extraction setup. A non-imprinted polymer (NIP) was synthesized as a reference material in the same way, however, without the presence of the target molecule.

6.2.4 Sensing system

The QCM crystals have a resonance frequency of 5 MHz and are modified with Cr/Au electrodes. The Q-sense E4 system allows for simultaneous measurements of up to 4 crystals. The system is temperature controlled and was kept at 22.00 ± 0.01 °C throughout the measurements. On the top electrode a layer of PVC (PVC 0.35 wt % in tetrahydrofuran) was spincoated (5000 rpm with 990 rpm/s) to obtain a layer of 100 nm thickness. The MIP was then applied onto the surface using a poly(dimethylsiloxane) (PDMS) stamp, which was pressed against the active sensing surface. This resulted in a thin layer of MIPs on the surface. Subsequently, the PVC was heated to 120°C for 15 min. As this temperature is well above the glass transition temperature of 80°C, the MIP particles partially sink into the polymer layer. The samples were then cooled and the excessive MIP powder was rinsed off with deionized water. QCM measurements were performed as follows: First, the system was left to stabilize in the fluid (dH_2O or 0.1 x PBS at pH value of pH 9) in which the performance of the MIP was to be tested. This was with a flow of 200 µl/min. After the signal was stable, L-nicotine spiked saliva or urine samples were diluted with the measuring fluid (dH_2O or PBS) to achieve various concentrations that were then consecutively connected to the flow system starting with the lowest concentration while keeping the flow rate constant. This results in a dose-response curve for the frequency and dissipation of the QCM-D system. The frequency noise was 0 ± 0.84 Hz on average while the noise on the dissipation signal was 0 ± 0.43 x 10^{-6} on average. All measurements were performed 6 times per concentration in dH_2O or 0.1 x PBS with pH value of pH 9. In the results section, the average response per concentration is presented while the error bars correspond to the standard deviation.

6.2.5 Sample preparation

In Figure 6.1 the sample preparation protocol is schematically presented. In order to collect saliva a non-smoker test person was asked to deposit saliva in a sterilized Falcon tube every minute until the desired amount of 40 ml

was met. This saliva was immediately centrifuged for 10 min with 10.000 rpm at 8°C (a). The supernatant was collected (b) and filtered using 1 µm syringe filters (c). This resulting saliva sample was split in two parts. One part of the collected saliva was spiked with L-nicotine (100 mM) (d) while the other half was unaltered (e) serving as a control fluid. The same procedure was used on urine samples. Fluids were stored at -18°C to prevent degradation. For measurement purposes, the L-nicotine spiked saliva- and urine samples were diluted from the stock solution to the desired concentrations using dH2O or PBS. These are indicated as "spiked with L-nicotine" in the resulting graphs. For example, a nicotine concentration of 100 µM was obtained by diluting 20 µl of the 100 mM stock solution (volume measured with a micropipette, precision < 0.5 µl) with dH2O or PBS to a final volume of 20 ml. The non-spiked saliva and urine sample volumes used are the same as the volumes of the L-nicotine spiked samples used to create the corresponding concentration. These are indicated as "without L-nicotine" in the resulting graphs.

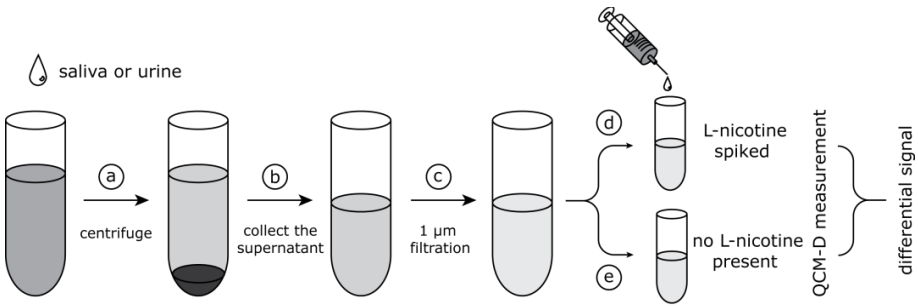

Figure 6.1 - Sample preparation. The collected non-smoker saliva or urine sample is first centrifuged at 10.000 rpm for 10 min (a), the supernatant is collected (b) and filtered (c). One half is spiked with L-nicotine (d) while the other half is not altered (e).

6.3 Results

An average surface coverage of the QCM crystals was 19.4% for the MIP- and 20.2 % for the NIP powders, which is consistent with previously reported surface-coverage values (48). All shown QCM-D results (except for the raw data in Figure 6.2 A) are corrected for non-specific binding, by subtracting the non-specific NIP response from the MIP response. The NIP-channel serves as a control and will show the non-specific binding, while the MIP represents the specific binding of L-nicotine on top of non-specific events. By subtracting the NIP- from the MIP response, the specific binding of the L-nicotine is obtained, which gives a direct insight in the performance of the sensor.

6.3.1 L-nicotine detection in saliva

The saliva was collected according to section 2.5. One part was spiked with L-nicotine (100 mM) and subsequently diluted with dH_2O or 0.1 x PBS at pH value of pH 9 to obtain the required concentrations. The other part remained unaltered and served as a control. The results of these measurements are shown in Figure 6.2.

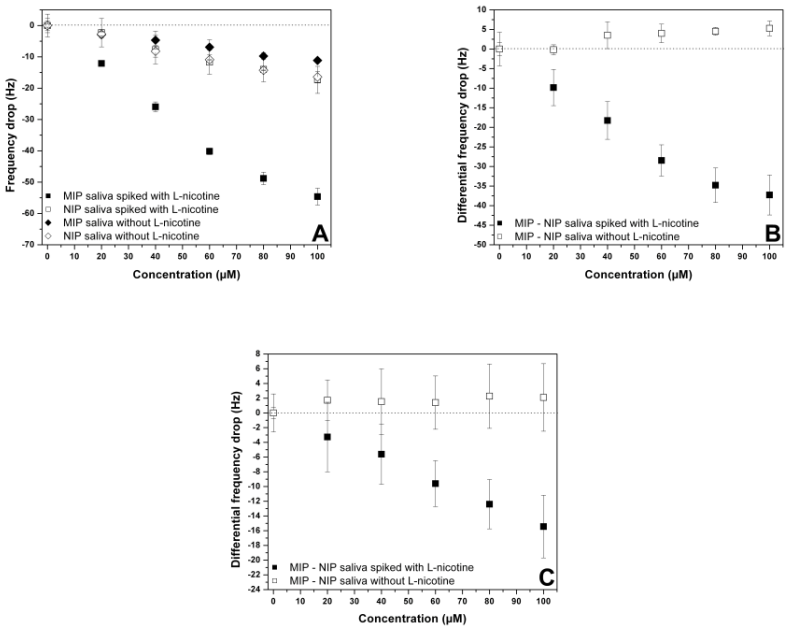

Figure 6.2 A) shows the dose-response curve for the saliva samples spiked with L-nicotine: the spiked saliva was diluted with dH_2O to obtain the required concentrations. Data for the MIP are given as solid squares while the NIP data are presented by open squares. The same measurements, however with non-spiked saliva, are presented as solid diamonds (MIP) and open diamonds (NIP). B) Figure 6.2 B displays the differential MIP – NIP signal for spiked- (solid squares) and non-spiked saliva samples (open squares), diluted in dH_2O C) Figure 6.2 C shows the differential MIP - NIP signal when the spiked- (solid squares) and non-spiked saliva samples (open squares) were diluted in 0.1 x PBS at pH value of pH 9.

As can be seen in Figure 6.2 A, the MIP and NIP gave no significant frequency response with non-spiked saliva of a non-smoking test person. This means that there is little tendency to bind other molecules than L-nicotine in saliva. With spiked saliva, the frequency drop for the MIP is significantly stronger than for the NIP, indicating specific binding of the L-nicotine. Figure 6.2 B shows the MIP - NIP difference signal between spiked-

and non-spiked saliva. With spiked saliva, the frequency drops in a sub-linear way with increasing concentration. A spiked concentration of 10 µM L-nicotine results in a frequency shift of 10 Hz ± 4 Hz, while a spiked concentration of 100 µM L-nicotine causes a 37 Hz ± 5 Hz frequency drop. The saliva sample without L-nicotine does not show a frequency drop and stays stable, suggesting that non-specific binding to MIP and to NIP is comparable and weak. This means that the MIP is able to recognize and bind the L-nicotine present in the spiked saliva in a specific manner. While measuring the frequency change, the QCM-D simultaneously measures changes in the dissipation. The same experiment was also performed with saliva diluted in 0.1 x PBS at pH value of pH 9, as PBS mimics the ionic composition of body liquids. The pH value of pH 9 was used on purpose because earlier studies suggested that the employed MIP has an optimal binding capacity for L-nicotine at this pH value (see section 5.3.1).From Figure 6.2 C, it is clear that the sensitivity of the MIP decreases significantly in comparison to measurements in dH_2O. A concentration of 100 µM of L-nicotine results in a 15 Hz ± 4 Hz frequency drop in 0.1 x PBS at pH value of pH 9 while in dH_20 the frequency drop is 37 Hz ± 5 Hz. On average, the MIP is able to bind almost 3 times more L-nicotine from the same spiked saliva sample when measured in dH_2O than in 0.1 x PBS at pH value of pH 9. The lowered binding capacity of the MIP in 0.1 x PBS at pH value of pH 9 may be attributed to interfering ions in the electrolyte, which hinder the formation of hydrogen bridges between the MIPs and the L-nicotine molecules.

In Figure 6.3 the change in dissipation is shown for saliva spiked and non-spiked samples, which were diluted in dH_2O. It is apparent that only the L-nicotine spiked saliva samples resulted in changes in dissipation, again confirming that the MIP is able to bind L-nicotine specifically. The difference between the L-nicotine spiked sample and the non-spiked sample is less pronounced than the frequency changes documented in Figure 6.2 B, nevertheless a distinction can be made between the two. This proves that also dissipation measurements can serve for the detection of low molecular weight molecules in diluted body fluids. The dissipation is determined by the viscoelastic properties of the interface between the quartz crystal and the liquid under study. We point out that the increasing nicotine concentration

goes along with a larger portion of saliva diluted in dH_2O, leading by itself to a higher dissipation. However, the differential measurement shown in Figure 6.3 corrects for this viscoelastic response, proving that the recognition of nicotine alters the viscoelastic behavior of the MIP layer itself. To our knowledge, this observation has not been reported in prior literature.

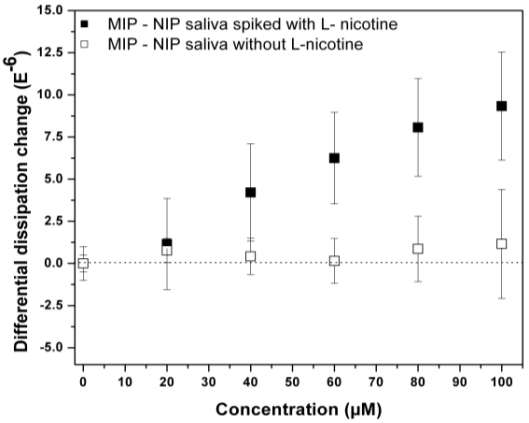

Figure 6.3 - Differential MIP - NIP dose-response curve of the dissipation signal for increasing concentrations of spiked L-nicotine saliva (solid squares) and non-spiked saliva (open squares). All measurements were performed on spiked- and non-spiked saliva samples diluted in dH_2O.

To further prove the ability of MIPs to bind L-nicotine specifically in complex matrices, the same tests were performed in urine. Urine was chosen because in smokers' urine there are still traces of L-nicotine present. In addition, urine is a complex matrix with a composition distinctly different from saliva. It should be noted that most of the L-nicotine is metabolized in the body to cotinine, which is excreted through urine (137). The MIP and NIP were previously tested for cross selectivity towards cotinine, which did indeed not show significant binding (49). Although the other molecules present in urine differ strongly from the ones present in saliva, the results obtained with urine samples are similar to the ones obtained with saliva. In Figure 6.4 the differential signal for the L-nicotine spiked urine and non-spiked urine are presented. A concentration of 10 µM L-nicotine results in a frequency shift of

31 Hz ± 1 Hz, while a concentration of 100 µM L-nicotine causes a 54 Hz ± 2 Hz frequency drop. It should be noted that the signal seems to saturate at a concentration of 60 µM. The L-nicotine spiked samples cause a stronger frequency change than the non-spiked urine sample indicating that L-nicotine is specifically bound to MIPs from the urine matrix. This proves that the MIP can specifically detect L-nicotine in at least two different diluted body fluids.

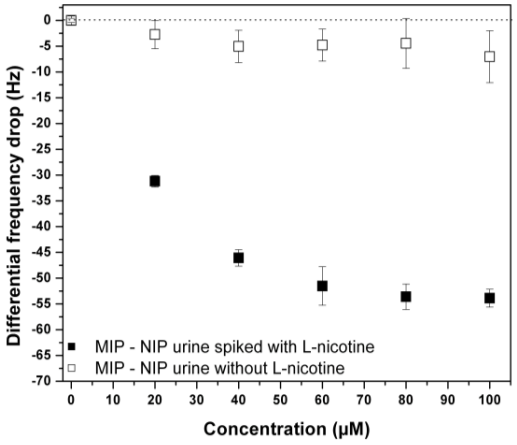

Figure 6.4 - Differential MIP - NIP dose-response curves for urine samples spiked with L-nicotine (solid squares) and non-spiked urine samples (open squares). The spiked- and non-spiked urine samples were diluted in dH_2O to obtain the indicated concentrations.

6.3.2 Detection of L-nicotine from saliva collected while chewing nicotine gums and smokeless tobacco

As a confirmation test for the selective and specific binding of L-nicotine from a complex matrix, the MIP sensor was applied to saliva samples collected while chewing nicotine gums with 2 mg and with 4 mg L-nicotine per tablet. The nicotine-free 'taste samples' of the Nicorette® gums were used for reference purposes, allowing correcting for a theoretical, non-

specific sensor response due to flavorings, colorants, and other additives. The test person chewed the nicotine gums for 60 minutes, meanwhile collecting saliva in a sterilized Falcon tube. Prior to collecting saliva, the test person had no intake of nicotine in any form for at least 24 hours in order to avoid possible offset effects. Additionally, saliva samples were obtained during the consumption of 2 grams of smokeless tobacco (SKOAL® Wintergreen) with a nominal nicotine content of 10 mg L-nicotine per gram as determined in prior literature (138). Saliva collection, centrifugation, filtration, and storage were handled in the same way as for all other saliva and urine samples (see Figure 6.1, except for the spiking in step D).

Figure 6.5 shows the differential frequency response (response of the MIP-loaded QCM minus the response of NIP-loaded QCM crystals) for the saliva samples obtained with 0 mg, 2 mg, and 4 mg Nicorette® tablets. For all experiments, 0.25 ml of saliva was diluted in 19.75 ml dH_2O to a total sample volume of 20 ml. Differential sensing is a necessity allowing to correct for non-specific adsorption effects inherent to the complex mixture of proteins and enzymes in saliva and additives of the Nicorette® tablets. All measurements were performed 6 times and averaged while the error bars represent the scattering of the data. As expected, the strongest signal change is found with the 4 mg samples (21 Hz ± 3 Hz), it is weaker for the samples obtained with 2 mg tablets (14.5 Hz ± 1.5 Hz) and with the nicotine-free testing tablet we measured a signal change of 1 Hz ± 1 Hz. Within the experimental resolution, this corresponds to the complete absence of a recognition effect. Note that the 4 mg samples do not result in twice the response observed with the 2 mg tablets because the dose-response curves are sub-linear and consuming tablets with higher nicotine concentration stimulates a stronger release of saliva, resulting in dilution. In the sense of the dose-response curve shown in Figure 6.2 B, the frequency drop of 21 Hz observed with the 4 mg tablet would correspond to a concentration in the range of 40 µM. Assuming that all nicotine from the tablet (4 mg, molecular weight 162.23 g/mol) is transferred to saliva (volume of approximately 10 ml after centrifugation), we expect a nicotine concentration of 2.5 mM in the actual saliva sample. Keeping in mind that these samples were diluted 80 times (0.25 ml of saliva in 19.75 ml dH_2O) we

end up with a final concentration of about 30 µM. Within the error bars, this is in reasonable agreement with the expected value of 40 µM from the dose-response curve.

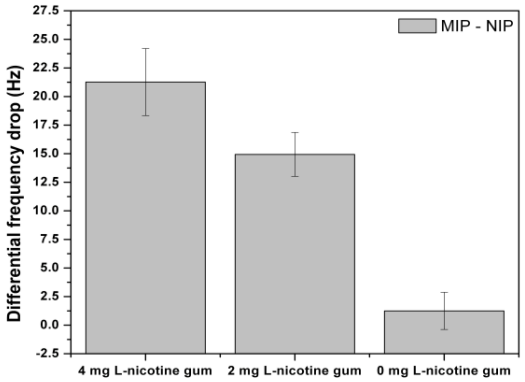

Figure 6.5 - Differential frequency response of the QCM-D for saliva samples of 4 mg nicotine gum, 2 mg nicotine gum and 0 mg nicotine gum. Measurements were performed in dH2O.

Finally, we evaluated whether it is possible to define a sensor base-line in case that neither nicotine-free tablets nor nicotine-free saliva are available as reference materials. For these experiments, two 5 mL samples of diluted saliva (dilution as described above) from the '4 mg nicotine batch' were extracted using either 20 mg of MIP powder or 20 mg of NIP powder. This procedure is schematically illustrated in Figure 6.6 A, B. The extraction treatment was performed for 120 minutes at room temperature on a rocking table followed by filtering and collecting the supernatant. In addition to the extraction of proteins and enzymes, which is already achieved by the NIP powder, the MIP powder will also extract the nicotine present in the diluted saliva sample. It is shown in Figure 6.6 C that the NIP-extraction has only a minor influence on the sensor response when compared to the non-extracted samples in Figure 6.5. On the other hand, Figure 6.6 C demonstrates that extraction with MIP powder removes all nicotine and, within error bars, the differential signal remains indeed at the base line.

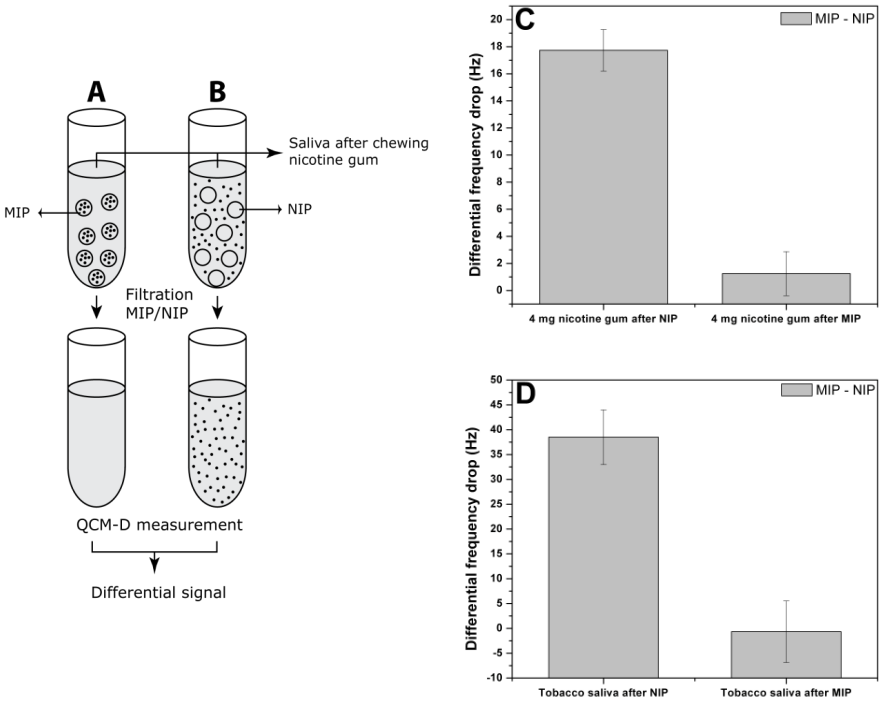

Figure 6.6 - QCM-D measurements on saliva samples obtained with 4 mg nicotine tablets and with smokeless tobacco. Each sample was either extracted with MIP powder (Figure 6.6 A) or with NIP powder (Figure 6.6 B) with negligible nicotine absorption. Figure 6.6 C shows the differential sensor response for NIP- or MIP-extracted samples obtained with a 4 mg nicotine tablet. The results for NIP- and MIP extracted saliva obtained while consuming smokeless tobacco are shown in Figure 6.6 D.

The differential sensor response with the NIP-extracted smokeless tobacco sample corresponds to 39 Hz ± 5 Hz, being more than twice as strong as the response obtained with the 4 mg nicotine-gum samples. This is in principle not surprising, since the nominal total nicotine content of 2 grams of smokeless tobacco is not less than 20 mg. In the sense of the dose-response

curve in Figure 6.2 B, the frequency drop by 40 Hz is equivalent to a concentration in the range of about 100 µM. Here, we point out that this concentration is only indicative because smokeless tobacco also contains salts and pH agents besides flavorings, which stimulate the actual nicotine uptake *via* the mucous tissue in the oral cavity. Nevertheless, experiments indicate that there must be a massive release of nicotine, exceeding the response obtained with tablets that are usually employed to reduce the withdrawal symptoms of former smokers.

6.4 Conclusion

A MIP with a high affinity and specificity towards L-nicotine has been developed for the use in aqueous fluids. This MIP was successfully integrated in a QCM-D sensor crystal by immobilizing them into a spincoated PVC layer on top of the upper gold electrode. The MIP performance to specifically bind L-nicotine in biological solutions was tested with spiked saliva and urine samples diluted into dH_2O or 0.1 x PBS. First, the MIP was tested with dH_2O where it showed a sub-linear frequency response to increasing L-nicotine concentration in the lower micromolar range while the control samples showed no specific response. Dissipation-response results were also promising and may serve as an alternative way to differentiate between nicotine-spiked- and non-spiked saliva samples. The same experiment was also performed in 0.1 x PBS at pH value of pH 9 with L-nicotine spiked saliva samples. The frequency response was lower in comparison with dH_2O, however L-nicotine could still be successfully detected in the micromolar range. The use of the MIP sensor in patients' samples was tested with saliva obtained during chewing of nicotine gums with different standard concentrations and while using smokeless tobacco. The sensor was indeed able to distinguish between different concentrations of L-nicotine in saliva while chewing nicotine gums. Consistently, we observed a strong nicotine release when consuming smokeless tobacco. This illustrates that MIPs are versatile receptors for small-molecule detection in complex fluids when combined with quartz-crystal microbalances or other analytical techniques used in the pharmaceutical, environmental, and bioanalytical sectors.

7 Conclusions

The main goal of the work described in this thesis was to examine the viability of molecular imprinted polymers as a recognition layer in biosensor for low molecular weight molecules in real life samples. To achieve this goal multiple MIPs were meticulously prepared and tested with multiple detection methods, each with their own advantages.

MIPs were created for histamine, malachite green and L-nicotine. The histamine and L-nicotine MIPs were created *via* bulk polymerization while the malachite green MIP was created *via* suspension polymerization. Bulk polymerization is a straightforward process in the creation of MIPs. The target molecule is mixed together with functional monomers and crosslinker. This mixture is polymerized, crushed and sieved. After removal of the target molecule, a nanocavity that can rebind the analyte is left behind. The sensitivity, specificity and overall working performance can be analyzed with UV-Vis spectroscopy. This can be used as a first assessment step in the development of an optimal MIP for sensor purposes. With the use of binding isotherms the MIP and corresponding NIP are selected on basis of binding affinity, heterogenic distribution, amount of binding sites per gram and specificity toward the target analyte.

These selected MIPs were immobilized onto the polymer surface of the sensor setup (OC_1C_{10}-PPV for impedance spectroscopy and PVC for QCM measurements) *via* the PDMS stamp techniques. This resulted in a surface coverage of 38.6 % for the histamine MIP, 30.0 % for the malachite green MIP and 20.2 % for the L-nicotine MIP. The MIP coverage on the sensor surface is dependent on the hardness and size of the MIP particles. The softer and the smaller the MIP particles are the better the coverage will be. Furthermore, the choice of the porogen is vital for sensor coverage as this will determine the characteristics of the MIP. In order to improve the surface

coverage other imprinting techniques can be used. Ideally the growing of the MIP directly on sensor electrodes would provide a 100% surface coverage.

The histamine and malachite green MIPs were both implemented in the impedimetric and the QCM sensor setup, whereas L-nicotine was tested with the QCM setup. The two detection techniques used in the sensor setup each have their own advantages and disadvantages. The primary advantage of the impedimetric setup is the sensitivity that can be achieved for low molecular weight molecules. Using impedimetric measurements, malachite green could be detected in the sub nano-molar range while histamine detection could be achieved under 10 nM. Another major advantage is that impedance spectroscopy is a label-free technique, which is favorable as the need for labeling can influence the obtained results. Sensing of the analyte in actual biological fluids is possible in the ppb range as shown with histamine sensing in tuna brine. The impedance spectroscopy techniques also allows for miniaturization of the apparatus making this a very feasible technique for 'point of care' sensors.

The quartz crystal microbalance main advantage as a sensing technique is the straightforward use. Although the sensitivity for MIP sensing is lower as compared to impedance spectroscopy, the QCM is an excellent device for examining the binding characteristics of the MIP receptors. The QCM was used to measure histamine, malachite green and L-nicotine. Histamine and L-nicotine could be detected in sub micro molar range in demi-water. Malachite green, being almost four times as heavy as histamine and L-nicotine, could successfully be measured in the sub nanomolar range. L-nicotine was also tested in various PBS solutions of different ionic strength and different pH values. The L-nicotine MIP had the optimal binding capacity at pH value of pH 9. The binding capacity also decreases when the ionic strength of the solution increases. The L-nicotine MIP detection was also demonstrated making use of dissipation sensing technique of the QCM-D setup. Finally, L-nicotine detection was also tested in actual biological fluids using QCM. First of all, QCM surfaces with L-nicotine MIPs were successfully tested to measure the presence of L-nicotine in spiked saliva and urine

samples in the submicro molar range. In addition, similar results could be obtained with dissipation detection of L-nicotine in spiked saliva. L-nicotine was also successfully detected in saliva samples collected after chewing nicotine gum with varying concentrations. Saliva samples were also successfully tested after chewing Skoal wintergreen chewing tobacco. This proves that the L-nicotine MIP is well suited to bind the analyte in complex matrices, proving that the MIPs are future proof for sensor applications.

8 References

1. Thévenot DR, Toth K, Durst RA, Wilson GS. Electrochemical biosensors: recommended definitions and classification. Biosens Bioelectron. 2001 Jan;16(1-2):121–31.

2. Yang J, Deng S, Lei J, Ju H, Gunasekaran S. Electrochemical synthesis of reduced graphene sheet–AuPd alloy nanoparticle composites for enzymatic biosensing. Biosensors and Bioelectronics. 2011 Nov 15;29(1):159–66.

3. Prodromidis MI, Karayannis MI. Enzyme Based Amperometric Biosensors for Food Analysis. Electroanalysis. 2002;14(4):241–61.

4. Zhao W-W, Yu P-P, Xu J-J, Chen H-Y. Ultrasensitive photoelectrochemical biosensing based on biocatalytic deposition. Electrochemistry Communications. 2011 May;13(5):495–7.

5. Cooreman P, Thoelen R, Manca J, vandeVen M, Vermeeren V, Michiels L, et al. Impedimetric immunosensors based on the conjugated polymer PPV. Biosensors and Bioelectronics. 2005 Apr 15;20(10):2151–6.

6. Frederix F, Bonroy K, Laureyn W, Reekmans G, Campitelli A, Dehaen W, Maes G. Enhanced Performance of an Affinity Biosensor Interface Based on Mixed Self-Assembled Monolayers of Thiols on Gold. Langmuir. 2003 May 1;19(10):4351–7.

7. Vermeeren V, Grieten L, Vanden Bon N, Bijnens N, Wenmackers S, Janssens SD, et al. Impedimetric, diamond-based immmunosensor for the detection of C-reactive protein. Sensors and Actuators B: Chemical. 2011 Sep 20;157(1):130–8.

8. Naessens M, Tran-Minh C. Whole-cell biosensor for direct determination of solvent vapours. Biosensors and Bioelectronics. 1998 Mar 1;13(3–4):341–6.

9. Peter J, Hutter W, Stöllnberger W, Hampel W. Detection of chlorinated and brominated hydrocarbons by an ion sensitive whole cell biosensor. Biosensors and Bioelectronics. 1996;11(12):1215–9.

10. Akyilmaz E, Yaşa İ, Dinçkaya E. Whole cell immobilized amperometric biosensor based on Saccharomyces cerevisiae for selective determination of vitamin B1 (thiamine). Analytical Biochemistry. 2006 Jul 1;354(1):78–84.

11. Vermeeren V, Bijnens N, Wenmackers S, Daenen M, Haenen K, Williams OA, et al. Towards a real-time, label-free, diamond-based DNA sensor. Langmuir. 2007 Dec 18;23(26):13193–202.

12. Grinsven B van, Vanden Bon N, Grieten L, Murib M, Janssens SD, Haenen K, et al. Rapid assessment of the stability of DNA duplexes by impedimetric real-time monitoring of chemically induced denaturation. Lab Chip. 2011 May 7;11(9):1656–63.

13. Schöning MJ, Poghossian A. Bio FEDs (Field-Effect Devices): State-of-the-Art and New Directions. Electroanalysis. 2006;18(19-20):1893–900.

14. Je S, Aj B. The pathogenesis of diabetic foot problems: an overview. Diabetes. 1997 Sep;46 Suppl 2:S58–61.

15. Boron WF, Boulpaep EL. Medical Physiology E-Book. Elsevier Health Sciences; 2008, ISBN 0721632564, Amsterdam

16. Agarwal PK. Enzymes: An integrated view of structure, dynamics and function. Microbial Cell Factories. 2006 Jan 12;5(1):2.

17. Nairn R, Helbert M. Immunology for Medical Students. Mosby; 2007, ISBN 0-323-04331-3, Philadelphia.

18. Kim K-K, Won H-H, Cho SS, Park JH, Kim M-J, Kim S, et al. Comparison of identical single nucleotide polymorphisms genotyped by the GeneChip Targeted Genotyping 25K, Affymetrix 500K and Illumina 550K platforms. Genomics. 2009 Aug;94(2):89–93.

19. Gabl R, Feucht H-D, Zeininger H, Eckstein G, Schreiter M, Primig R, et al. First results on label-free detection of DNA and protein molecules using a novel integrated sensor technology based on gravimetric detection principles. Biosensors and Bioelectronics. 2004 Jan 15;19(6):615–20.

20. Rodriguez MC, Kawde A-N, Wang J. Aptamer biosensor for label-free impedance spectroscopy detection of proteins based on recognition-induced switching of the surface charge. Chem. Commun. 2005 Aug 22;(34):4267–9.

21. Tran DT, Vermeeren V, Grieten L, Wenmackers S, Wagner P, Pollet J, et al. Nanocrystalline diamond impedimetric aptasensor for the label-free detection of human IgE. Biosensors and Bioelectronics. 2011 Feb 15;26(6):2987–93.

22. Owens P., Karlsson L, Lutz ES., Andersson L. Molecular imprinting for bio- and pharmaceutical analysis. TrAC Trends in Analytical Chemistry. 1999 Mar;18(3):146–54.

23. Cormack PAG, Elorza AZ. Molecularly imprinted polymers: synthesis and characterisation. Journal of Chromatography B. 2004 May 5;804(1):173–82.

24. Sellergren B. Molecular imprinting by noncovalent interactions. Enantioselectivity and binding capacity of polymers prepared under conditions favoring the formation of template complexes. Die Makromolekulare Chemie. 1989;190(11):2703–11.

25. Spivak DA. Optimization, evaluation, and characterization of molecularly imprinted polymers. Advanced Drug Delivery Reviews. 2005 Dec 6;57(12):1779–94.

26. Jahanzad F, Sajjadi S, Yianneskis M, Brooks BW. In situ mass-suspension polymerisation. Chemical Engineering Science. 2008 Sep 1;63(17):4412–7.

27. Chaitidou S, Kotrotsiou O, Kotti K, Kammona O, Bukhari M, Kiparissides C. Precipitation polymerization for the synthesis of nanostructured particles. Materials Science and Engineering: B. 2008 Aug 25;152(1–3):55–9.

28. Pietrzyk A, Suriyanarayanan S, Kutner W, Chitta R, D'Souza F. Selective Histamine Piezoelectric Chemosensor Using a Recognition Film of the Molecularly Imprinted Polymer of Bis(bithiophene) Derivatives. Anal. Chem. 2009 Apr 1;81(7):2633–43.

29. Pérez-Moral N, Mayes A. Comparative study of imprinted polymer particles prepared by different polymerisation methods. Analytica Chimica Acta. 2004 Feb 16;504(1):15–21.

30. Li S, Ge Y, Piletsky SA, Lunec J. Molecularly Imprinted Sensors: Overview and Applications. Elsevier; 2012.

31. Panasyuk-Delaney T, Mirsky VM, Wolfbeis OS. Capacitive Creatinine Sensor Based on a Photografted Molecularly Imprinted Polymer. Electroanalysis. 2002;14(3):221–4.

32. Pernites R, Ponnapati R, Felipe MJ, Advincula R. Electropolymerization molecularly imprinted polymer (E-MIP) SPR sensing of drug molecules: Pre-polymerization complexed terthiophene and carbazole electroactive monomers. Biosensors and Bioelectronics. 2011 Jan 15;26(5):2766–71.

33. Horemans F, Alenus J, Bongaers E, Weustenraed A, Thoelen R, Duchateau J, et al. MIP-based sensor platforms for the detection of histamine in the nano- and micromolar range in aqueous media. Sensors and Actuators B: Chemical. 2010 Jul 15;148(2):392–8.

34. Haupt K, Mosbach K. Plastic antibodies: developments and applications. Trends in Biotechnology. 1998 Nov 1;16(11):468–75.

35. Yang Z, Zhang C. Designing of MIP-based QCM sensor for the determination of Cu(II) ions in solution. Sensors and Actuators B: Chemical. 2009 Oct 12;142(1):210–5.

36. Bolisay LD, Culver JN, Kofinas P. Molecularly imprinted polymers for tobacco mosaic virus recognition. Biomaterials. 2006 Aug;27(22):4165–8.

37. Ogiso M, Minoura N, Shinbo T, Shimizu T. DNA detection system using molecularly imprinted polymer as the gel matrix in electrophoresis. Biosensors and Bioelectronics. 2007 Apr 15;22(9–10):1974–81.

38. Shi H, Tsai W-B, Garrison MD, Ferrari S, Ratner BD. Template-imprinted nanostructured surfaces for protein recognition. Nature. 1999 Apr 15;398(6728):593–7.

39. Lu C-H, Zhang Y, Tang S-F, Fang Z-B, Yang H-H, Chen X, et al. Sensing HIV related protein using epitope imprinted hydrophilic polymer coated quartz crystal microbalance. Biosensors and Bioelectronics. 2012 Jan 15;31(1):439–44.

40. Hayden O, Bindeus R, Haderspöck C, Mann K-J, Wirl B, Dickert FL. Mass-sensitive detection of cells, viruses and enzymes with artificial receptors. Sensors and Actuators B: Chemical. 2003 Jun 1;91(1–3):316–9.

41. Alizadeh T, Zare M, Ganjali MR, Norouzi P, Tavana B. A new molecularly imprinted polymer (MIP)-based electrochemical sensor for monitoring 2,4,6-trinitrotoluene (TNT) in natural waters and soil samples. Biosensors and Bioelectronics. 2010 Jan 15;25(5):1166–72.

42. Sun H, Mo ZH, Choy JTS, Zhu DR, Fung YS. Piezoelectric quartz crystal sensor for sensing taste-causing compounds in food. Sensors and Actuators B: Chemical. 2008 Apr 14;131(1):148–58.

43. Bereczki A, Tolokán A, Horvai G, Horváth V, Lanza F, Hall AJ, et al. Determination of phenytoin in plasma by molecularly imprinted solid-phase extraction. Journal of Chromatography A. 2001 Sep 28;930(1–2):31–8.

44. Masqué N, Marcé R., Borrull F. Molecularly imprinted polymers: new tailor-made materials for selective solid-phase extraction. TrAC Trends in Analytical Chemistry. 2001 Sep;20(9):477–86.

45. Feng Q, Zhao L, Lin J-M. Molecularly imprinted polymer as micro-solid phase extraction combined with high performance liquid chromatography to determine phenolic compounds in environmental water samples. Analytica Chimica Acta. 2009 Sep 14;650(1):70–6.

46. Alvarez-Lorenzo C, Concheiro A. Molecularly imprinted polymers for drug delivery. Journal of Chromatography B. 2004 May 5;804(1):231–45.

47. Strikovsky A, Hradil J, Wulff G. Catalytically active, molecularly imprinted polymers in bead form. Reactive and Functional Polymers. 2003 Jan;54(1–3):49–61.

48. Thoelen R, Vansweevelt R, Duchateau J, Horemans F, D'Haen J, Lutsen L, et al. A MIP-based impedimetric sensor for the detection of low-MW molecules. Biosensors and Bioelectronics. 2008 Jan 18;23(6):913–8.

49. Alenus J, Galar P, Ethirajan A, Horemans F, Weustenraed A, Cleij TJ, et al. Detection of L-nicotine with dissipation mode quartz crystal microbalance using molecular imprinted polymers. physica status solidi (a). 2012 May 1;209(5):905–10.

50. Valero-Navarro A, Salinas-Castillo A, Fernández-Sánchez JF, Segura-Carretero A, Mallavia R, Fernández-Gutiérrez A. The development of a MIP-optosensor for the detection of monoamine naphthalenes in drinking water. Biosensors and Bioelectronics. 2009 Mar 15;24(7):2305–11.

51. Lai EP, Fafara A, VanderNoot VA, Kono M, Polsky B. Surface plasmon resonance sensors using molecularly imprinted polymers for sorbent assay of theophylline, caffeine, and xanthine. Canadian Journal of Chemistry. 1998 Mar;76(3):265–73.

52. Kugimiya A, Takeuchi T. Surface plasmon resonance sensor using molecularly imprinted polymer for detection of sialic acid. Biosensors and Bioelectronics. 2001 Dec;16(9–12):1059–62.

53. Matsunaga T, Hishiya T, Takeuchi T. Surface plasmon resonance sensor for lysozyme based on molecularly imprinted thin films. Analytica Chimica Acta. 2007 May 15;591(1):63–7.

54. Eggins BR. Biosensors: an introduction. Wiley-Teubner; 1996.

55. Riley JF, West GB. The presence of histamine in tissue mast cells. J Physiol. 1953 Jun 29;120(4):528–37.

56. Inhibitability and Enhanceability of Basophil Histamine Release in Asthmatic and Normal Subjects. International Archives of Allergy and Immunology. 1985;76(4):344–9.

57. Lagunoff D, Martin TW, Read G. Agents that Release Histamine from Mast Cells. Annual Review of Pharmacology and Toxicology. 1983;23(1):331–51.

58. Thompson WG, Longstreth GF, Drossman DA, Heaton KW, Irvine EJ, Muller-Lissner SA. Functional bowel disorders and functional abdominal pain. Gut. 1999 Sep 1;45(Supplement 2):ii43–ii47.

59. Saito YA, Schoenfeld P, Iii GRL. The epidemiology of irritable bowel syndrome in North America: a systematic review. The American Journal of Gastroenterology. 2002;97(8):1910–5.

60. Talley NJ. Irritable bowel syndrome: definition, diagnosis and epidemiology. Best Practice & Research Clinical Gastroenterology. 1999 Oct;13(3):371–84.

61. Smout AJPM. Prikkelbare Darm Syndroom. Inmerc; 2003, ISBN 9066113979, Wormer.

62. Wood JD, Alpers DH, Andrews PLR. Fundamentals of neurogastroenterology. Gut. 1999 Sep 1;45(Supplement 2):ii6–ii16.

63. Drossman DA. Review article: an integrated approach to the irritable bowel syndrome. Alimentary Pharmacology & Therapeutics. 1999;13:3–14.

64. Drossman DA. The functional gastrointestinal disorders and the Rome II process. Gut. 1999 Sep 1;45(Supplement 2):ii1–ii5.

65. O'Sullivan M, Clayton N, Breslin NP, Harman I, Bountra C, Mclaren A, O'Morain CA. Increased mast cells in the irritable bowel syndrome. Neurogastroenterology & Motility. 2000;12(5):449–57.

66. Weston AP, Biddle WL, Bhatia PS, Miner PB. Terminal ileal mucosal mast cells in irritable bowel syndrome. Digestive Diseases and Sciences. 1993;38(9):1590–5.

67. Santos J, Saperas E, Nogueiras C, Mourelle M, Antolín M, Cadahia A, et al. Release of mast cell mediators into the jejunum by cold pain stress in humans. Gastroenterology. 1998 Apr;114(4):640–8.

68. Barbara G, Stanghellini V, De Giorgio R, Cremon C, Cottrell GS, Santini D, et al. Activated mast cells in proximity to colonic nerves correlate with abdominal pain in irritable bowel syndrome. Gastroenterology. 2004 Mar;126(3):693–702.

69. Lehane L, Olley J. Histamine fish poisoning revisited. International Journal of Food Microbiology. 2000 Jun 30;58(1–2):1–37.

70. Chen H-C, Huang Y-R, Hsu H-H, Lin C-S, Chen W-C, Lin C-M, et al. Determination of histamine and biogenic amines in fish cubes (Tetrapturus angustirostris) implicated in a food-borne poisoning. Food Control. 2010 Jan;21(1):13–8.

71. Taylor SL, Stratton JE, Nordlee JA. Histamine Poisoning (Scombroid Fish Poisoning): An Allergy-Like Intoxication. Clinical Toxicology. 1989 Jan;27(4-5):225–40.

72. Tsai Y-H, Lin C-Y, Chien L-T, Lee T-M, Wei C-I, Hwang D-F. Histamine contents of fermented fish products in Taiwan and isolation of histamine-forming bacteria. Food Chemistry. 2006;98(1):64–70.

73. Histamine Toxicity from Fish. 2012 Jun 17 [cited 2012 Sep 5]; Available from: http://emedicine.medscape.com/article/1009464-overview

74. Ding F, Li X-N, Diao J-X, Sun Y, Zhang L, Ma L, et al. Potential toxicity and affinity of triphenylmethane dye malachite green to lysozyme. Ecotoxicology and Environmental Safety. 2012 Apr 1;78(0):41–9.

75. Yonar ME, Yonar SM. Changes in selected immunological parameters and antioxidant status of rainbow trout exposed to malachite green (Oncorhynchus mykiss, Walbaum, 1792). Pesticide Biochemistry and Physiology. 2010 May;97(1):19–23.

76. Fernandes C, Lalitha VS, Rao KVK. Enhancing effect of malachite green on the development of hepatic pre-neoplastic lesions induced by N-nitrosodiethylamine in rats. Carcinogenesis. 1991 Jan 5;12(5):839–45.

77. Meyer FP, Jorgenson TA. Teratological and Other Effects of Malachite Green on Development of Rainbow Trout and Rabbits. Transactions of the American Fisheries Society. 1983;112(6):818–24.

78. Srivastava S, Sinha R, Roy D. Toxicological effects of malachite green. Aquatic Toxicology. 2004 Feb 25;66(3):319–29.

79. Kietzmann M, Hapke HJ, Beeke M, Stehle S. [Problems with malachite green use in fish]. DTW. Dtsch. Tierärztleche Wochenschr. 1990 Jul;97(7):290–3.

80. Henningfield JE, Cohen C, Slade JD. Is nicotine more addictive than cocaine? British Journal of Addiction. 1991;86(5):565–9.

81. Weinberger AH, Sofuoglu M. The Impact of Cigarette Smoking on Stimulant Addiction. The American Journal of Drug and Alcohol Abuse. 2009 Jan;35(1):12–7.

82. Benowitz NL. Nicotine Addiction. N Engl J Med. 2010 Jun 17;362(24):2295–303.

83. Hoffmann D, Djordjevic MV, Hoffmann I. The Changing Cigarette. Preventive Medicine. 1997 Jul;26(4):427–34.

84. Schrek R, Baker LA, Ballard GP, Dolgoff S. Tobacco Smoking as an Etiologic Factor in Disease. I. Cancer. Cancer Res. 1950 Jan 1;10(1):49–58.

85. Doll R, Peto R. The causes of cancer: quantitative estimates of avoidable risks of cancer in the United States today. Journal of the National Cancer Institute. 1981 Jun;66(6):1191.

86. Mayer AS, Newman LS. Genetic and environmental modulation of chronic obstructive pulmonary disease. Respiration Physiology. 2001 Oct;128(1):3–11.

87. Ambrose JA, Barua RS. The pathophysiology of cigarette smoking and cardiovascular disease: An update. Journal of the American College of Cardiology. 2004 May 19;43(10):1731–7.

88. Bergström J. Tobacco smoking and chronic destructive periodontal disease. Odontology. 2004;92(1):1–8.

89. Yang X-L, Luo M-B, Ding J-H. Rapid Determination of Nicotine in Saliva by Liquid Phase Microextraction-High Performance Liquid Chromatography. Chinese Journal of Analytical Chemistry. 2007 Feb;35(2):171–4.

90. Louwet F, Vanderzande D, Gelan J. A general synthetic route to high molecular weight poly(p-xylylene)-derivatives: a new route to poly(p-phenylene vinylene). Synthetic Metals. 1995 Mar 1;69(1-3):509–10.

91. Ansell RJ, Kriz D, Mosbach K. Molecularly imprinted polymers for bioanalysis: chromatography, binding assays and biomimetic sensors. Current Opinion in Biotechnology. 1996 Feb;7(1):89–94.

92. Umpleby II RJ, Baxter SC, Bode M, Berch Jr. JK, Shah RN, Shimizu KD. Application of the Freundlich adsorption isotherm in the characterization of molecularly imprinted polymers. Analytica Chimica Acta. 2001 May 17;435(1):35–42.

93. Umpleby II RJ, Baxter SC, Rampey AM, Rushton GT, Chen Y, Shimizu KD. Characterization of the heterogeneous binding site affinity distributions in molecularly imprinted polymers. Journal of Chromatography B. 2004 May 5;804(1):141–9.

94. Pei R, Cheng Z, Wang E, Yang X. Amplification of antigen–antibody interactions based on biotin labeled protein–streptavidin network complex using impedance spectroscopy. Biosensors and Bioelectronics. 2001 Aug;16(6):355–61.

95. Wang M, Wang L, Wang G, Ji X, Bai Y, Li T, et al. Application of impedance spectroscopy for monitoring colloid Au-enhanced antibody immobilization and antibody–antigen reactions. Biosensors and Bioelectronics. 2004 Jan 15;19(6):575–82.

96. Martinsen OG, Grimnes S. Bioimpedance and Bioelectricity Basics. Academic Press; 2008, ISBN 0123740045.

97. Sauerbrey G. Verwendung von Schwingquarzen zur Wägung dünner Schichten und zur Mikrowägung. Zeitschrift für Physik A Hadrons and Nuclei. 1959 Apr 1;155(2):206–22.

98. Modin C, Stranne A-L, Foss M, Duch M, Justesen J, Chevallier J, et al. QCM-D studies of attachment and differential spreading of pre-osteoblastic cells on Ta and Cr surfaces. Biomaterials. 2006 Mar;27(8):1346–54.

99. Atashbar MZ, Bejcek B, Vijh A, Singamaneni S. QCM biosensor with ultra thin polymer film. Sensors and Actuators B: Chemical. 2005 Jun 29;107(2):945–51.

100. Tammelin T, Saarinen T, Österberg M, Laine J. Preparation of Langmuir/Blodgett-cellulose Surfaces by Using Horizontal Dipping Procedure. Application for Polyelectrolyte Adsorption Studies Performed with QCM-D. Cellulose. 2006;13(5):519–35.

101. Richter RP, Brisson AR. Following the Formation of Supported Lipid Bilayers on Mica: A Study Combining AFM, QCM-D, and Ellipsometry. Biophysical Journal. 2005 May;88(5):3422–33.

102. Harsing LG, Nagashima H, Duncalf D, Vizi ES, Goldiner PL. Determination of histamine concentrations in plasma by liquid chromatography/electrochemistry. Clinical Chemistry. 1986 Jan 10;32(10):1823–7.

103. Von Mach-Szczypiński J, Stanosz S, Sieja K, Stanosz M. Metabolism of histamine in tissues of primary ductal breast cancer. Metabolism. 2009 Jun;58(6):867–70.

104. Auerswald L, Morren C, Lopata AL. Histamine levels in seventeen species of fresh and processed South African seafood. Food Chemistry. 2006;98(2):231–9.

105. Gosetti F, Mazzucco E, Gianotti V, Polati S, Gennaro MC. High performance liquid chromatography/tandem mass spectrometry determination of biogenic amines in typical Piedmont cheeses. Journal of Chromatography A. 2007 May 18;1149(2):151–7.

106. Claeys-Bruno M, Vandenabeele-Trambouze O, Sergent M, Geffard M, Bodet D, Dobrijevic M, et al. Methodological approaches for histamine quantification using derivatization by chloroethylnitrosourea and ELISA measurement. Part II: Optimisation of the derivatization step. Chemometrics and Intelligent Laboratory Systems. 2006 Feb 15;80(2):186–97.

107. Peeters M, Troost FJ, van Grinsven B, Horemans F, Alenus J, Murib MS, et al. MIP-based biomimetic sensor for the electronic detection of serotonin in human blood plasma. Sensors and Actuators B: Chemical. 2012 Aug;171–172:602–10.

108. Umpleby II RJ, Bode M, Shimizu KD. Measurement of the continuous distribution of binding sites in molecularly imprinted polymers. The Analyst. 2000;125(7):1261–5.

109. Freundlich H. Üeber die Adsorption in Lösungen.: Engelmann; 1906, Leipzig.

110. Rogers PL, Staruszkiewicz WF. Histamine Test Kit Comparison. Journal of Aquatic Food Product Technology. 2000;9(2):5–17.

111. Haginaka J. Monodispersed, molecularly imprinted polymers as affinity-based chromatography media. Journal of Chromatography B. 2008 Apr 15;866(1–2):3–13.

112. Stammati A, Nebbia C, Angelis ID, Albo AG, Carletti M, Rebecchi C, et al. Effects of malachite green (MG) and its major metabolite, leucomalachite green (LMG), in two human cell lines. Toxicology in Vitro. 2005 Oct;19(7):853–8.

113. Bergwerff AA, Scherpenisse P. Determination of residues of malachite green in aquatic animals. Journal of Chromatography B. 2003 May 25;788(2):351–9.

114. Cheng D, Li B. Simple and sensitive fluorometric sensing of malachite green with native double-stranded calf thymus DNA as sensing material. Talanta. 2009 May 15;78(3):949–53.

115. Lee S, Choi J, Chen L, Park B, Kyong JB, Seong GH, et al. Fast and sensitive trace analysis of malachite green using a surface-enhanced Raman microfluidic sensor. Analytica Chimica Acta. 2007 May 8;590(2):139–44.

116. Tsai W-T, Chen H-R. Removal of malachite green from aqueous solution using low-cost chlorella-based biomass. Journal of Hazardous Materials. 2010 Mar 15;175(1–3):844–9.

117. Hameed BH, El-Khaiary MI. Batch removal of malachite green from aqueous solutions by adsorption on oil palm trunk fibre: Equilibrium isotherms and kinetic studies. Journal of Hazardous Materials. 2008 Jun 15;154(1–3):237–44.

118. Hameed BH, El-Khaiary MI. Kinetics and equilibrium studies of malachite green adsorption on rice straw-derived char. Journal of Hazardous Materials. 2008 May 1;153(1–2):701–8.

119. Bekçi Z, Özveri C, Seki Y, Yurdakoç K. Sorption of malachite green on chitosan beads. Journal of Hazardous Materials. 2008 Jun 15;154(1–3):254–61.

120. Yan S, Gao Z, Fang Y, Cheng Y, Zhou H, Wang H. Characterization and quality assessment of binding properties of malachite green molecularly imprinted polymers prepared by precipitation polymerization in acetonitrile. Dyes and Pigments. 2007;74(3):572–7.

121. Su LQ, Qiao S, Zhang WB. Studies on the synthesis and properties of malachite green imprinted polymer. Chinese Chemical Letters. 2007 Feb;18(2):229–32.

122. Li Y, Yang T, Qi X, Qiao Y, Deng A. Development of a group selective molecularly imprinted polymers based solid phase extraction of malachite green from fish water and fish feed samples. Analytica Chimica Acta. 2008 Aug 29;624(2):317–25.

123. Long C, Mai Z, Yang Y, Zhu B, Xu X, Lu L, et al. Determination of multi-residue for malachite green, gentian violet and their metabolites in aquatic products by high-performance liquid chromatography coupled with molecularly imprinted solid-phase extraction. Journal of Chromatography A. 2009 Mar 20;1216(12):2275–81.

124. Martínez Bueno MJ, Herrera S, Uclés A, Agüera A, Hernando MD, Shimelis O, et al. Determination of malachite green residues in fish using molecularly imprinted solid-phase extraction followed by liquid chromatography–linear ion trap mass spectrometry. Analytica Chimica Acta. 2010 Apr 14;665(1):47–54.

125. García-Calzón JA, Díaz-García ME. Characterization of binding sites in molecularly imprinted polymers. Sensors and Actuators B: Chemical. 2007 May;123(2):1180–94.

126. Cacho C, Schweitz L, Turiel E, Pérez-Conde C. Molecularly imprinted capillary electrochromatography for selective determination of thiabendazole in citrus samples. Journal of Chromatography A. 2008 Feb 1;1179(2):216–23.

127. Yan H, Row KH. Characteristics of a Monolithic Molecularly Imprinted Column and Its Application for Chromatographic Separation. J. Ind. Eng. Chem. 2007;13(4):552–7.

128. Reimhult K, Yoshimatsu K, Risveden K, Chen S, Ye L, Krozer A. Characterization of QCM sensor surfaces coated with molecularly imprinted nanoparticles. Biosensors and Bioelectronics. 2008 Jul 15;23(12):1908–14.

129. Larsson C, Bramfeldt H, Wingren C, Borrebaeck C, Höök F. Gravimetric antigen detection utilizing antibody-modified lipid bilayers. Analytical Biochemistry. 2005 Oct 1;345(1):72–80.

130. Höök F, Rodahl M, Brzezinski P, Kasemo B. Measurements Using the Quartz Crystal Microbalance Technique of Ferritin Monolayers on Methyl-Thiolated Gold: Dependence of Energy Dissipation and Saturation Coverage on Salt Concentration. Journal of Colloid and Interface Science. 1998 Dec 1;208(1):63–7.

131. Michanek A, Kristen N, Höök F, Nylander T, Sparr E. RNA and DNA interactions with zwitterionic and charged lipid membranes — A DSC and QCM-D study. Biochimica et Biophysica Acta (BBA) - Biomembranes. 2010 Apr;1798(4):829–38.

132. Bongaers E, Alenus J, Horemans F, Weustenraed A, Lutsen L, Vanderzande D, et al. A MIP-based biomimetic sensor for the impedimetric detection of histamine in different pH environments. physica status solidi (a). 2010 Apr 1;207(4):837–43.

133. Peeters M, Troost FJ, Mingels RHG, Welsch T, van Grinsven B, Vranken T, et al. Impedimetric Detection of Histamine in Bowel Fluids Using Synthetic Receptors with pH-Optimized Binding Characteristics. Anal. Chem. 2013 Feb 5;85(3):1475–83.

134. Kevin J. Ivey MD F, PhD EJT. Absorption of nicotine by the human stomach and its effect on gastric ion fluxes and potential difference. Digest Dis Sci. 1978 Sep 1;23(9):809–14.

135. Neal L. B. The Role of Nicotine in Smoking-Related Cardiovascular Disease. Preventive Medicine. 1997 Jul;26(4):412–7.

136. Zander A, Findlay P, Renner T, Sellergren B, Swietlow A. Analysis of nicotine and its oxidation products in nicotine chewing gum by a molecularly imprinted solid phase extraction. Anal. Chem. 1998 Aug 1;70(15):3304–14.

137. Behera D, Uppal R, Majumdar S. Urinary levels of nicotine & cotinine in tobacco users. Indian J. Med. Res. 2003 Sep;118:129–33.

138. Henningfield JE, Radzius A, Cone EJ. Estimation of available nicotine content of six smokeless tobacco products. Tob Control. 1995 Mar;4(1):57–61.

References

9 Scientific Publications

- E. Bongaers, **J. Alenus**, F. Horemans, A. Weustenraed, L. Lutsen, D. Vanderzande, T. Cleij, F. J. Troost, R.J. Brummer and P. Wagner, A MIP-based biomimetic sensor for the impedimetric detection of histamine in different pH environments, Phys. Status Solidi A 207 (4), 837-843 (2010).

- E. Bongaers, **J. Alenus**, L. Grieten, P. Wagner, F. Troost, R.J. Brummer, Development of a biosensor for the detection of Histamine and Tryptase, Physicalia Magazine 25 (3), 123-131, 2007.

- F. Horemans, **J. Alenus**, E. Bongaers, A. Weustenraed, R. Thoelen, J. Duchateau, L. Lutsen, D. Vanderzande, P. Wagner and T.J. Cleij, MIP-based sensor platforms for the detection of histamine in the nano- and micromolar range in aqueous media, Sens. Actuators, B 148, 392-398 (2010)

- **J. Alenus**, P. Galar, A. Ethirajan, F. Horemans, A. Weustenraed, T.J. Cleij and P. Wagner, Detection of L-nicotine with dissipation mode quartz crystal microbalance using molecular imprinted polymers, Phys. Status Solidi A 209 (5), 905 -910 (2012).

- M. Peeters, F.J. Troost, B. Van grisven, F. Horemans, **J. Alenus**, M. S. Murib, D. Keszthelyi, A. Ethirajan, R. Thoelen, T.J. Cleij and P. Wagner, MIP-based biomimetic sensor for the electronic detection of serotonin in human blood plasma, Sensors and Actuators, B 171 - 172, 602–610 (2012).

- F. Horemans, **J. Alenus**, A. Weustenraed, K. Eersels, L. Lutsen, D. Vanderzande, P. Wagner and T.J. Cleij, Using MIP Beads as Novel Sensor Recognition Elements for the Detection of Malachite Green in Aqueous Media. (under preparation, 2013).

- **J. Alenus**, A. Ethirajan, F. Horemans, A. Weustenraed, T.J. Cleij and P. Wagner, Molecularly imprinted polymers as synthetic receptors for the QCM-D based detection of L-nicotine in saliva- and urine samples, submitted to Analytical and Bioanalytical Chemistry (February 2013).

10 Posters and oral presentations

- Belgian Physical Society, General Scientific Meeting, 30/05/2007, Antwerp (Belgium). E. Bongaers, L. Grieten, **J. Alenus**, P. Wagner, F. Troost, RJ. Brummer. Development of a biosensor for the detection of histamine and tryptase, (Poster).
    - **Best poster award**

- Belgian Polymer Group General Meeting 22-23/05/2008, De Haan (Belgium). R. Thoelen, **J. Alenus**, F. Horemans, J. Duchateau, L. Lutsen, D. Vanderzande, T.J. Cleij, and P. Wagner. Piezoelectric and Electrochemical Sensing of Small Molecules using Synthetic MIP-based Receptor, (Poster).

- The Tenth World Congress on Biosensors 14-16/05/2008, Shanghai (China). R. Thoelen, **J. Alenus**, F. Horemans, J. Duchateau, L. Lutsen, D. Vanderzande, T.J. Cleij, and P. Wagner. Piezoelectric and Electrochemical Sensing of Small Molecules using Synthetic MIP-based Receptor, (Poster).

- Tech Transfer Offices Flanders, 2009 Gent (Belgium). F. Horemans, A. Weustenraed, **J. Alenus**, L. Lutsen, D. Vanderzande, T.J. Cleij, P. Wagner. Development of molecularly imprinted polymers (MIPs) for Novel Bioanalytical Applications, (Poster).

- Belgian Physical Society, General Scientific Meeting, 01/04/2009, Hasselt. E. Bongaers, **J. Alenus**, F. Horemans, F.J Troost, R.J Brummer. A MIP-based Biosensor for the detection of Histamine, (Poster).

- Belgian Physical Society, General Scientific Meeting, 01/04/2009, Hasselt. **J. Alenus**, E. Bongaers, J. Duchateau, F. Horemans, L.

Lutsen, D. Vanderzande, T.J. Cleij, and P. Wagner. Piezoelectric detection of small molecules using synthetic MIP based receptors, (Poster).

- **Best poster award**

- Fysica 2010, 23/04/2010, Utrecht (The Netherlands). **J. Alenus**, F. Horemans, M. Leekens, A. Weustenraed, L. Lutsen, D. Vanderzande, T.J. Cleij, and P. Wagner. Impedimetric and piezoelectric detection of malachite green with molecular imprinted polymer beads as recognition element, (Poster).

- The Eleventh World Congress on Biosensors, 25-28/05/2010, Glasgow. **J. Alenus**, F. Horemans, A. Weustenraed, L. Lutsen, D. Vanderzande, T.J. Cleij, and P. Wagner. Malachite green detection with molecular imprinted polymer beads as recognition element in microgravimetric and impedimetric sensors, (Poster).

- Engineering of Functional Interfaces 15-16/06/2010, Marburg. **J. Alenus**, F. Horemans, E. Bongaers, A. Weustenraed, L. Lutsen, D. Vanderzande, T.J. Cleij, P. Wagner. Impedimetric and piezoelectric detection of low MW molecules using molecular imprinted polymers as recognition element, (Poster and Oral presentation).

- Belgian Physical Society, General Scientific Meeting 25/05/2011, Namur. **J. Alenus**, P. Galar, F. Horemans, E. Bongaers, A. Weustenraed, J. duchateau, , L. Lutsen, D. Vanderzande, T.J. Cleij, and P. Wagner. Impedicmetric and piezoelectric detection of low MW molecules using molecular imprinted polymers as recognition element, (Poster).

- Biomedica 07/04/2011, Eindhoven. **J. Alenus**, P. Galar, F. Horemans, E. Bongaers, A. Weustenraed, L. Lutsen, D. Vanderzande, T.J. Cleij, P. Wagner. Impedimetric and piezoelectric detection of low

MW molecules using molecular imprinted polymers as recognition element, (Poster).

- Interuniversitaire attractive polen 2011, **J. Alenus**, M. Peeters, F. Horemans, A. Weustenraed, T. Welsh, D. Vandezander, T.J. Cleij, and P. Wagner. Molecularly imprinted nanocavities: Synthetic receptor for small molecules, (Poster).

- Engineering of functional interfaces 19-20/07/2011, Linz. **J. Alenus**, P. Galar, F. Horemans, E. Bongaers, A. Weustenraed, L. Lutsen, D. Vanderzande, T.J. Cleij, and P. Wagner. Impedicmetric and piezoelectric detection of low MW molecules using molecular imprinted polymers as recognition element, (Poster).

- Graduate student symposium on molecular imprinting 28-30/09/2011. London. **J. Alenus**, P. Galar, F. Horemans, E. Bongaers, A. Weustenraed, L. Lutsen, D. Vanderzande, T.J. Cleij, P. Wagner. Impedimetric and piezoelectric detection of low MW molecules using molecular imprinted polymers as recognition element, (Poster and Oral).

11 Appendix 1: List of abbreviations

- AA Acryl amide
- AC Alternating current
- AIBN Azobisisobutyronitrile
- Al Aluminum
- CNS Central nervous system
- DMSO Dimethylsuffoxide
- DNA Deoxyribonucleic acid
- EGDM Ethylene glycol dimethacrylate
- EIS Electrochemical impedance spectroscopy
- ELISA Enzyme linked immunosorbant assay
- ENS Enteric nervous system
- GC Gas chromatography
- hCG Human chorionic gonadotropin
- HEMA Hydroxy ethyl methacrylate
- HPLC High performance liquid chromatography
- IBS Irritable bowel syndrome
- IS Impedance spectroscopy
- MAA methacrylic acid
- MG Malachite green
- MIP Molecular imprinted polymer
- NIP Non imprinted polymer
- PBS Phosphate buffered saline
- PCB Printed circuit board
- PDMS Poly(dimethylsiloxane)
- PPV Poly(p-phenylene vinylene)
- PVA Poly vinyl alchohol
- PVC Poly vinyl chloride
- PVD Physical vapor deposition
- QCM Quartz crystal microbalance

Appendix 1: List of abbreviations

- QCM-D Quartz crystal microbalance – dissipation
- SDS Sodium dodecyl sulfate
- SEM Scanning electron microscopy
- TDMA Tetramethylene dimethacrylate
- THF Tetra hydrofuran
- TRIM trimethyle propane trimethacrylate
- UV Ultraviolet
- VIS Visible

12 Appendix 2: List of figures

Appendix 2: List of figures

Appendix 2: List of figures

13 Appendix 3: List of tables